The Dissertation Committee for Francis Jude Martinez Certifies that this is the approved version of the following dissertation:

Digital Gamma-Gamma Coincidence Measurements for Neutron Activation Analysis

Committee:

_____
Sheldon Landsberger, Supervisor

_____
Peter Bode

_____
William Charlton

_____
Derek Haas

Digital Gamma-Gamma Coincidence Measurements for Neutron Activation Analysis

By

Francis Jude Martinez

Dissertation

Presented to the Faculty of the Graduate School of

The University of Texas at Austin

in Partial Fulfillment

of the Requirements

for the Degree of

DOCTOR OF PHILOSOPHY

The University of Texas at Austin

December 2021

Dedication

To my beautiful and amazing wife, Alicia, our perfect daughter Isabella Alessandra, our amazing sons Christopher Xavier and Dominic Patrick, and to our child in heaven that we never got to meet.
You are all my motivation in everything that I do.
This was done out of love for all of you.

Acknowledgements

I want to first thank my advisor, Dr. Sheldon Landsberger for his guidance, support and mentoring over the last 5 years. I started this PhD program knowing that I would be stretched to learn a lot but learned more about nuclear engineering, NAA and gamma-gamma coincidence than I could have ever imagined. It has been an honor and a pleasure to have had the opportunity to work with and learn from you.

I would like to thank Dr. Peter Bode, Dr. Bill Charlton, and Dr. Derek Haas for their support along the way and for all the constructive feedback that they provided as part of my dissertation committee.

I want to thank Jim Terry, Dr. Brandon de Luna, and Conny Egozi for all their help. Jim made it possible for me to work on my PhD during Covid by setting up the Pixie-16 system to be remotely accessible. Brandon and Conny helped me by running a number of experiments and helped me with resolving a number of problems along the way. Brandon's coding prowess allowed for an efficient way to process data by the development of the software used on this project.

I want to thank my group leader at Los Alamos National Laboratory, Dr. Dan Borovina, for supporting his employees to the point that he motivates them to continue furthering their educations. Through his support and motivation, he helps change lives by making us all better employees and better people.

I want to thank my deputy group leader Tom Stepan, and all my colleagues in W-10 at LANL. I am truly blessed to work with such supportive and caring people who all enjoy working with one another.

I want to thank my brother, sisters, brothers-in-law, sister-in-law and nephews for their love and their support. I want to thank them for helping keep life fun and never too serious.

I want to thank my Mom and Dad. They taught my brother, my sisters and me to always work hard in all that we do. They always told us that they would be proud of us as long as we always did our best. All my successes in life have been because I have tried to do my best just as they taught me. I try to instill this same principle in my own children.

Two people that I don't have the right words to thank are Mark Armijo and Justine Davidson. Mark, Justine, and I started this journey together as a group of LANL employees who wanted to get our PhDs. Their support with doing homework, studying for exams, studying for the qualifying exam and keeping me grounded when it seemed too much to handle is what has made it possible for me to make it here today. I would not have succeeded without the two of you.

I thank God for all the blessings he has bestowed on me, especially the gift of my family.

Lastly, but most importantly, I want to thank my amazing and beautiful wife and our wonderful children. They stood behind me when I proposed this crazy idea of getting a PhD while working full-time. They are patient, caring, supportive, and have always been my biggest cheerleaders. They deserve the PhD more than I do as they did the hard work while I got to have fun learning NAA and gamma-gamma coincidence! I would have never been successful without all of you. Words will never be able to describe how thankful I am for all that you have done and I can never begin to explain how much I love you all.

Digital Gamma-Gamma Coincidence Measurements for Neutron Activation Analysis

Francis Jude Martinez, Ph.D.

The University of Texas at Austin, 2021

Supervisor: Sheldon Landsberger

The ability to perform low level counting, specifically gamma spectroscopy, for unknown radionuclides provides some challenges. In many cases, the ability to assess a material requires the use of neutron activation analysis (NAA) to excite the unknown sample to allow for the use of gamma ray measurement techniques to determine the radionuclides that are present. Quite often, the ability to identify unique gamma rays is challenging due to the fact that many radionuclides have gamma rays that have energies that are nearby other gamma rays from other radionuclides. The Compton continuum and high background radiation levels also contribute to the difficulty to make these measurements.

This research has explored the use of an advanced digital gamma-gamma coincidence system, XIA Pixie-16, for use in neutron activation analysis. The reason for performing this research is that, although gamma-gamma coincidence in NAA is not a new area of research, there has not been a comprehensive study of the use of gamma-gamma coincidence for all NAA products. This research has the potential to benefit research and experiments that utilize NAA techniques for identifying unknown samples.

The new XIA Pixie-16 system was first assembled and characterized. It was then used to perform measurements for all applicable short-lived, medium-lived and long-lived NAA products.

The gamma-gamma coincidence system was utilized to identify radionuclides in different samples that have been demonstrated to be difficult to identify using standard gamma spectroscopy techniques. A thorough evaluation of the results of this research should serve as a reference for all future NAA research.

Table of Contents

Table of Tables

Table of Figures

Chapter 1: Introduction

Techniques for low-level radioactivity counting for alpha and beta particles, as well as gamma rays, have been used for many decades. The ability to make low-level counting successful has been a focus in many areas including nuclear engineering, nuclear physics, environmental monitoring, etc. Some examples of the use of low-level counting include the effect of uranium mining and remediation in the environment (Niese, 1996), the determination of ^{241}Pu in environmental samples (Lee & Lee, 1999), and radioactivity in food products (Kaihola, 2011). Different techniques for low-level counting have been explored and implemented over the past few decades with varying levels of success.

One of the primary issues in low-level radiation counting in gamma ray spectroscopy comes from the radiation emitted by natural radionuclides in the detector crystal and construction materials of the gamma ray detector (Knoll, 2010). Because this cannot be changed easily, the greatest area for improvement is with the control of external background radiation. This is most often done by implementing shielding techniques for reducing background radiation. This is implemented via the installation of shielding (typically lead, but also steel and tungsten) around the experimental setup to try to minimize external radiation making it to the detectors.

Another method for reducing background radiation for low-level radiation counting has been the design of underground laboratories. These laboratories have been constructed and installed to try to eliminate any and all background radiation, including cosmic radiation (Niese & Kohler, 1996). This technique is often coupled with the addition of external shielding for the counters and other external counting equipment. This technique has proven to be extremely effective with the background radiation count typically reduced by upwards of two orders of

magnitude when compared to a similar above-ground configuration. The largest challenge for these types of laboratories is the cost and difficulty to design and construct the laboratory.

The technique of Compton suppression has been utilized to reduce or eliminate the contribution of the Compton effect in gamma ray spectroscopy, in addition to the reduction of cosmic radiation, for low-level counting applications (Landsberger & Peshev, 1996). A Compton suppression system accounts for the contribution of the gamma ray and also the scattering photon and recoil electron which are formed when the gamma ray interacts with the detector. A Compton suppression system is designed to independently measure both the singles spectrum as well as the spectrum where the scattering photons of the continuum have been suppressed. A typical system is seen in Figure 1 while comparison of Compton suppression for thermal and epithermal neutron activation analysis (NAA) is shown in Figure 2.

Figure 1: Compton suppression system with germanium detector, four photomultiplier tubes and one central NaI detector.

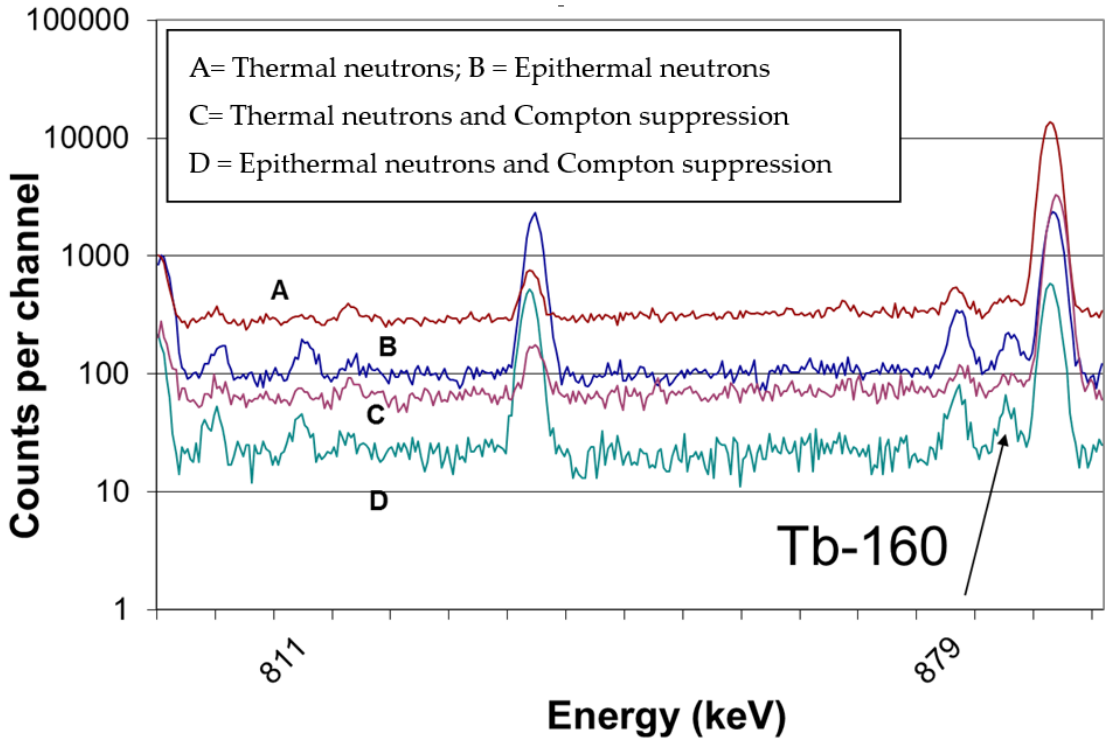

Figure 2: Determination of ^{160}Tb in NAA under different irradiation and counting conditions.

This technique has been successfully used in NAA for many years in various environmental and geological measurement applications (Canion & Landsberger, 2013; Landsberger & Wu, 1995; Stokley & Landsberger, 2018; Landsberger & Yellin, 2018).

While Compton suppression can reduce the background significantly within the Compton continuum, gamma-gamma coincidence (GCC) can reduce the background level across all energies by rejecting events that don't occur in coincidence. One specific application that this research will investigate is utilizing gamma-gamma coincidence for samples that have undergone neutron activation. Neutron activation analysis (NAA) is a well-established multielement technique to determine a wide variety of matrices. However, in many instances the continuum that exists are spectral interferences which are major deterrents to determine many elements in very low concentrations. While gamma-gamma coincidence has been used in NAA in the past for very specific applications, there has never been a comprehensive study of its optimization for use for

all NAA products. The two main goals of this dissertation are to implement and characterize an advanced digital system, the XIA Pixie-16, for use in gamma-gamma coincidence and to demonstrate its utility for use in NAA through the evaluation of a subset of NAA products contained within various certified reference materials.

Chapter 2: Literature Review

This section is intended to provide an overview of the use of gamma-gamma coincidence techniques from its earliest use through the implementation of digital gamma-gamma coincidence systems up to the current day.

Due to the evolution of the efficacy of gamma-gamma coincidence measurements over several decades, nuclear physicists started utilizing this technique, and continue to do so to elucidate nuclear decay schemes. The ability to gate gamma energies has also proven to be extremely beneficial due to its ability to effectively demonstrate which gamma rays are specifically in coincidence with one another. A few examples of gated spectra are shown below.

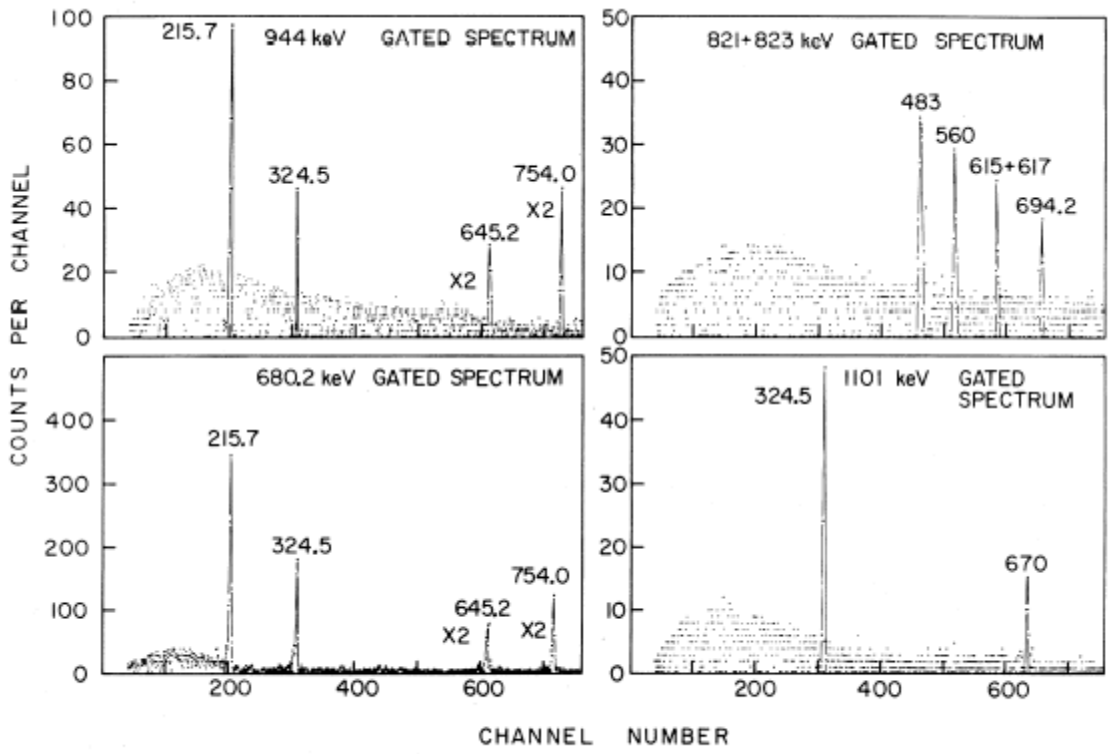

FIG. 2. Some γ-γ coincidence spectra which have an important bearing on the decay scheme of ^{97}Tc. Energies are in keV and the spectra have been corrected for random and background coincidences.

Figure 3: Example of electronically gated gamma-rays for ^{97}Tc (Kajrys et al., 1982)

When an unknown radioactive material is evaluated, it is possible that much of the gamma ray information that is being emitted is being hidden amongst the background information that exists in the gamma ray spectrum or can suffer spectral interference, especially in complex spectra. Much of this background comes from the Compton continuum that exists within the spectrum which raises the background levels within the spectrum.

It can be difficult to properly identify a photopeak when gamma rays with similar energy values overlap one another. These gamma rays may effectively hide nearby gamma ray information within the spectrum. A significant amount of background and interfering gamma ray peaks can be reduced using gamma-gamma coincidence counting.

Gamma-gamma coincidence counting techniques take advantage of cascading gamma-ray emissions. When a radioactive material decays, it prefers to return to a stable state by shedding its excess energy which can be in the form of alpha, beta, and gamma-ray emission. Beta decay often has gamma ray emission with alpha decay to a lesser degree. Often, radioactive isotopes will undergo two or more cascading gamma-ray emissions in an effort to return to a more stable state. These cascading gamma-ray emissions occur "in coincidence," or within a very short period of time of one another, most often in the picosecond range.

The technique of trying to measure only coincident gamma-rays allows for a researcher to reject gamma-rays that are not in coincidence, and thus, can potentially lower the background level and any potential spectral interferences. If the background level can be lowered, the coincident peaks that exist in the gamma spectra become more visible amongst the background levels. A discussion of the theory and application of how coincidence measurements are made can be found in Chapter 4.

2.1 Early Uses of Coincidence Measurements

The first attempt at the implementation of coincidence measurements was performed in 1924 by Walter Bothe and Hans Geiger (Bonolis, 2011). They utilized the technique to validate that a recoil electron is produced simultaneously with a gamma-ray during Compton scattering. They utilized two newly developed Geiger needle counters that were separated with a very thin window of aluminum foil. One counter was setup to detect the recoil electron from the Compton-scattering process while the second counter was set up to detect the recoil electron which was generated by a secondary photon which passed through a thin platinum foil and gave way to another Compton-scattering process. Both detectors were fed into separate electrometers which were recorded on fast photoelectric film and deemed to be in coincidence if they occurred within 1ms. A few years later, Bothe and Werner Kolhörster applied the same coincidence technique with a newly developed Geiger-Müller counter to study cosmic rays.

As gamma-gamma coincidence research and the understanding of cosmic rays grew, so did the development of more advanced and more sophisticated coincidence-counting techniques. In the early 1930s, a physicist by the name of Bruno Rossi published his version of a coincidence circuit. He was also performing cosmic ray research and needed a better counting system for coincidence measurements (Rossi, 1930; Bonolis, 2011). He utilized a triode as an automatic switch which evaluated whether current was flowing or not flowing which would open and close a "switch." This design allowed for a tenfold improvement in coincidence timing and also reduced the rate of change coincidences.

Over the next few decades, there were a number of different efforts related to the use gamma-gamma coincidence. Technology continued to advance over the that period of time which improved detectors and also improved the sophistication of counting systems. A select collection

of this research follows to give an overall understanding of the evolution of gamma-gamma coincidence measurements and the various applications that it has in the field of nuclear science and engineering.

Bramlitt published his research of the use of gamma-gamma coincidence as applied to neutron activation analysis (Bramlitt, 1966). This was one of the early attempts to couple the use of gamma-gamma coincidence with neutron activation analysis. Bramlitt was attempting to use neutron activation analysis to detect trace quantities of chlorine in organics. This was important as chlorine is often obscured by other elements in a compound mixture, e.g., ^{38}Cl can be hidden by ^{56}Mn, ^{24}Na, or ^{41}Ar in organic materials. Through the coincidence techniques of normal sum mode and sum peak coincidence, he was able to demonstrate the ability to reduce and/or eliminate spectra that belongs to elements other than chlorine.

Cooper published the results of his research in which he utilized lithium drifted germanium detectors for gamma-gamma coincidence measurements with and without anticoincidence shielding for radioanalytical applications (Cooper, 1971). For his research, he utilized two high efficiency Ge(Li) detectors. He utilized "standard" coincidence circuitry of the time which included Ortec and Canberra preamplifiers, discriminators, amplifiers, and single channel analyzers (SCA). He was able to adjust the coincidence time window from between 300 nanoseconds to 3 milliseconds. One phenomenon that he identified was that Compton events were also caused by higher energy gamma rays. He believed that it would be unlikely to resolve two major gamma-ray peaks and instead, utilized gamma-gamma coincidence techniques to reduce the interference due to the Compton events. He showed an improvement in the Compton interference for a mixture of ^{133}Ba and ^{75}Se. He also showed an improvement in the sensitivity for

the 265 keV gamma ray belonging to ^{75}Se when mixed with ^{32}P, a pure β emitter. It was virtually impossible to resolve the 265 keV spectra from a single detector.

Based on his data, he concluded that there was background reduction of about 4 orders of magnitude and a five times improvement in sensitivity for materials which emit low energy coincident gamma rays (Cooper, 1971). In addition, he developed a table of radionuclides which have the potential of showing an improvement in sensitivity when utilizing gamma-gamma coincidence techniques. However, he also noted the limitation in his experimentation based on the limitations of the detectors that were available at the time.

Researchers from Los Alamos Scientific Laboratory (LASL) decided to perform a similar study to Cooper's 1971 research (Wangen et al., 1980). They performed coincidence measurements with the use of Ge(Li) detectors to determine ^{75}Se in Standard Reference Materials (SRM). The team recognized the difficulty in determining low mass fractions of selenium in environmental samples and sought to utilize neutron activation analysis coupled with gamma-gamma coincidence techniques to try to improve this. The LASL research team showed similar results to Cooper with regards to the sensitivity for low energy coincident gamma rays. They generally saw reduction in the Compton background which assisted with the detection of ^{75}Se in many cases. However, in other cases, the reduction in the Compton background was not sufficient to improve the sensitivity to ^{75}Se.

At the same time, another researcher, Crane, at LASL was utilizing coincidence measurements for use on a non-NAA application. He was utilizing coincidence measurements to measure uranium and plutonium in solid waste (Crane, 1980). He utilized the coincidence method to evaluate coincident neutrons due to spontaneous fissions. One of his primary focuses was to isolate the alpha-n reaction from the spontaneous fission reactions. His coincidence techniques

utilized the use of shift register circuits. He showed these techniques to be successful for the evaluation of plutonium in quantities for 200 mg.

2.2 Implementation of Digital Systems for Coincidence Measurements

The advancement of technology over the next decade gave the ability to utilize new counting and measurement techniques for implementation in gamma-gamma coincidence measurements. Digital data acquisition systems were becoming more sophisticated and could now be utilized in the implementation of coincidence counting which gave the potential of better resolution and tighter coincidence timing windows.

In 1998, a group of researchers developed a gamma-gamma coincidence system which utilized two high purity germanium detectors and nuclear instrumentation model (NIM) spectrometric modules in either a VME (Verma module Eurocard) or CAMAC (computer automated measurement and control) based data acquisition system (Jakůbek et al., 1998). Their purpose was to build this system to support coincidence instrumental NAA studies and to support conventional non-coincidence neutron activation analysis. The reason for the NIM based modules in either a VME or CAMAC based system was to provide flexibility in the analysis of the coincidence data based on the capabilities of the data acquisition systems. This was one of the big advantages of the capabilities of data acquisition systems at that point in time. The discussion of their results was brief but they claimed to have improved background radiation by an order of four or lower when comparing the coincident data to single detector data for detecting scandium, cobalt and cesium in a Standard Reference Material of Bovine Liver and then comparing the results to published data.

The next year, two members from that team collaborated with some other researchers because they recognized some of the limitations with the NIM module-based data acquisition systems and set on a path to minimize those limitations (Vobecký et al., 1999). One of the limitations of gamma-gamma coincidence in the past, and with the early use of the NIM type configurations, was the limitation in memory which made it difficult to store enough spectrometric data to make the measurements valid. This research group decided to build a coincidence system using two HPGe detectors but they utilized NIM modules which were then output to a computer via VME or CAMAC modules. This enabled them to capture sufficient amounts of data for their experimentation to better understand and evaluate the benefits of gamma-gamma coincidence measurements. They successfully utilized this updated system for the determination of scandium, cobalt, cesium and iridium.

The team found improvement in the detection of these elements. As part of their reporting, they specifically discussed how the 296 keV peak of ^{192}Ir is influenced by the peaks of ^{152}Eu and ^{160}Tb. However, by utilizing the coincidence data, it was possible to detect and understand those peaks. With the improved data storage capability, they determined that the application of a coincidence method decreased the probability of energy interference and thus, gives more accurate results for very low elemental concentrations (Vobecký et al., 1999).

In 2006, researchers from the Japan Atomic Energy Agency, Tohoku University and Hokkaido University attempted to develop a multiparameter coincidence method (Hatsukawa et al., 2007). They utilized 19 separate Germanium detectors which they called GEMINI-II. Their intended use of this system was to detect iridium content in geological samples with the use of NAA. Utilizing this highly complex system, they were successful in detecting the 468–316 keV

gamma-gamma coincident peaks in ^{192}Ir which allowed them to resolve as little as 10 ppt (picogram per gram) of iridium in the geological sample.

In 2008, the Analytical Chemistry Division of National Institute of Standards and Technology explored the use of two HPGe gamma-ray detectors and an all-digital data-acquisition system for the purpose of exploring coincidence techniques utilized in NAA and its value in characterizing reference materials (Tomlin et al., 2008). They utilized an XIA, LLC Pixie-4 system for coincidence measurements. The Pixie-4 system is a digital data acquisition system that takes the output from the detectors and continually samples and digitizes the data via an analog-to-digital converter. One big advantage that the Pixie-4 system had is its ability to capture significant amounts of data and due to it being a 14-bit system, the data can be finely discretized. In addition, the Pixie-4 system was used to capture data utilizing a list-mode technique which stores pairs of digitized detector data and timestamps. Due to the pairing of detector data and timestamps, this data format is ideal for coincidence measurements.

The team utilized both single channel information and coincidence data for their analysis. The sample that underwent the NAA analysis was bovine tissue liver (Tomlin et al., 2008). In analyzing the data that was collected, they were able to discern a couple of peaks, 884 keV and 937 keV due to ^{100m}Ag, in the coincidence data that were not visible in the spectrum from the individual detectors. They account this to the high-degree of background reduction that is achieved in the coincidence data.

In 2012, Horne and Landsberger utilized gamma-gamma coincidence counting and Compton suppression to determine trace amounts of mercury and selenium in biological materials (Horne & Landsberger, 2012). They analyzed the 279 keV photopeak of ^{203}Hg after neutron activation which interferes with the 279 keV photopeak of ^{75}Se after neutron activation. The 279

keV peak produced by ^{75}Se is in coincidence with a 121 keV peak whereas the 279 keV by ^{203}Hg is not coincident with anything else. Thus, the lack of coincidence was utilized to assist with separating the 279 keV peak due to ^{75}Se from the 279 keV peak due to ^{203}Hg. The coincidence data and the Compton suppressed data were utilized and post processed to determine the number of 279 keV counts that came from ^{75}Se and the number of 279 keV count that came from ^{203}Hg. When the calculated/measured values were compared to the reference value for the standard sample that was evaluated, it was found to be accurate.

In 2014, a set of researchers utilized two bismuth germanate scintillators (BGO) and an XIA Pixie-4 system for coincidence measurements (Zhang et al., 2014). The intention of this research was to improve spectroscopy sensitivity for low-level cosmogenic ^{22}Na and ^{7}Be in air samples due to the use of coincidence and anticoincidence counting. The research team was able to demonstrate that when compared to a single HPGe detector setup, the gamma-gamma coincidence/anticoincidence system was more effective in identifying ^{22}Na and ^{7}Be. As a matter of fact, it was found that the gamma-gamma coincidence system improved the capability for detecting ^{22}Na by an order of magnitude.

Although much of the research in gamma-gamma coincidence has been centered around biological and environmental samples, in 2015 researchers from the Atomic Weapon Establishment (AWE) utilized coincidence techniques in support of nuclear weapons research (Britton et al., 2015). The team attempted to utilize gamma-gamma coincidence for the purpose of improving the ability to monitor for the detection of the testing of nuclear weapons and other radiological-based incidents in support of the Comprehensive Nuclear Test-Ban Treaty. For their gamma-gamma coincidence system, they utilized two large area, planar Canberra BEGe-6530

HPGe detectors which were both ultimately output to two separate digital data acquisition systems for redundancy and testing purposes.

As the goal was to utilize this in support of the Test Ban Treaty, this system would need to be capable of detecting the 83 different radionuclides that are characteristic of nuclear weapon testing and other nuclear reactor-based incidents. Thus, they calculated and evaluated a number of different radionuclides as part of their research. For the radionuclides that were tested and evaluated, they found that the gamma-gamma coincidence system that was developed, including the software that was developed as part of this research, showed potential in quickly identifying relevant radionuclides.

In 2017, researchers from the National Institute of Standards and Technology (NIST) published details of a new gamma-gamma coincidence system that they developed (Zeisler et al., 2017). The purpose for developing the new system was to specifically support neutron activation analysis. The researchers utilized a configuration of both 2 and 4 detectors to try to evaluate both configurations to determine which configuration would be more effective. Both configurations utilized the XIA Pixie-4 data acquisition for all data collection. The team used custom NIST software for all data processing and analysis. The team evaluated the system for Ag, Cs, Co and Se in several different reference materials. They compared the gamma-gamma results against standard NAA techniques. The team concluded that the both the 2- and 4-detectors configurations showed to be more effective than a single detector. However, they determined that the 2-detector configuration provided better performance due to the highly efficient counting geometry.

In 2017, Marković, Roos, and Nielsen, published results of their attempt to utilize digital gamma-gamma coincidence of an HPGe system for the use in environmental analysis (Marković et al., 2017). They utilized a new spectrometer called Nutech Coincidence Low Energy

Germanium Sandwich (NUCLeGeS). This detector was developed at the surface gamma laboratory at the Radioecology Section of DTU Center for Nuclear Technologies. It consisted of two Canberra HPGe detectors which were placed in a low activity lead shield. The setup also utilized a digital acquisition system comprised of Canberra preamplifiers and a CAEN Digital Multi Channel Analyzer to collect the data in time-stamped list mode. The coincident events were identified during post processing rather than actively during the measurement

The system was tested by utilizing NBL 103 certified reference material to try to detect ^{210}Pb and also by utilizing a standardized set of filters with different activities of ^{134}Cs and ^{137}Cs. For the measurements of ^{210}Pb, they identified a 15% decrease in the background for the ^{210}Pb peak. For the measurements of ^{134}Cs and ^{137}Cs, not only was there a reduction in the background, but the efficiency was also reduced. They concluded that the system was an effective technique for improving the minimum detectable activity values for cascade emitting isotopes

Also in 2017, researchers from the University of Texas of Austin (UT) and Pacific Northwest National Laboratory (PNNL) developed a gamma-gamma spectroscopy system through the use of two cerium doped lanthanum bromide (LaBr3:Ce) scintillation detectors rather than using high-purity germanium detectors (Drescher et al., 2017). The purpose of this research was to determine if gamma-gamma coincidence measurements using LaBr3:Ce could prove to be effective. An XIA, LLC Pixie-4 system was utilized to perform the coincidence measurements from the detectors.

The experimentation not only used the LaBr3:Ce detectors in coincidence, but also a single LaBr3:Ce and a single HPGe detector. The data in their research showed that the coincidence configurations contained much better signal-to-noise values than the single detectors. It was also shown that the HPGe detectors performed better in lower count rate scenarios but in high count

rate scenarios, the HPGe detectors paralyzed the detectors. This is where the LaBr3:Ce detectors in coincidence can benefit over HPGe detectors. It was determined that the coincident configuration provided an improvement in signal to noise (SNR) relative to a measurement using a single detector.

In 2018, researchers at UT attempted to do a more thorough determination on the ability to use gamma-gamma coincidence to evaluate complex gamma spectroscopy spectra after a sample had undergone neutron activation analysis (Drescher et al., 2018). The work was performed at the TRIGA Mark II reactor at the Nuclear Engineering Test Laboratory. The researchers utilized two HPGe Canberra detectors. An XIA Pixie-4 module was used for acquisition of the data and an in-house developed software package was used for evaluating the coincident and single channel data. (Drescher et al., 2018).

The experiment showed that it was possible to determine the existence of ^{76}As, ^{160}Tb, and ^{169}Yb in a few NIST-certified standard reference materials. The ability to distinguish these peaks was only possible due to the gamma-gamma coincidence technique as some of these peaks are extremely difficult to distinguish from the background in a single detector configuration.

Chapter 3: Background and Theory

This section describes the theory behind the use of gamma-gamma coincidence in NAA. First, the theory behind gamma-gamma coincidence will be described. Secondly, the principle of NAA will be described. This will provide the basis required to understand how gamma-gamma techniques are used in NAA.

3.1 Gamma-gamma coincidence

To explain the concept of gamma-gamma coincidence, some sample gamma ray spectra will first be examined and then the idea of gamma-gamma coincidence will be described. This concept can be easily understood with the use of sample gamma ray spectra to visually demonstrate what constitutes gamma-gamma coincidence.

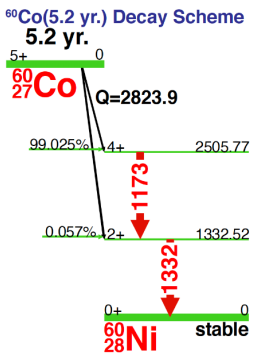

Figure 4: ^{60}Co Decay Scheme

Figure 4 is a simple example of an isotope, ^{60}Co, which has 2 major gamma rays that are in coincidence with one another. As ^{60}Co decays, it emits an 1173 keV gamma ray to get to its first energy state. It then subsequently emits a 1332 keV gamma ray to ultimately end up as ^{60}Ni, which is stable.

When evaluating Figure 5, the decay scheme for ^{95}Zr, the differences between it and the ^{60}Co decay are quite obvious. When ^{95}Zr decays, it emits a 756 keV gamma ray and/or a 724 keV gamma ray to get to its stable energy state. The two decays are not subsequent to one another and therefore, this isotope does not have a coincident decay.

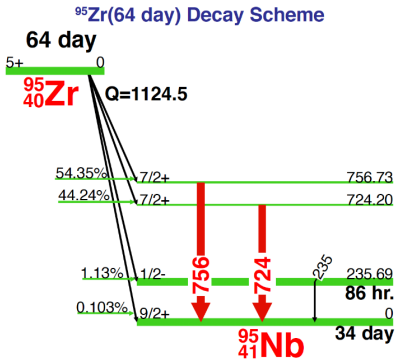

Figure 5: ^{95}Zr Decay Scheme

When an isotope decays and emits gamma rays, the gamma ray emissions can occur either in coincidence or not in coincidence. When an isotope decays to one energy level by emitting a characteristic gamma ray and then subsequently decays to another energy level, emitting a second gamma ray, these gamma emissions occur within a very small window of time. This time window is normally considered to be within picoseconds and thus, if the gamma ray decays occur within a very short time window, nanoseconds or less, they are considered to be "in coincidence" of one another. Therefore, isotopes that have subsequent energy decays that emit subsequent gamma rays have gamma rays that occur in coincidence.

However, in the example of ^{95}Zr, the two gamma ray emissions occur at "random" times with respect to one another due to the fact that the isotope can randomly emit either one or both of

the gamma rays. This does not occur subsequently. Gamma rays that are not emitted due to subsequent decays are not considered to be in coincidence as their relative timing is typically random with respect to one another.

Figure 6 is an example of a decay that has both gamma rays that do not occur in coincidence and also gamma rays that do occur in coincidence. For the decay of ^{59}Fe, it can be seen that there are 3 major gamma rays, 192 keV, 1099 keV and 1291 keV. Note that the 192 keV and the 1291 keV both occur when the isotope decays from its 1291 keV state. As they are both emitted from the decay of that energy state, they both occur randomly in time with respect to one another. When looking at the 192 keV and 1099 keV gamma rays, it can be seen that the 192 keV gamma is emitted during the transition of the 1291 keV state and the 1099 keV state. The 1099 keV gamma ray is subsequently emitted during the subsequent decay from 1099 keV to the stable decay state of ^{59}Co.

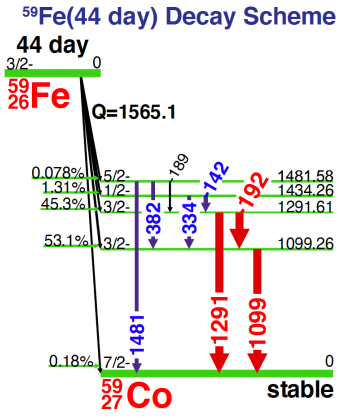

Figure 6: Fe-59 Decay Scheme

When considering coincident gamma rays and measuring the time of gamma rays occurring with respect to one another, one must also consider that random coincidences may also exist. A

random coincidence results from the emissions of two gamma rays that are not subsequent, may randomly be registered within the coincidence time window. Due to the large number of gamma ray emissions from a decaying isotope, this happens regularly but is possible to identify random coincidences due to the fact that true coincidences have many more occurrences than random coincidences do.

The count rate for gamma-gamma coincidence can be described with the following set of equations. A transition occurs in one of the detectors, detector A, which has an efficiency of εA, and a similarly defined one εB for the second detector, detector B, will register a number of counts in in both of the detectors within time T (the coincidence time), for a source rate N (Crouthamel, 1970):

$$N_A = \varepsilon_A NT \quad or \quad N_B = \varepsilon_B NT$$

when every coincident pair of transitions registered in the detectors is counted:

$$N_{AB} = \varepsilon_A \varepsilon_B NT$$

If the coincidences are measured with a coincidence arrangement with a resolving time, 2τ the number of accidental or random pulses will be given by:

$$N_R = 2\tau \varepsilon_A \varepsilon_B N^2 T$$

The total measured count rate ends up being the sum of the true and random coincidence rate.

$$N_T = N_{AB} + N_R$$

To implement a gamma-gamma coincidence measurement system, two or more detectors are used to measure the gamma spectra of a sample. The data from the two detectors is evaluated against one another using a coincidence timing window. All data from gamma rays that do not fall within that coincidence timing window are rejected. This technique reduces interferences between

photopeaks and also effects due to the Compton continuum which allows for a more definitive identification of an unknown isotope utilizing the coincidence peaks.

3.2 Neutron Activation Analysis

In neutron activation analysis, a sample is exposed to a flux of neutrons, most often from a nuclear research reactor. This process causes a radiative capture reaction for many samples. In radiative capture, the target nucleus typically captures the extra neutron which causes the formation of a compound nucleus in an excited state. The compound nucleus proceeds to transition to a stable state by shedding excess energy, which might be in the form of a (prompt) gamma ray. An illustration of such an (n, γ) reaction can be seen in Figure 7.

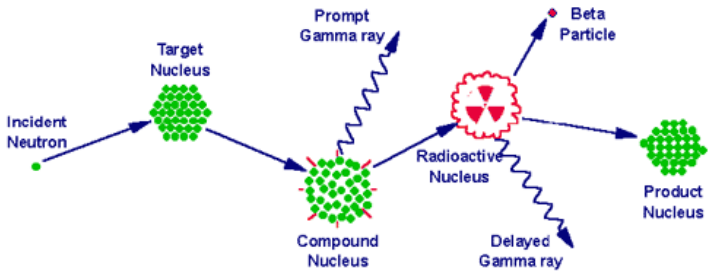

Figure 7: Process of Neutron Activation (University of Missouri, 2012)

The reaction for this process, radiative capture, can be seen in *Equation 1*.

$$n + {}^{A}Z \rightarrow {}^{A+1}Z^{*} \rightarrow {}^{A+1}Z + \gamma$$

Equation 1: NAA equation

where n is the bombarding neutron, ${}^{A}Z$ is the nucleus that will be bombarded, and ${}^{A+1}Z^{*}$ is the newly excited compound nucleus. After de-excitation, the newly formed nucleus ${}^{A+1}Z$ may be stable or radioactive. In the latter case, the radioactive ${}^{A+1}Z$ nucleus sheds its excess energy by the emission of radiation via either ionizing (like alpha, beta or gamma) radiation or via the emission of neutrons.

Both the prompt and/or delayed gamma ray energies that are emitted are characteristic to the target nuclei that have been irradiated. This is the basic analytical principle in gamma-ray spectroscopy for the identification of the specific elemental composition of the sample.

One major advantage for the use of NAA is that it is typically a nondestructive process; no need for dissolution is required. This allows for identification of elements without having to physically contact the sample which proves to have major benefits. Further, NAA is a sensitive technique which means it proves to be effective for use in samples that have low elemental concentrations. It can also be used for solids, liquids or powders which makes the technique extremely versatile.

For NAA, the radionuclides that are produced are characterized as short-lived (decay times less than approximately 12 hours), medium-lived (decay times between approximately 12 hours and 3 days) and long-lived (decay times longer than approximately 3 days). The most common ones can be found in Table 1, Table 2 and Table 3 (Landsberger, 1994).

.

Table 1: Short-lived radionuclides

TABLE 1.
Properties of reactions producing short lived radionuclides

Element	Isotope	Half-life	Gamma-ray energies (keV)
Ag	^{110}Ag	24.6 s	657.8
Al	^{28}Al	2.24 min	1778.9
Ba	^{139}Ba	83.2 min	165.9
Br	^{80}Br	17.7 min	616.2
Br	^{80m}Br	4.42 h	37.1
Ca	^{49}Ca	8.7 min	3084.4
Cl	^{38}Cl	37.3 min	1642.4, 2167.5
Co	^{60m}Co	10.48 min	58.6
Cu	^{66}Cu	5.1 min	1039.4
Dy	^{165}Dy	2.33 h	94.7
F	^{20}F	11.0 s	1633.8
I	^{128}I	25.0 min	442.3
In	^{116m}In	54.2 min	416.9, 1097.3
K	^{42}K	12.36 h	1524.7
Mg	^{27}Mg	9.45 min	843.8, 1014.4
Mn	^{56}Mn	2.58 h	846.7, 1810.7
Na	^{24}Na	15.0 h	1368.6, 2754.1
Se	^{77m}Se	17.4 s	161.7
Sb	^{122m}Sb	4.15 min	61.5
Si	^{29}Al[a]	6.6 min	1273.0
Sr	^{87m}Sr	2.81 h	388.4
Ti	^{51}Ti	5.8 min	320.1
U	^{239}U	23.5 min	74.6
V	^{52}V	3.76 min	1434.1

[a] Si is detected by the ^{29}Si(n,p)^{29} Al reaction.

Table 2: Medium-lived radionuclides

TABLE 2.
Properties of reactions producing medium lived radionuclides

Element	Isotope	Half-life	Gamma-ray energies (keV)
As	^{76}As	26.3 h	559.1
Au	^{198}Au	2.7 d	411.8
Br	^{82}Br	35.3 h	554.3, 776.5
Cd	^{115m}In[a]	53.5 h	336.3
Ga	^{72}Ga	14.1 h	834.0, 629.9
Ge	^{77}Ge	11.3 h	264.4
Hg	^{197}Hg	64.1 h	77.4
Ho	^{166}Ho	26.8 h	80.6
K	^{42}K	12.36 h	1524.7
La	^{140}La	40.23 h	1596.2, 328.8, 487.0
Mo	^{99}Mo	66.02 h	140.5
Na	^{24}Na	15.02 h	1368.6, 2754.1
Pd	^{109}Pd	13.7 h	88.0
Sb	^{122}Sb	2.72 d	564.0
Sm	^{153}Sm	46.7 h	103.2
U	^{239}Np[b]	2.35 d	277.7
W	^{187}W	23.9 h	85.8
Zn	^{69m}Zn	13.8 h	438.6

[a] Cd is determined from the ^{114}Cd(n, $\gamma\beta$) ^{115}Cd → ^{115}In reaction.
[b] U is determined from the ^{238}U (n, $\gamma\beta$)^{239}U → ^{239} Np reaction.

Table 3: Long-lived radionuclides

TABLE 3.
Properties of reactions producing long lived radionuclides

Element	Isotope	Half-life	Gamma-ray energies (keV)
Ag	^{110m}Ag	249.8 d	657.8
Ce	^{141}Ce	32.5 d	145.4
Cr	^{51}Cr	27.72 d	320.0
Cs	^{134}Cs	2.06 y	795.8
Co	^{60}Co	5.27 y	1173.2, 1332.4
Eu	^{152}Eu	13.4 y	1408.0
Fe	^{59}Fe	44.5 d	1099.2, 1291.6
Hf	^{181}Hf	42.4 d	482.2
Hg	^{203}Hg	46.6 d	279.2
Lu	^{177m}Lu	160 d	378.5
Nd	^{147}Nd	10.99 d	91.1
Ni	^{58}Co[a]	70.9 d	810.8
Rb	^{86}Rb	18.7 d	1076.6
Sb	^{124}Sb	60.2 d	1691.0
Sc	^{46}Sc	83.8 d	889.3, 1120.5
Se	^{75}Se	119.8 d	136.0, 264.7, 400.7
Sn	^{113}Sn	114.4 d	391.7
Sr	^{85}Sr	64.84 d	514.0
Ta	^{182}Ta	115.0 d	1221.4
Tb	^{160}Tb	72.1 d	879.4,
Th	^{233}Pa[b]	27.0 d	311.9
Tm	^{170}Tm	129 d	84.3
Yb	^{175}Yb	4.19 d	396.3
Zn	^{65}Zn	243.8 d	1115.5
Zr	^{95}Zr	64.0 d	756.7

[a] Ni is determined using the ^{58}Ni(n, p) ^{58}Co reaction.
[b] Th is determined using the ^{232}Th(n, $\gamma\beta$) ^{233}Th $\rightarrow$ ^{233}Pa reaction.

An evaluation of a subset of radionuclides from each decay range will be made against gamma-gamma coincidence techniques using the XIA Pixie-16 system for this research. To be able to implement the XIA Pixie-16 system as a useful tool for NAA, it must be shown that it is capable of successfully implementing gamma-gamma coincidence for short-, medium- and long-lived NAA products with the ability to produce spectra that are accurate.

Chapter 4: Implementation of gamma-gamma coincidence using the XIA, LLC Pixie-16 system

This section describes the implementation of gamma-gamma coincidence using the XIA Pixie-16 system. A discussion of the physical and electrical configuration will be discussed as well as the theory behind the implementation of gamma-gamma coincidence via the comparator method. Lastly, as the implementation of gamma-gamma coincidence using the Pixie-16 system must provide valid results, a number of different qualification tests were performed and will be discussed.

4.1 Configuration of the Pixie-16 system for gamma-gamma coincidence

The XIA Pixie-16 based gamma-gamma coincidence system utilizes two high-purity germanium (HPGe) detectors. One of the HPGe detectors is a Canberra CG2518 which has a relative efficiency of 25% and an energy resolution of 1.8 keV at the full width half maximum (FWHM) at 1.332 MeV. The second HPGe detector is a Canberra CG2519 which has a relative efficiency of 15% and an energy resolution of 1.8 keV at the FWHM at 1.332 MeV. Unfortunately, midway through this research, one of the detectors stopped functioning and a poor resolution detector was used as a replacement. As a reference, a measurement of this detector in singles mode, via the Pixie-16 system, produced a FWHM measurement of approximately 3.1 keV at 1.332 MeV.

For the gamma-gamma coincidence system, the output of the two HPGe detectors were input into 4 separate channels of the Pixie-16 system. Each detector output was split into two separate channels on the Pixie-16 system. The Pixie-16 system was configured so that one of the

channels for each detector was set to capture the full, unedited spectrum. The second channel was configured to capture the data in coincidence mode. Configuring the system in this manner allowed for a comparison between the singles and coincident data sets to help evaluate the effectiveness of the system in performing its coincidence analysis. The layout of the Pixie-16 based gamma-gamma coincidence system can be seen in Figure 8 and photos of the hardware can be seen in Figure 9.

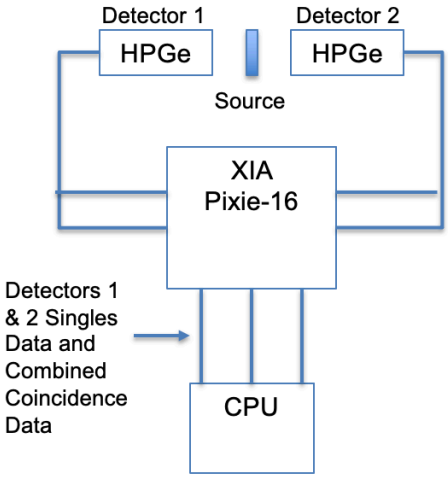

Figure 8: Block Diagram of Pixie-16 gamma-gamma coincidence system

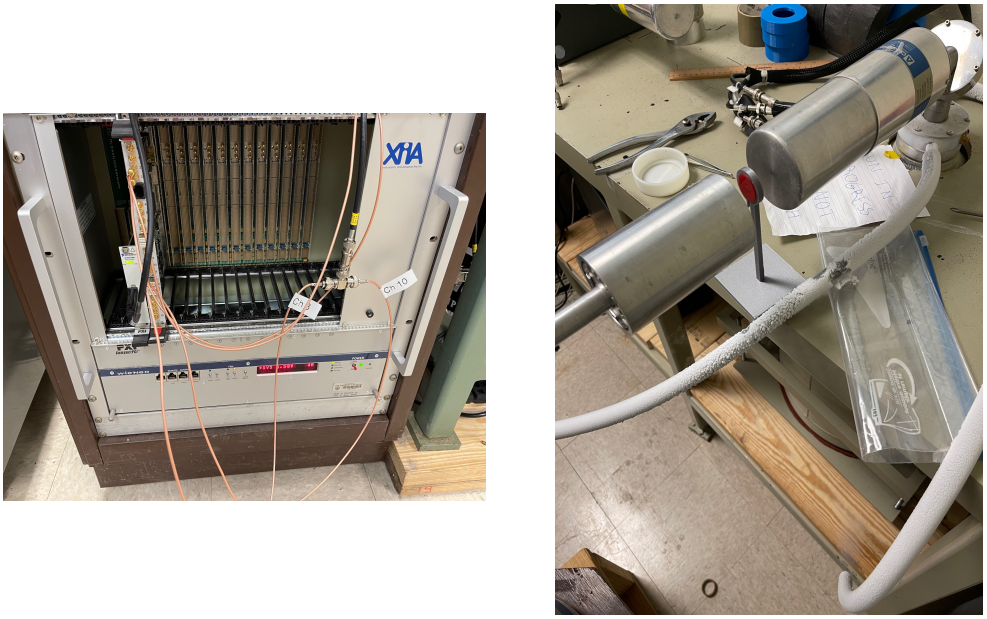

Figure 9: Pixie-16 system (left) and gamma-gamma detector configuration (right)

The coincidence timing window was set up to operate at a maximum of 80 ns, although the Pixie-16 has the capability of single nanosecond resolution. The coincidence time window was determined by consulting with personnel from XIA and also through trial and error to try to maximize net counts of coincidences but also to minimize random coincidences. The Pixie-16 modules were configured and controlled utilizing the software that was included from XIA, Pixie-16, Version 2.3.0. The data was captured in list mode which provided a file in binary format (.bin).

The binary data that was output by the Pixie-16 system was read into a custom python-based software package which allows for each channel's coincident data to be analyzed and plotted. The software is capable of generating heatmaps (not used in this dissertation) which plot the coincident data of one detector (in energy) against the coincident data of the second detector (in energy). Lastly, the software allows the user to configure a specific energy-gated window to evaluate which gamma ray energies occur within coincidence of a specific gamma ray energy.

While one can employ efficiency curves and k-zero techniques for the use of gamma-gamma coincidence for NAA, a common technique, the comparator method, has been implemented for use on the Pixie-16 system. This simplifies a lot of the analysis. Further, constructing an efficiency curve for gamma-gamma coincidence can be very involved and this is not the focus of this research. If one was interested in identification of a specific radionuclide(s) using gamma-gamma coincidence, at that point, the development of an efficiency curve may be warranted.

The basic determination of the amount of specific elements in NAA can be performed using *Equation 2*. For the comparator method, many of the complex variables are simplified as a number of them fall out of the equation.

$$A = \sigma\ \Phi \left(\frac{m}{M}\right) N_A\ S\ D\ C\ \ \theta P_\gamma\ \xi$$

Equation 2: Radioactive decay law

where A ---measured activity (Bq) from the product of an expected reaction,

σ ---activation cross section of the reaction (cm^2),

Φ ---activating flux (neutrons/cm^2 sec),

m ---amount of the element determined (g),

M ---atomic weight of the element to be determined (g/mole),

N_A---Avogadro constant (6.022 x 10^{23} molecules/mole**),**

S ---[1 - exp($-\lambda t_i$)] saturation factor (λ is decay constant of the radioactive product, t_i is duration of the irradiation time),

D ---exp($-\lambda t_d$) decay factor (t_d is duration of the decay time),

C ---[1 - exp($-\lambda\ t_c$)] correction factor for nuclide decay during the counting time (t_c is duration of the counting time),

θ ---relative natural isotopic abundance of the activated isotope,

P_γ ---probability of emission of a photon with energy E, and

ξ --- detector efficiency for the measured radiation energy.

In the comparator method, the terms that drop out include σ, P_γ, ξ, and Φ which then makes the need for an efficiency curve superfluous. The equation is simplified to:

$$C_{sam} = C_{std} * \left(\frac{A_{sam}}{A_{std}}\right) * \left(\frac{S_{std}}{S_{sam}}\right) * \left(\frac{D_{std}}{D_{sam}}\right) * \left(\frac{C_{std}}{C_{sam}}\right) * \left(\frac{W_{std}}{W_{sam}}\right) * \left(\frac{F_{std}}{F_{sam}}\right)$$

Equation 3: Comparator method: Concentration of sample, full equation

where W_{sam} -- weight of sample,

W_{std} -- weight of standard,

F_{std} --neutron fluence of standard, and

F_{sam} -- neutron fluence of sample.

The equation can be simplified further as the decay factor and saturation factor of the radionuclide of interest is the same for both the sample and source, and the weight of the sample and standard are identical, as well as neutron fluence.

$$C_{sam} = C_{std} * \frac{A_{sam}}{A_{std}}$$

Equation 4: Comparator method: Concentration of sample, simplified

This use of the most simplified version of the equation is usually not the case due to the difference in irradiation, decay, and counting times. However, an effort was made to try to

minimize and/or eliminate these variables in the experiments performed for this dissertation, and therefore, this equation can be implemented for this research.

4.2 Qualification testing of the Pixie-16 system

Several experiments were performed to certify that the system was effective in performing gamma-gamma measurements to qualify the Pixie-16 system for use in gamma-gamma coincidence. Many of the basic gamma spectroscopy principles were evaluated to ensure that the system functioned properly. This was important to do prior to trying to utilize the system for the measurements of NAA samples. These experiments included evaluating how the digital electronics affected the resolution of the detectors, evaluating the ability for the system to lower the background count, evaluating the relationship between counts and distance between the source and the detector, and verifying the Poisson distribution for gamma spectroscopy.

4.2.1 Evaluating the resolution of HPGe detectors as configured within the Pixie-16 system

An experiment was performed to evaluate the resolution of the Pixie-16 as configured for use in gamma-gamma coincidence measurements. This was done to determine the effect of the use of the digital electronics in the Pixie-16 system and whether or not any degradation of the resolution of the two HPGe detectors might exist. A ^{60}Co source was measured for 3 hours with the Pixie-16 system utilizing a single channel, non-coincidence setup to be able to evaluate the Full Width Half Max (FWHM) of the detectors through the Pixie-16 system. The files were processed utilizing the Ortec Maestro software to measure the FWHM of each of the two detectors. The spectra and the FWHM for each of the detectors for the 1332 keV gamma ray in ^{60}Co can be seen below.

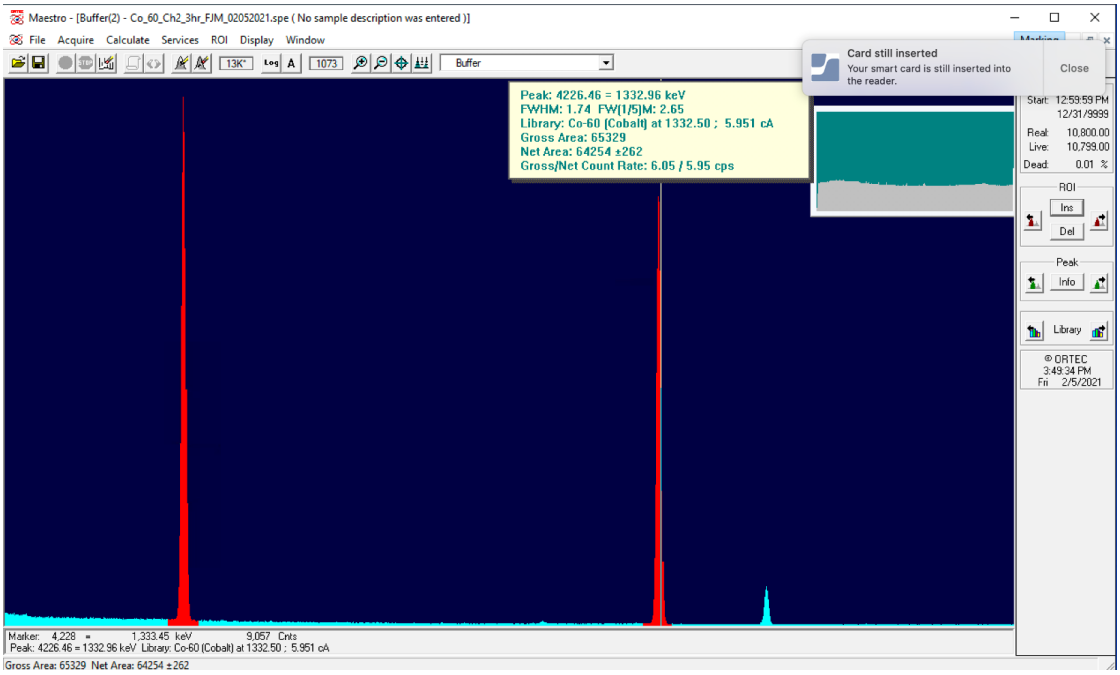

Figure 10: Resolution of HPGe detector 1 used with Pixie-16 system

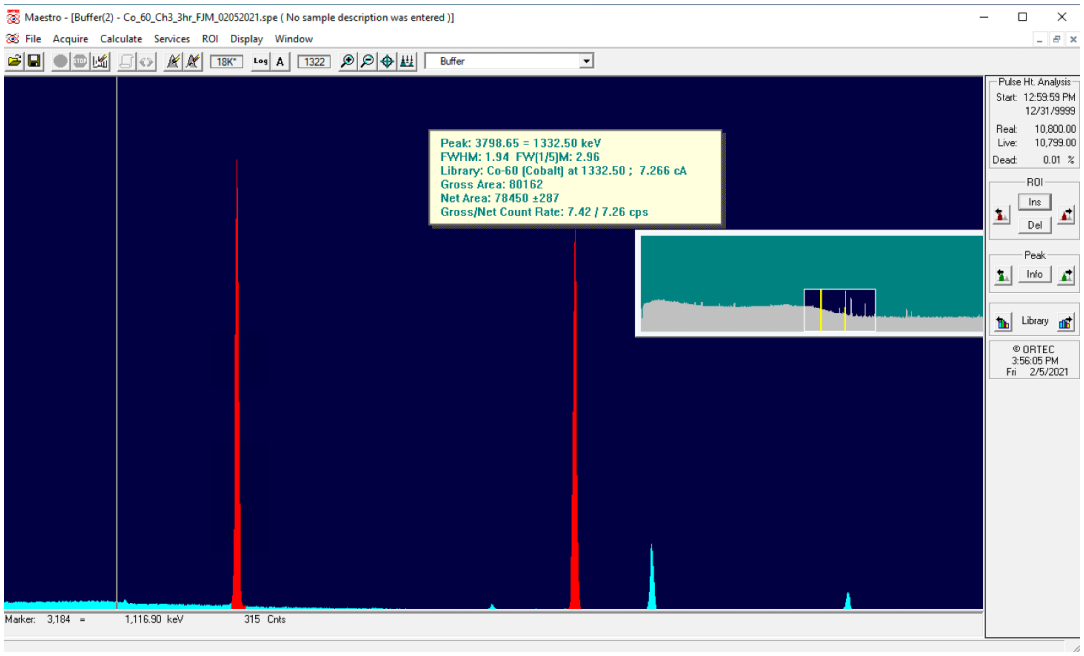

Figure 11: FWHM of HPGe detector 2 used with Pixie-16 system

Table 4 summarizes the FWHM data for the detectors and the manufacturer's FWHM specifications for the detectors. The table demonstrates that the measured FWHM data is actually better than the manufacturer's FHWM specifications for detector 1. Detector 2 shows to have a slight degradation from the manufacturer's FHWM specifications. This may be due to the age of the detector. The data for detector 1 demonstrates that the Pixie-16 system is maintaining the resolution of the detectors while setup in the experimental configuration. Experiments that were performed later within this body of research further validate the ability of the Pixie-16 to maintain the resolution of the detectors and are discussed later within this document.

Table 4: FWHM of detectors

Detector	**FWHM @ 1.332 MeV**
Detector 1 (measured)	1.74
Detector 1 (specification)	1.8
Detector 2 (measured)	1.94
Detector 2 (specification)	1.8
Detector 3, replacement for detector 2 (measured)	3.1
Detector 1 - Canberra CG2518, Detector 2 - Canberra CG2519	

4.2.2 Evaluating the effect of gamma-gamma coincidence on the background count

An experiment was performed to evaluate the effect that gamma-gamma coincidence has on the background level that is measured by the system. One of the most significant benefits of gamma-gamma coincidence counting is the ability to reduce the dramatically reduce the

background information, thus, allowing for better sensitivities for the gamma ray data which is being measured.

For this experiment, the system was configured to capture data for 18,000 seconds for both singles data and also coincidence data. The system was setup in a gamma laboratory. The Pixie-16 based system and thus, specifically the HPGe detectors, had no shielding from the background. There was no source in or around the experimental setup. The system was configured to capture data in both singles mode and gamma-gamma coincidence mode. The results from the experiment can be seen in Figure 12.

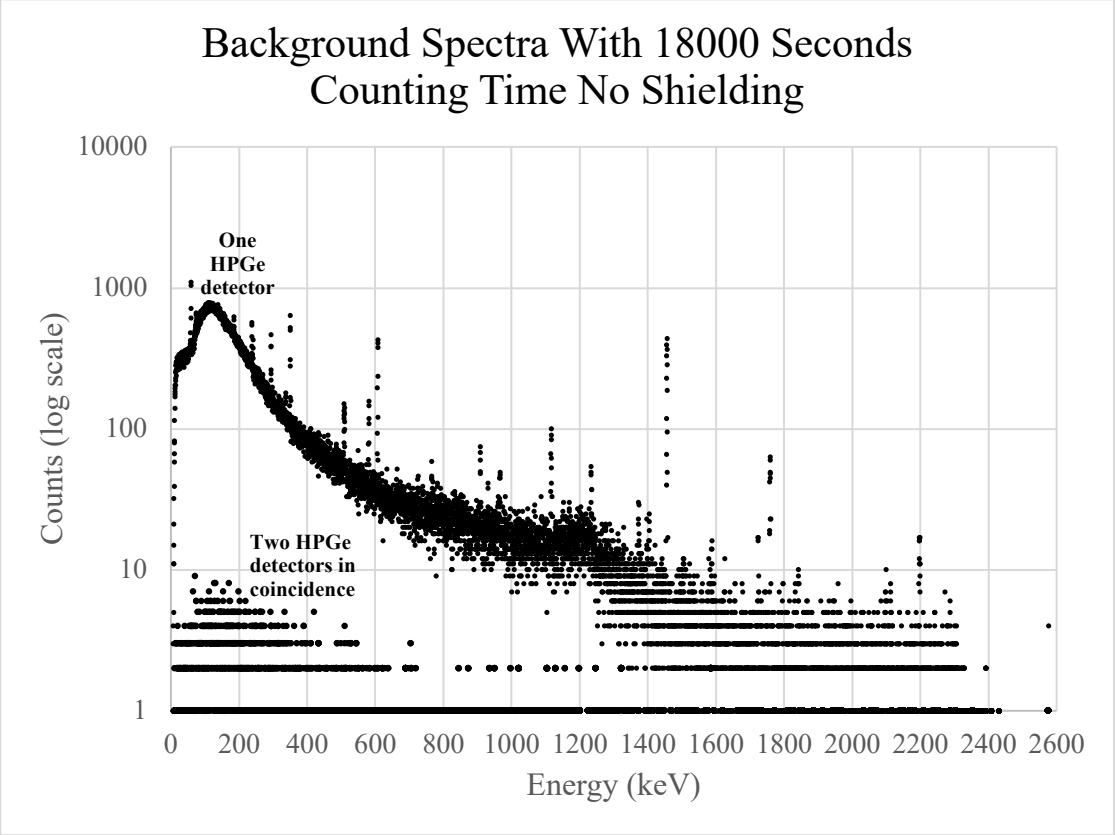

Figure 12: Background count with singles and coincidence data

An inspection of the data shows a dramatic reduction in the background spectrum across all energy ranges. When reviewing the data at energies up to approximately 1200 keV, the reduction is even more significant. If one is to look at a specific energy, for example, 150 keV, the single detector measured approximately 1000 counts for the background. At this same energy, the coincidence channel captured a background level that was less than 10 counts, a reduction of 2 orders of magnitude. This data demonstrates a major advantage for the use of gamma-gamma coincidence.

The energy regions between 150 keV and upwards to 1200 keV show a significant reduction in background where gamma peaks can easily get hidden due to backscatter and the Compton continuum. There is also a dramatic reduction in the background information across the entire energy range. The benefit from the reduction of the background information will make itself evident as the implementation of this system for measuring NAA samples is explored further. The addition of being able to gate specific energies will also contribute to a further reduction in the background levels and is explored later within this dissertation.

4.2.3 Evaluating the effect of increasing the distance between the source and detector

An experiment was performed to determine the effect that increasing the distance between the source and detector has on the net counts in the gamma-gamma coincidence configuration. This will allow for a direct comparison and understanding of how the net counts measured by a single detector compares to the net counts measured by a coincidence system relative to distance between the detector(s) and source.

To validate these concepts, the experiment consisted of a ^{60}Co source that was placed on a sample holder. The detectors were then incrementally moved away from the source with identical

distance measurements being made relative to the face of the detector. At each incremental distance from the source, a measurement was made. Note that the thickness of the source was 0.62 cm and thus, any measurement that had the source directly against the surface of the detector, was considered to be 0.31cm from the source.

A set of calipers was used to measure the distance between the source and each of the detectors. It is understood that there was potentially some human error in the movement of the detectors and thus, potentially some error in the exact distances between the source and each detector. However, the purpose of this experiment is to evaluate the effect that the distance between the source and the detectors has on the data and thus, the exact distances are not critical.

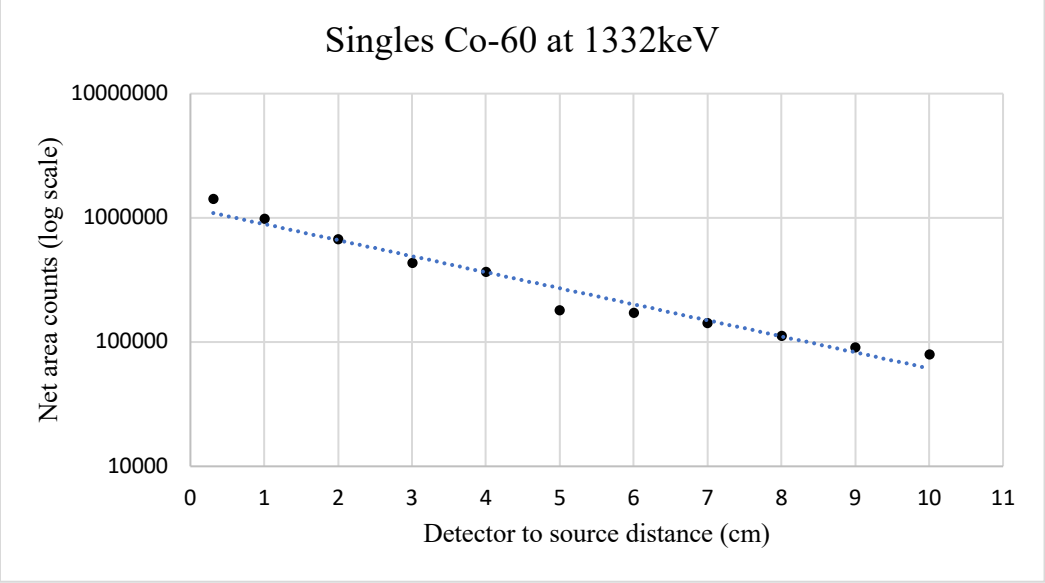

Figure 13: Results of source-detector distance experiment, ^{60}Co source

Figure 13 shows the results of this experiment from a single detector. Note the linear trend of the response when presented with a log scale on the vertical axis. This demonstrates a characteristic relationship as the distance and the detector are separated from one another. It is

also notable that the net counts are approximately 1,000,000 counts at a distance of 0.31cm (half the thickness of the source) and the net counts drop to just under 100,000 counts at a distance of 10cm. This is approximately a 1 order of magnitude reduction in total counts.

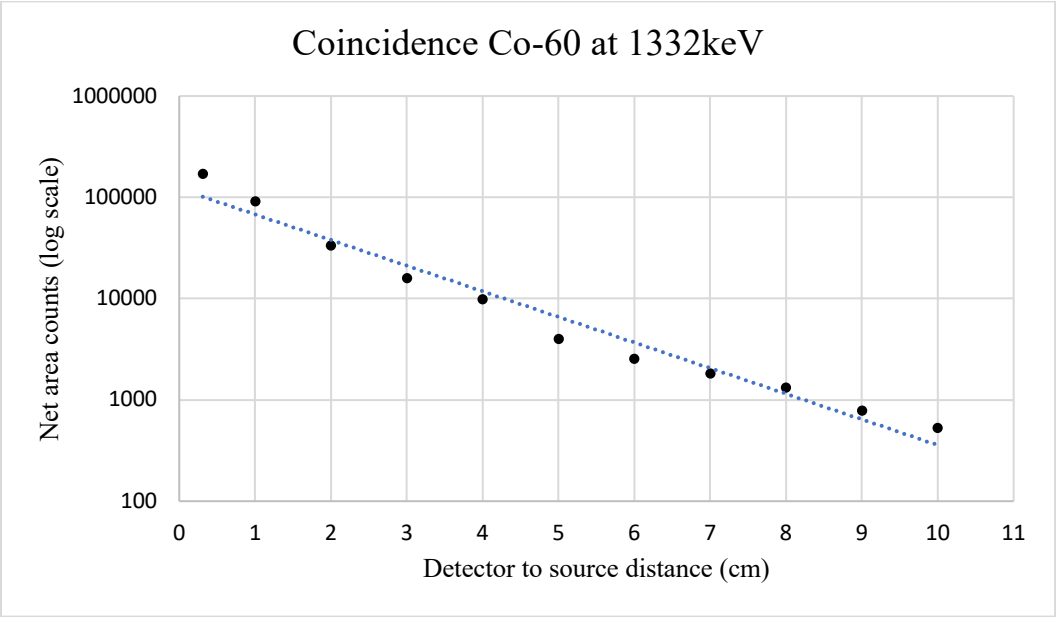

Figure 14: Results of source-detector distance experiment, gamma-gamma coincidence data, ^{60}Co source

Figure 14 shows the coincidence data from the same experiment. Note that there is a significant reduction in total counts and the significant drop off of counts as distance is increased when compared to the single detector data.

The data has also been represented as a ratio of net counts relative to the "zero" value, or 0.31cm value. This data is found in Figure 15 and Figure 16 for singles and coincidence experiments, respectively.

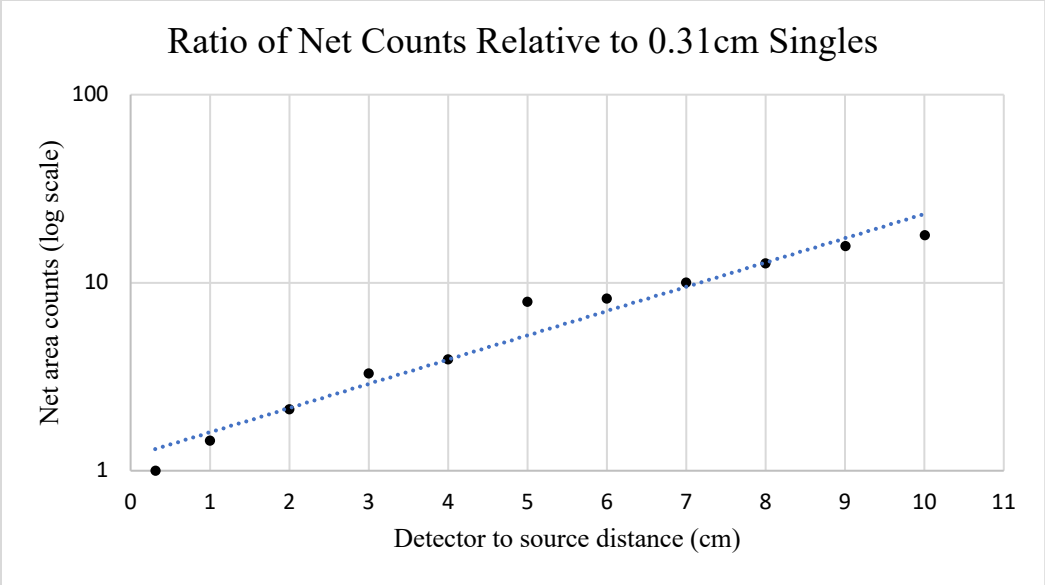

Figure 15: Ratio of net counts to 0.31cm data for single detector

Figure 15 demonstrates the effect of moving the source away from the detector. There is more than an order of magnitude reduction in net area counts as the distance is increased from 0.31 cm to 10 cm for a single detector.

When displaying the data for the gamma-gamma coincidence configuration in a similar manner, as shown in Figure 16, the data easily demonstrates that there is more than 100x reduction in net counts relative to the source being against the face of the detector. This is an order of magnitude greater reduction in net area counts than when looking at the single detector configuration.

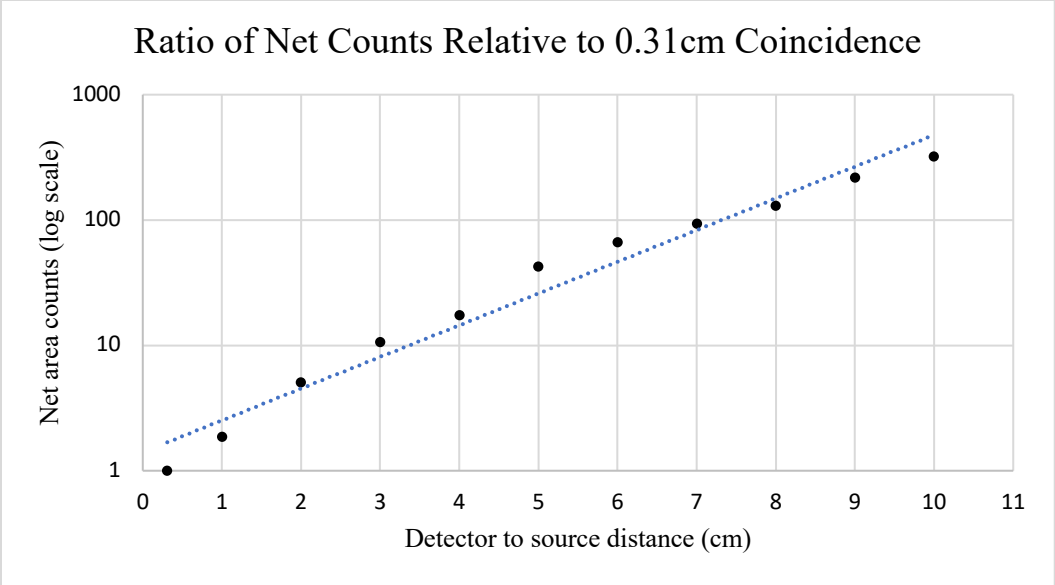

Figure 16: Ratio of net counts relative to .31cm, coincidence system

This experiment exposes one of the limitations of a gamma-gamma coincidence system. At close range, this can be a highly effective technique. However, as the distance is increased, the total net counts that are measured by the system are quickly reduced. This potentially makes the system less than adequate for use in a configuration where it is necessary to have the detectors relatively distant from the source or the sample that is being investigated. However, one can employ much larger-sized detectors that can decrease the solid angle or an array of detectors can be utilized, both of which will increase the efficiency. The effect of angular correlation is discussed in section 6.2.

4.2.4 Validation of the Poisson Distribution

Radioactive decay is understood to be a Poisson process, although it is often approximated to be Gaussian(Kirkpatrick & Young, 2009). An effort was made to develop an experiment using the Pixie-16 system to validate that the Poisson distribution holds true for both singles and

coincidence data for the system. To ensure it was statistically defensible, a custom software was written which allowed for a large number of samples to be captured without a user having to manually start and stop those measurements. A Python script was developed which automatically controlled the system to start counting and then stopped it after 200 seconds. It then saved the data and then started another 200 second count. It was configured to capture 2500 separate, 200-second counts. A ^{60}Co source was used for this experiment and the 1332 keV gamma ray was evaluated. The results of this experiment can be seen below.

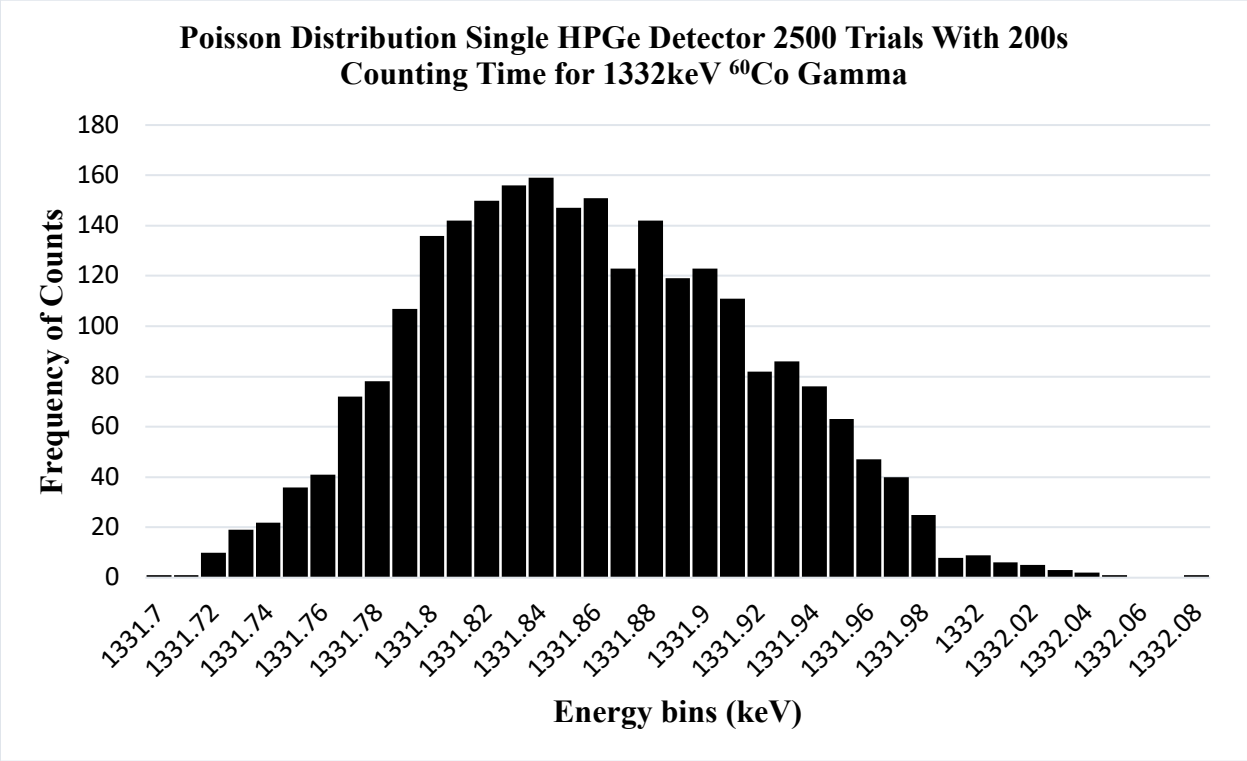

Figure 17: Poisson distribution for singles data, ^{60}Co

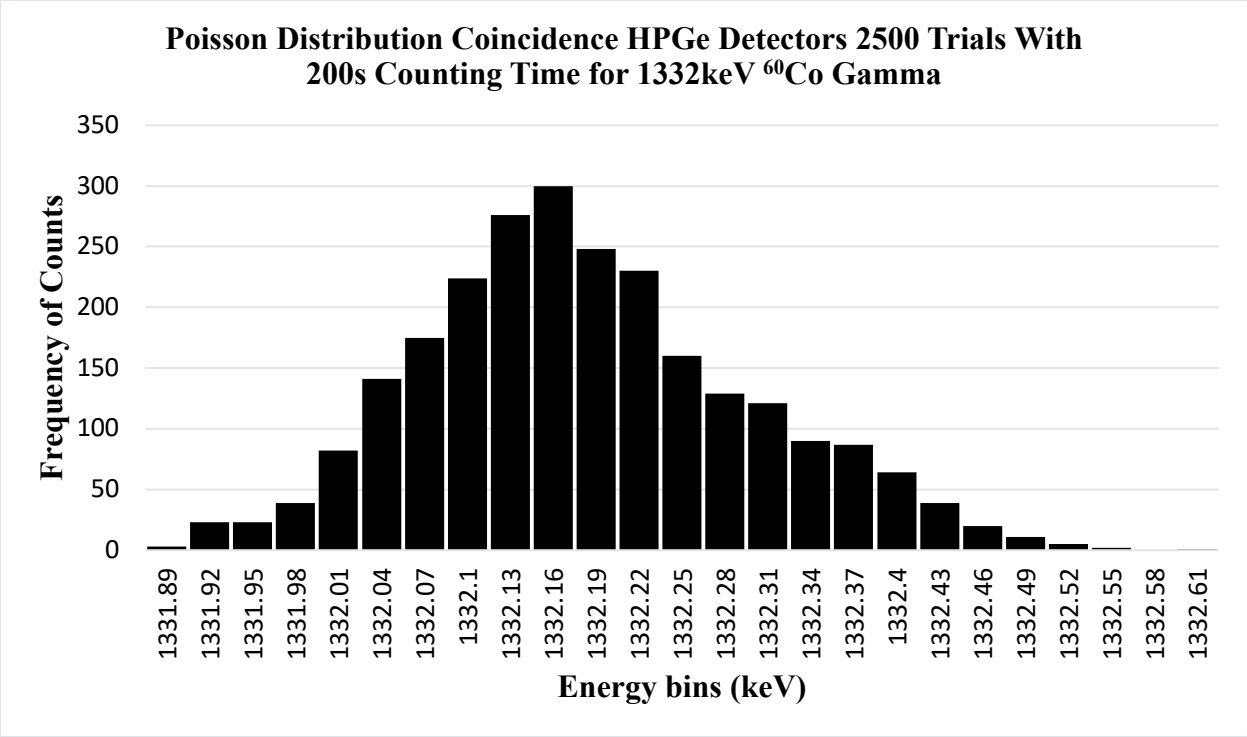

Figure 18: Poisson distribution for coincidence data, ^{60}Co

A quick inspection of both the singles and coincidence data shows the data to be Poisson in nature. Note that the distribution is not symmetric like a Gaussian distribution would be. This is representative of a typical gamma spectroscopy histogram which demonstrates that the coincidence data follows a Poisson distribution.

4.3 Validation of the effectiveness of gamma-gamma coincidence on Pixie-16

After performing the qualification tests, it was necessary to evaluate the Pixie-16 system's gamma-gamma coincidence capabilities against reference isotopes. A number of different experiments were performed to determine the effectiveness of the Pixie-16 system's gamma-gamma coincidence capabilities. The purpose of this set of experiments is to validate if the system can successfully reject gamma rays that aren't in coincidence with gamma-rays of interest. This

should eliminate spectral interferences of nearby gamma rays. As the comparator method is being used for gamma-gamma coincidence, this series of experiments demonstrates the ability for this system to be utilized for gamma-gamma coincidence measurements.

4.3.1 Validation utilizing ^{60}Co, ^{137}Cs and ^{152}Eu

The first isotope that the Pixie-16 system was evaluated against was ^{60}Co. ^{60}Co was selected because it only has two major gamma rays, 1173 keV and 1332 keV, that occur in coincidence with one another. To validate the efficacy of the gamma-gamma coincidence counting, a ^{137}Cs source was also measured with the ^{60}Co source. This was done to validate that the Pixie-16 would effectively screen out the single 661 keV gamma ray from the ^{137}Cs. The coincidence gamma spectrum output by the Pixie-16 system can be seen in Figure 19. Note that both the 1173keV and 1332 keV gamma rays are visible in the spectrum as they are in coincidence with one another but the 661keV gamma ray from the ^{137}Cs is effectively absent. The small peak that is visible is due to random coincidences due to the strong 661 keV peak in coincidence with itself.

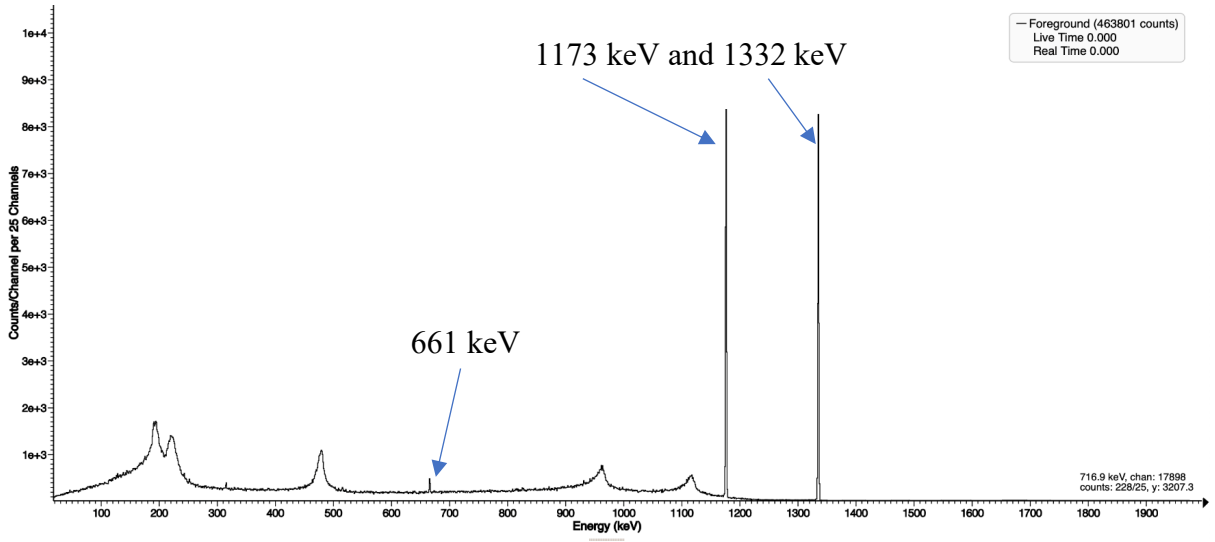

Figure 19: ^{60}Co Spectrum, coincidence

The next step for validation of the Pixie-16 is to demonstrate that the system can determine when a specific gamma ray is in coincidence with another specific gamma ray. This was done utilizing UT custom-written software to perform this process. When utilizing the software and applying an energy-gating window of 1173 keV, it is shown that the 1332 keV gamma ray is in coincidence specifically with the 1173 keV gamma ray as shown in Figure 20.

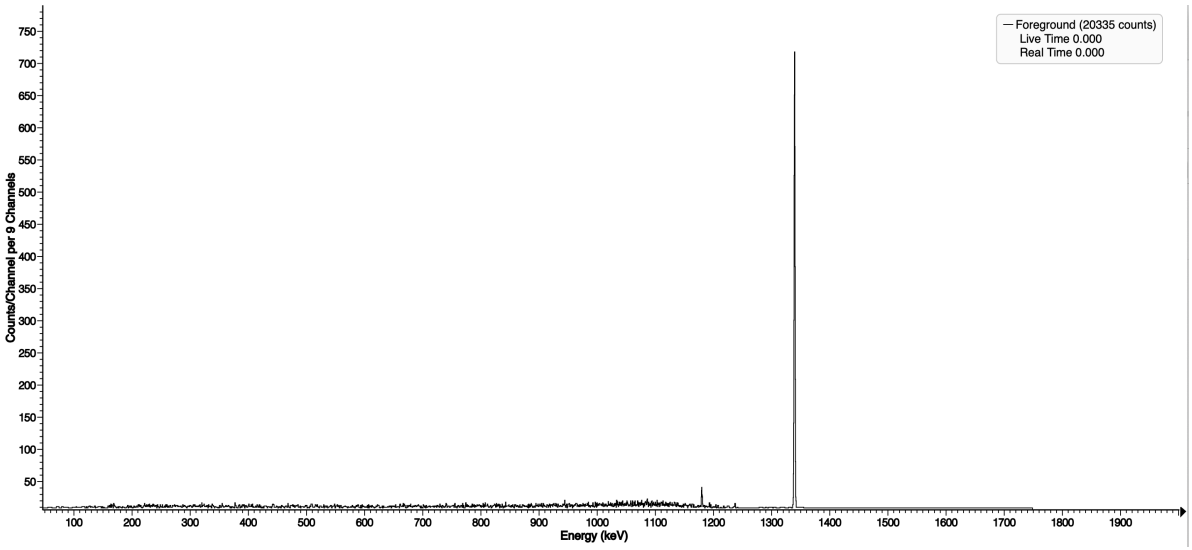

Figure 20: ^{60}Co, Energy gate applied at 1173 keV

For a simple decay like ^{60}Co with only two gamma rays, the energy-gating produces an obvious result. However, utilizing gamma-gamma coincidence and having the ability to perform energy-gating on the coincidence data to identify an isotope with a more complex decay scheme can prove to be extremely beneficial. For this reason, ^{152}Eu was utilized to fully evaluate the efficacy of gamma-gamma coincidence on the Pixie-16 system.

The complex decay scheme of ^{152}Eu, coupled with the fact that many different gammas are in coincidence with one another, makes it a very good isotope to evaluate the Pixie-16 system and

the software against. Figure 21 shows the coincident spectrum for ^{152}Eu as captured by the Pixie-16 system.

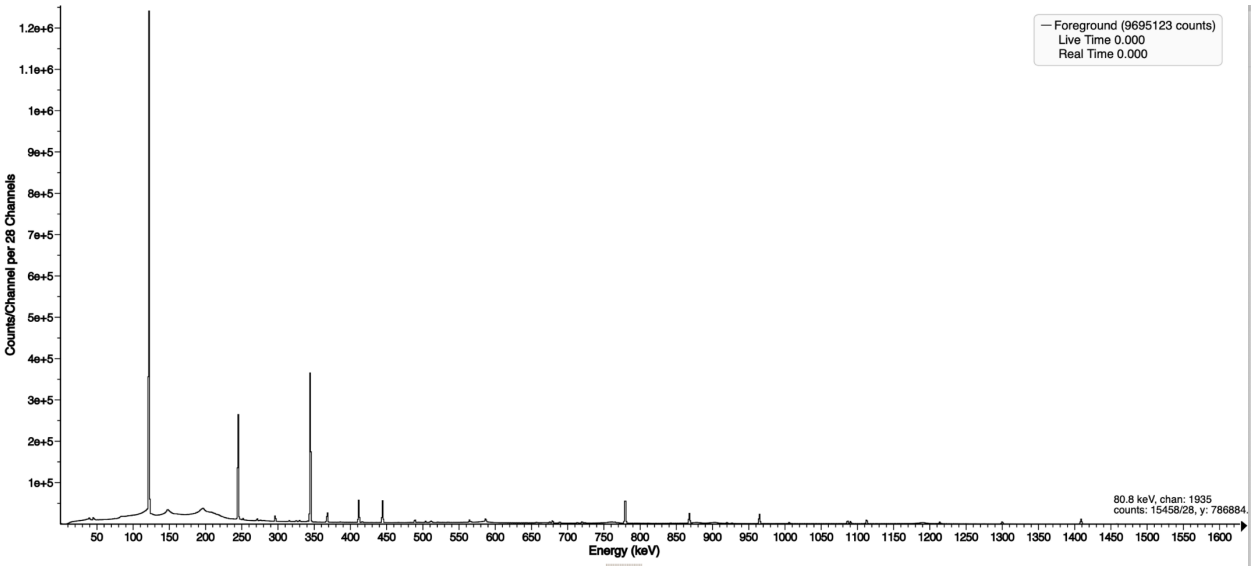

Figure 21: ^{152}Eu Coincidence Spectrum

Note that the gamma-gamma coincidence implementation on the Pixie-16 system evaluates which gamma emissions occur within a specific coincidence time window and it doesn't specifically identify which specific gammas are in coincidence with other specific gammas. Thus, the ability to energy gate proves to be extremely important as it makes it possible to determine which specific gamma rays are coincident with other specific gamma rays.

Figure 22, Figure 23, and Figure 24 provide a few specific energy-gating examples for ^{152}Eu to demonstrate the effectiveness of the UT custom-written software in gating a specific energy and thus, demonstrating which gammas are in coincidence with that specific gamma energy.

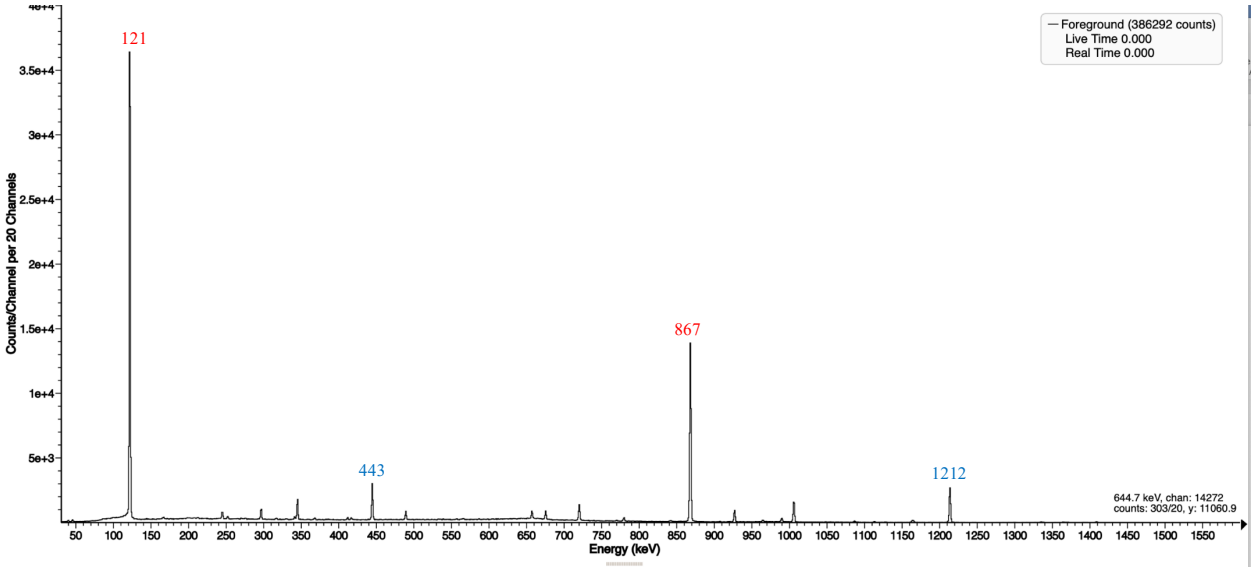

Figure 22: ^{152}Eu Energy gate at 244 keV

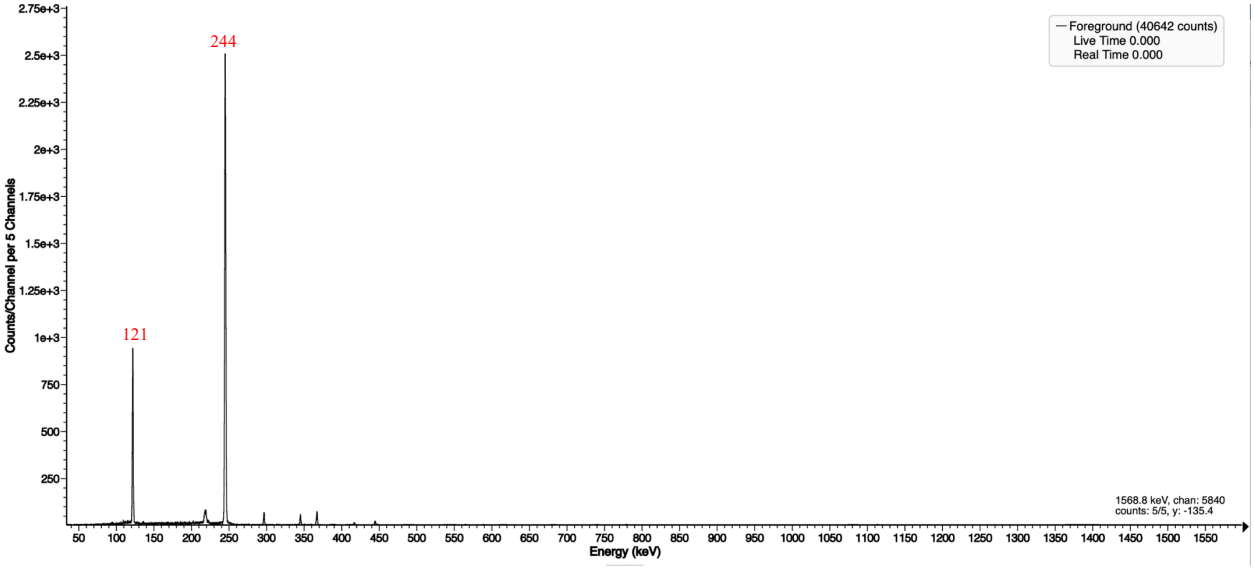

Figure 23: ^{152}Eu Energy gate at 867 keV

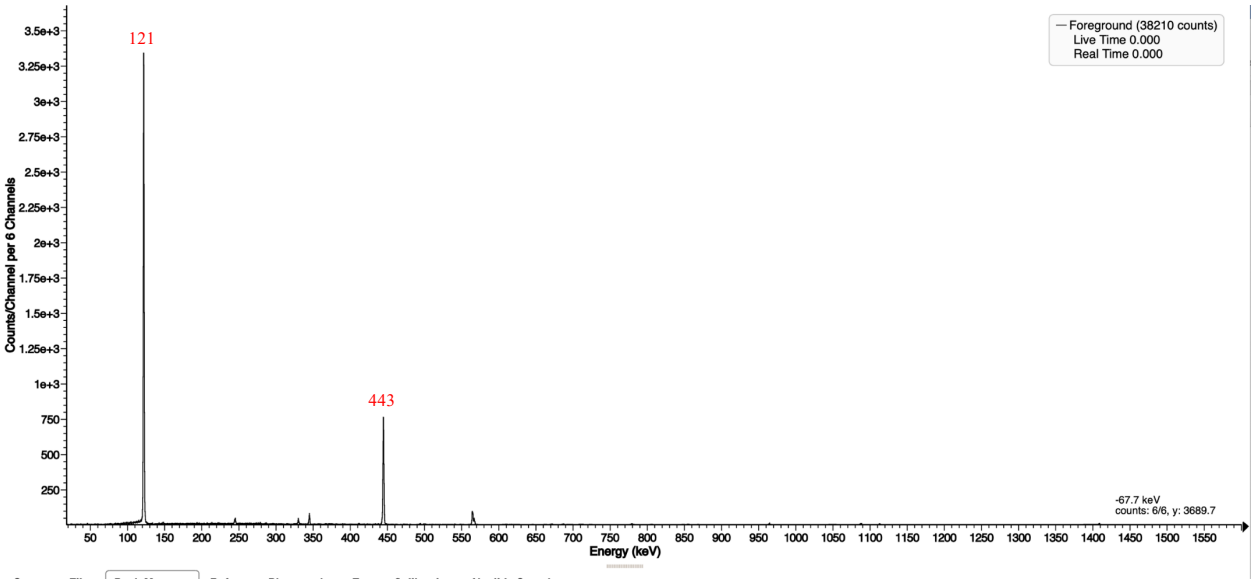

Figure 24: ^{152}Eu Energy gate at 964 keV

Figure 25 presents the spectrum for the ^{152}Eu sample with an energy gate at 344 keV which has a large number of different coincident gamma rays. The decay scheme for ^{152}Eu is included

in Figure 26 to allow the reader to match the gamma energies in Figure 26 with the decay scheme as an independent validation.

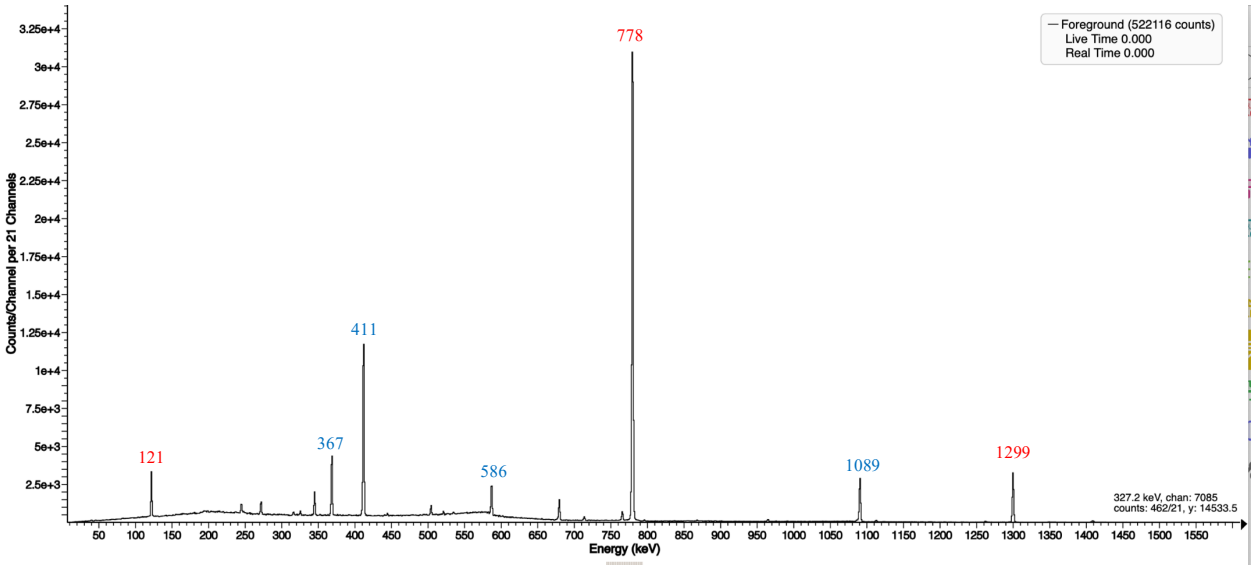

Figure 25: ^{152}Eu Energy gate at 344 keV

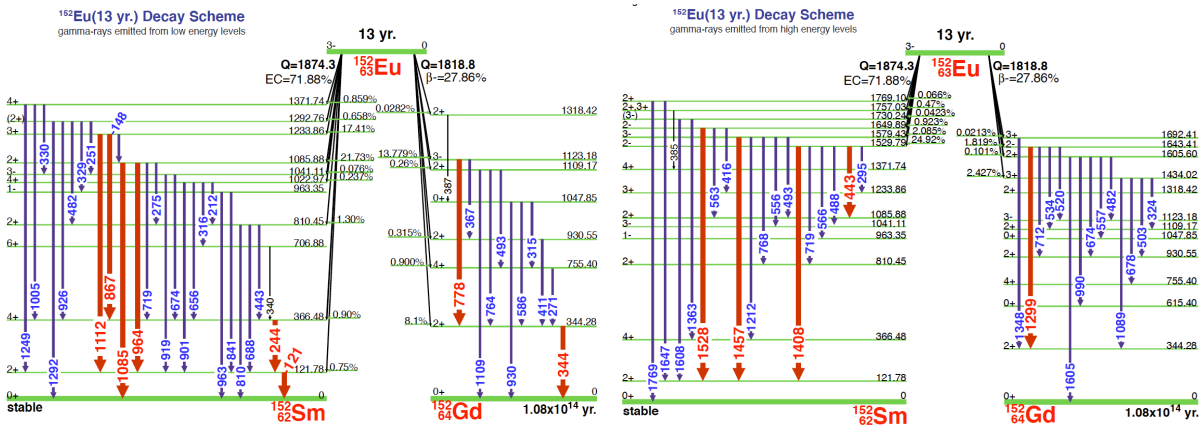

Figure 26: Decay of ^{152}Eu

4.3.2 ^{226}Ra versus ^{152}Eu

In 2018, Drescher, Yoho, and Landsberger utilized an XIA Pixie-4 system for research in Neutron Activation Analysis. As part of that research, they developed a quality control experiment for further validation of the gamma-gamma coincidence function of the Pixie-4 system (Drescher et al., 2018). The experiment was based on the idea that ^{152}Eu and ^{226}Ra both have a gamma ray that exists at approximately 1408 keV. For ^{152}Eu, there is a 121 keV gamma ray that is in coincidence with the 1408 keV gamma ray. However, for ^{226}Ra, there is not a gamma ray which is in coincidence with the 121 keV gamma ray. For their research, they took single detector spectrum data for ^{152}Eu, ^{226}Ra, and one experiment that contained both ^{152}Eu and ^{226}Ra. They also took 121 keV coincidence data for all 3 samples and were able to show the 121/1408 keV coincidence for ^{152}Eu, the lack thereof for ^{226}Ra and the 121/1408 keV coincidence due to the ^{152}Eu for the ^{152}Eu/^{226}Ra sample. Their data proved the effectiveness of the Pixie-4 system for gamma-gamma coincidence.

Due to its successful validation of the gamma-gamma coincidence of the Pixie-4 system, an effort was made to repeat this experiment for the Pixie-16 system. The same configurations of ^{152}Eu and ^{226}Ra were evaluated with the Pixie-16 system. However, as noted above, the Pixie-16 system is configured to output coincidence data. Thus, only the coincidence data spectra were evaluated for the 3 different source configurations. For the ^{226}Ra, the lack of a 1408 keV gamma ray from the spectrum showed that it was not in coincidence with any other gamma ray. For the ^{152}Eu spectrum, the existence of a 1408 keV gamma ray confirms that it is in coincidence with another gamma ray.

Figure 27 displays the output coincidence spectrum for ^{226}Ra. Note the lack of any significant data at 1408 keV. The limited data that is present at 1408 keV can be attributed to random coincidences.

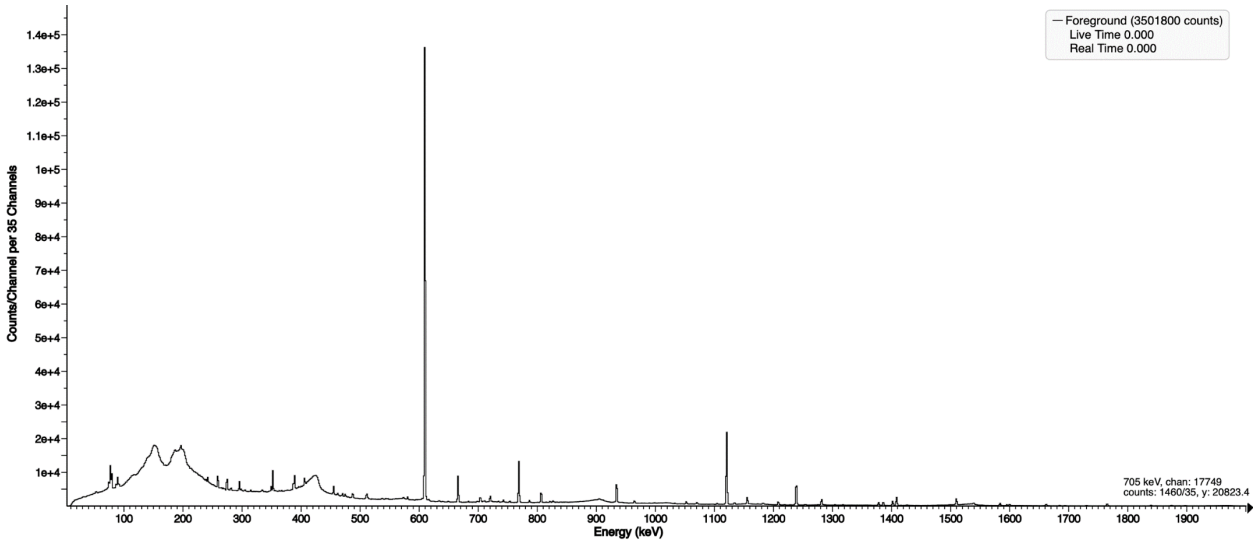

Figure 27: Pixie-16 coincidence data for ^{226}Ra

Figure 28 shows the output coincidence spectrum for ^{152}Eu which clearly shows the 1408 keV gamma ray.

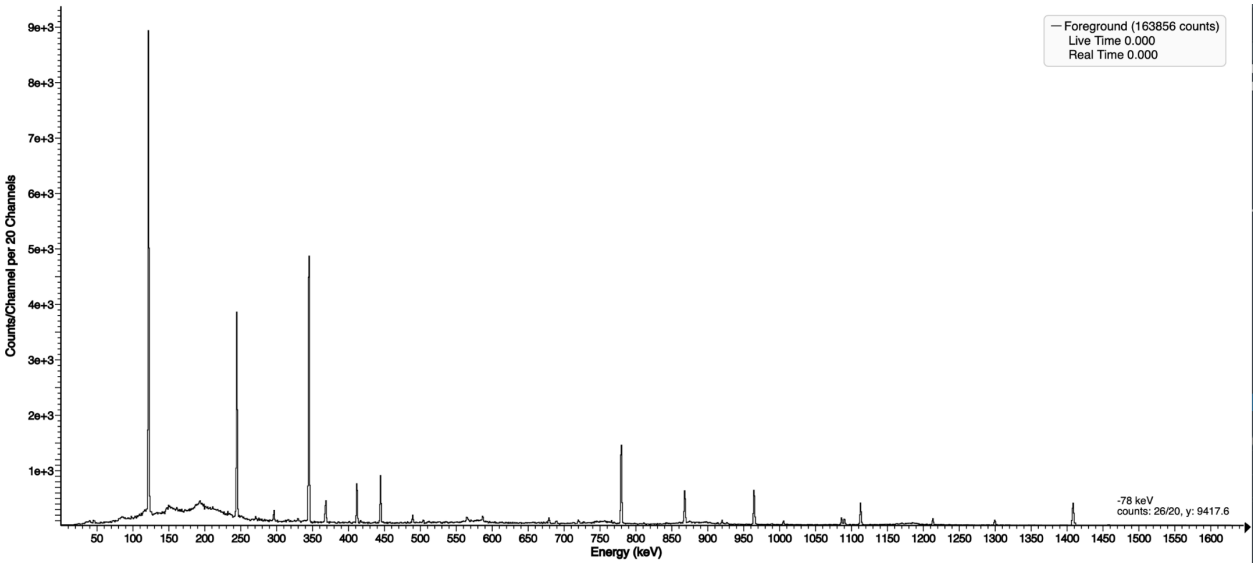

Figure 28: ^{152}Eu coincidence data

Figure 29 shows the output coincidence spectrum for the $^{152}Eu/^{226}Ra$ sample which shows the 1408 keV gamma due to the ^{152}Eu contribution.

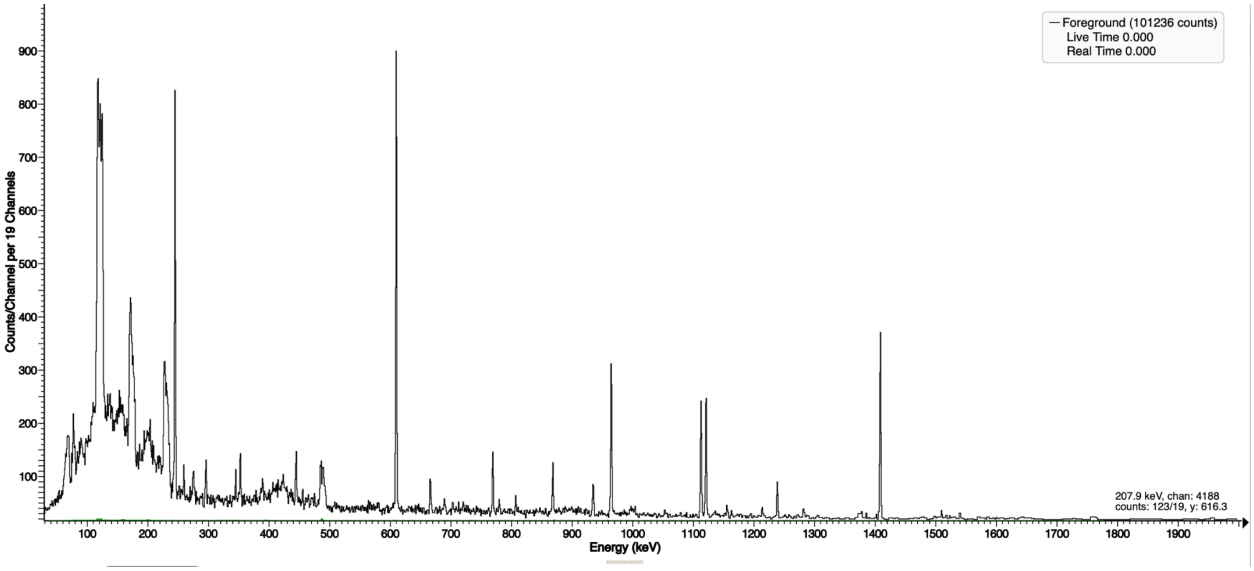

Figure 29: ^{226}Ra and ^{152}Eu, Gated at 121 keV

4.4 Evaluation of the dead-time correction on Pixie-16

All gamma ray spectroscopy systems suffer from what is known as dead time. The dead time of the system is the length of time that it takes a gamma spectroscopy system to respond to a subsequent photon after detecting and processing a previous one. The total dead time of the system includes the time it takes the detector to respond to a subsequent gamma ray, the delays caused by analog amplifiers, and the time it takes the data acquisition system to process and record the data (Usman & Patil, 2018). Until the dead time has cleared the system, the gamma spectroscopy system is incapable of capturing and processing any further signals. When a gamma spectroscopy system is utilized to measure a sample with high activity, the sample is often allowed to decay prior to counting it, the distance between the measured sample and the detector can be increased,

or the counting time can be extended to compensate for the loss due to the deadtime (Westphal, 2008).

One major benefit of the use of digital gamma spectroscopy systems is the ability to perform dead time corrections. Because of the nature of digital systems, there is no requirement to capture an analog signal and then convert it to a digital signal. As the signal is already a digital signal, this conversion step is eliminated. A number of different techniques exist to perform these dead time corrections. Some of the more novel approaches to this are the virtual pulse generator technique and Ortec's Zero Dead Time Counting (ZDTtm) technique (Westphal, 2008). Westphal also discussed the historical technique of using the pulser method, which is no longer required due to the use of digital systems.

The XIE Pixie-16 system, being a digital one, also has its own method of dead time correction. The system takes the filter sums, reconstructs the energy, and adds it back to the spectrum. The filter sums are continuously updated in a Field Programmable Gate Array (FPGA), and are captured into event buffers. Reconstructing the energy and incrementing the spectrum is done by the Digital Signal Processor (DSP), so that the FPGA is ready to take new data immediately (XIA LLC, 2019).

An experiment was developed to evaluate the effectiveness of the sophisticated dead-time correction as performed by the Pixie-16. To perform this experiment, a highly-shielded conventional "Clamshell" gamma spectroscopy system was used as the baseline. This system has been used at NETL for a number of years and is the system that is used to perform routine gamma spectroscopy measurements.

Two samples were simultaneously irradiated in the NETL TRIGA reactor with thermal neutrons for 1 hour with a reactor power of 950 kW. A 9.999 +/- .060 μg/g Scandium solution,

with a known density of 1.035 g/ml, from Inorganic Ventures (NIST traceable) was irradiated. The second sample was a NIST Coal Fly Ash sample, Standard 1633c, which contains a mass fraction of 37.6 ± mg/kg of Scandium. The samples were weighed prior to irradiation; the liquid mass used for the Scandium Standard was 0.6854g and solid mass used of Standard 1633c was 0.69147g. After the irradiation was complete, the samples were allowed to decay for 2 weeks. The irradiated samples were then both measured using both the Clamshell system and the Pixie-16 system.

The irradiated Scandium standard, which gave the radionuclide ^{46}Sc, was measured for 5 minutes live time on the Clamshell system with 25,858 ±170 net counts being captured. The irradiated coal fly ash sample, which also gave the radionuclide ^{46}Sc, was measured for 5 minutes live time as well with 90,447 ± 326 net counts being captured. The of the coal fly ash was measured to be 40% using the Clamshell system.

For the Pixie-16 gamma-gamma system, the system was set to capture data for 10,0000 seconds live time. Then the same samples, Scandium and coal fly ash, were measured in singles mode. For the Scandium sample, a total of 130,184 ± 585 counts were measured. For the coal fly ash sample, 484,596 ± 1129 counts were measured.

Utilizing these captured data, the concentration of the Scandium was then calculated utilizing the following equation which is based on Equation 4.

$$N\ C_1 \frac{\mu g}{g_1} = N\ C_2 \frac{\mu g}{g_2}$$

Equation 5: Simplified concentration equation, comparator method

For the Clamshell system, utilizing 9.66 μg/g (10 μg/ml / 1.035 g/ml), 25,858 ±170 counts for the Scandium standard and 90,447 ± 326 counts for NIST coal fly ash sample, 1633c, the

concentration of Scandium in NIST 1633c is calculated to be between 33.7 and 34.1 μg/g, when considering uncertainty. The mass fraction value as noted by the NIST certificate is 37.6 ± .6 μg/g. This is an error between 9.3% to 10.4% relative to the NIST sample.

For the Pixie-16 system, when utilizing 130,184 ± 585 counts for the Scandium standard and 484,596 ± 1129 counts for NIST coal fly ash sample 1633c, the concentration of Scandium in NIST 1633c is calculated to be 35.9 to 36.2 μg/g, when considering uncertainty. When comparing this calculated concentration to the NIST 1633c value, the error is between 3.7% to 4.5%. The concentration calculated from the Pixie-16 data is closer to the reference value in the NIST 1633c sample than the data calculated from the Clamshell data. This demonstrates that the Pixie-16 dead time correction is effective while maintaining the integrity of the data.

Chapter 5: Neutron Activation Analysis Products

This section will discuss the results of the primary focus area of this dissertation which was to implement the XIA Pixie-16 based gamma-gamma coincidence system for use on NAA products and then to characterize the results of the system for a subset of NAA products. The purpose for characterizing the results is to provide information that other researchers can use in implementing gamma-gamma coincidence for NAA when using an advanced digital system. The data that is generated using the Pixie-16 based system is not unique to this system alone, but may prove to be more successful at the reduction of background levels due to the capabilities of the hardware.

5.1 Characterization of NAA products for gamma-gamma coincidence

One aspect that must be considered with the implementation of gamma-gamma coincidence for NAA is that only a subset of its products has coincident gamma rays. As such, the implementation of gamma-gamma coincidence for all NAA products is not possible. Part of this research included reviewing the decay schemes for each of the NAA products to identify whether or not they had coincident gamma rays. This information is summarized in Table 7, Table 8, and Table 9. Rather than having the decay schemes for all NAA products distributed throughout this chapter, the NAA decay schemes which have coincident gamma rays can be found in Appendix A (Helmer et al., 1998).

It is impossible to evaluate all NAA products against all potential matrices that exist including samples that are challenging to identify specific radionuclides within and others that are much more straightforward. In some instances, advantages gained by implementation of gamma-

gamma coincidence is minor and in other instances, the advantages may be significant. *A focus was made to demonstrate what peaks can be identified for all applicable NAA products whether they are normally easy or difficult to identify.* Table 5 and Table 6 serve as a test matrix which documents which specific samples were evaluated for the different NAA products. Table 6 details how long each sample was irradiated, what power level the reactor was set at, and also whether it was irradiated with thermal or epithermal neutrons. In some cases, a few of the NIST reference materials were setup as two different samples, one irradiated with thermal neutrons and one irradiated with epithermal neutrons. Also note that NIST 1633C is coal fly ash, NIST 2710a is Montana I Soil, 1632d is coal (bituminous), NIST 2670 is freeze-dried urine, and NIST 1548a is a typical diet sample.

Table 5: NAA test matrix

	Biological Standards	Geological Standards	Freeze-Dried Urine (biological)
Long-Lived	X	X	
Medium-lived	X	X	X
Short-lived	X	X	X

Table 6: Parameters of NIST-traceable samples

NIST-traceable standards	Reactor Power	Epithermal Neutrons	Thermal Neutrons	Irradiation Time	Decay Time	Counting Time
1633C	950 kW		X	2 hrs	2 weeks	18 hrs
2710a	950 kW		X	2 hrs	2 weeks	18 hrs
1632d	500 kw	X	X	5 min	1 hr	3 hrs
2670	500 kW	X	X	30 min	1 hr	3 hrs
1548a	500 kW	X	X	30 min	1 hr	3 hrs

5.1.1 Long-lived NAA products

The best likelihood for success of the implementation for gamma-gamma coincidence in NAA products was in the use of long-lived radionuclides due to the fact that many of the radionuclides have multiple gamma rays in the beta decay. An overview of relevant information is contained in Table 7.

For each of the irradiations, the samples were counted using the Pixie-16 gamma-gamma coincidence system and then the coincidence spectra were analyzed. After these spectra were reviewed, the custom UT-developed software was used to apply energy gates to assist in determining which isotopes were identifiable through this process and which ones were not. The spectra of all long-lived NAA products that were successfully identified through this process are presented in this section of the dissertation and the successful NAA products are also noted in Table 5. The Pixie-16 has shown great promise for use of identification of NAA products through the use of gamma-gamma coincidence. Many of the spectra presented below will show large number of counts whereas others will have fewer counts but will be easily identifiable due to the significant reduction in the background levels due to gamma-gamma coincidence. Further, many of the spectra show a limited portion of the full spectrum to allow the reader to identify the coincident gamma ray peaks of interest. It should also be noted that many of the spectra for

geological material contain strong photopeaks at 889 keV and 1120 keV due to ^{46}Sc. These occur due to random coincidences of the 889 keV and 1120 keV peaks.

A more thorough discussion will be presented for NAA products that have been historically difficult to identify but were successfully identified through use of this process as part of this research.

Table 7: Long-lived NAA products coincidences

Element	Isotope	Half life	Major Gamma Coincidences	Was γ- γ coincidence successful?
Ag	Ag-110m	249.8d	YES	YES
Ce	Ce-141	32.5d	NO	N/A
Cr	Cr-51	27.72d	NO	N/A
Cs	Cs-134	2.06y	YES	YES
Co	Co-60	5.27y	YES	YES
Eu	Eu-152	13.4y	YES	YES
Fe	Fe-59	44.5d	YES	YES
Hf	Hf-181	42.4d	YES	YES
Hg	Hg-203	46.6d	NO	N/A
Lu	Lu-177m	160d	YES	YES
Nd	Nd-147	10.99d	YES	NO
Ni	Co-58	70.9d	YES	NO
Rb	Rb-86	18.7d	NO	N/A
Sb	Sb-124	60.2d	YES	YES
Sc	Sc-46	83.8d	YES	YES
Se	Se-75	119.8d	YES	YES
Sn	Sn-113	114.4d	NO	N/A
Sr	Sr-85	64.84d	NO	N/A
Ta	Ta-182	115.0d	YES	NO
Tb	Tb-160	72.1d	YES	YES
Th	Pa-233	27.0d	YES	NO
Tm	Tm-170	129d	NO	N/A
Yb	Yb-175	4.19d	YES	YES

5.1.1.1 Identification of ^{110m}Ag

During process of analyzing the data for ^{110m}Ag, it became evident that this radionuclide is a very strong example to demonstrate the successful implementation of the gamma-gamma coincidence technique coupled with the energy gating software. This will be demonstrated in detail. The singles, the coincidence, and lastly, energy gated spectra will be presented to demonstrate the improvement of detection capability through the progression of singles to coincidence to energy gating spectra.

The singles spectrum evaluated for ^{110m}Ag was NIST 2710a, Montana I Soil Highly Elevated Trace Elements; the mass fraction concentration of ^{110m}Ag in the sample is 40 ug/g. The singles spectrum for 2710a can be seen in Figure 30. The spectrum has also been adjusted in Figure 31 to focus on the energy regions of interest, 600 keV to 1000 keV, for the coincident gamma peaks in ^{110m}Ag. Note that in this spectrum, the 657 keV and 884 keV gamma ray peaks for ^{110m}Ag are visible. Although the step of applying the gamma-gamma function and energy gating may not be required for this radionuclide, it will be presented to demonstrate the full gamma ray spectral analysis that is available with the Pixie-16 system and the custom UT software.

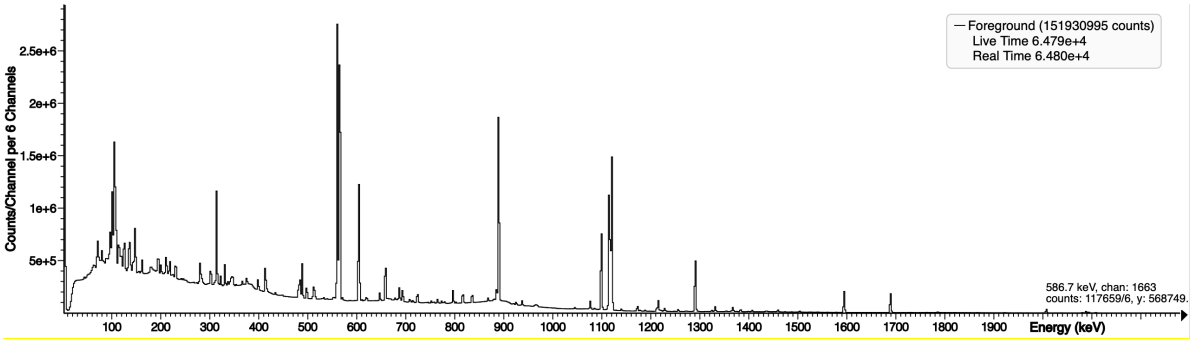

Figure 30: Singles spectrum for NIST 2710a

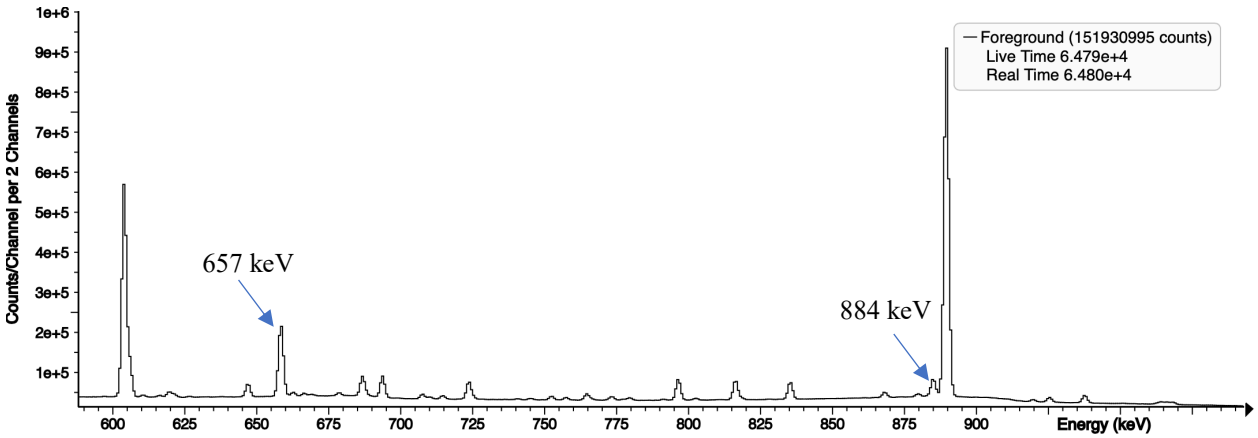

Figure 31: Singles spectrum for NIST 2710a, 600 keV - 1000 keV

Figure 32 presents the coincidence spectrum, from 600 keV to 1000 keV, that is generated with the Pixie-16 hardware. Figure 33 presents the spectrum after applying an energy gate at 884 keV. When this energy gate is applied, the coincident 657 keV gamma ray is visible.

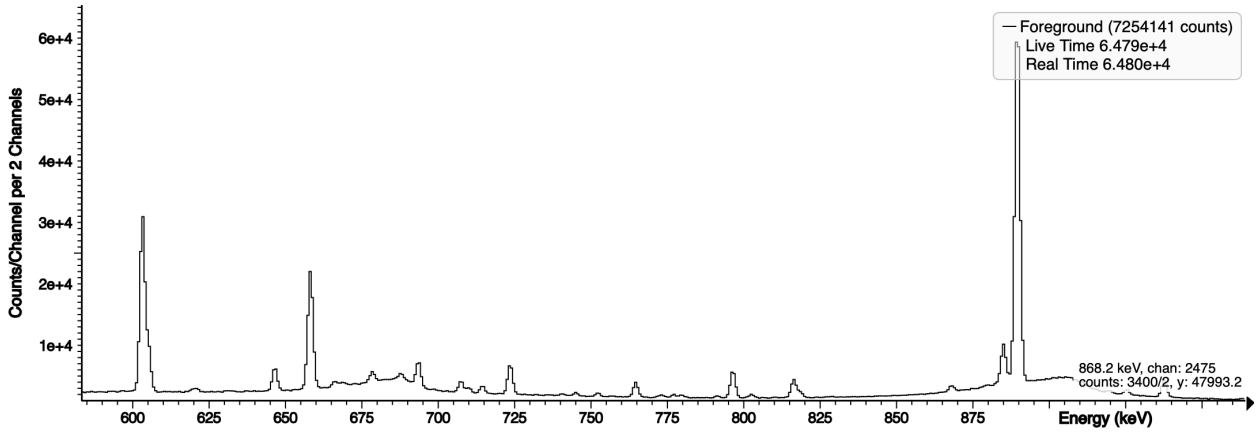

Figure 32: Coincidence spectrum for NIST 2710a, 600 keV - 1000 keV

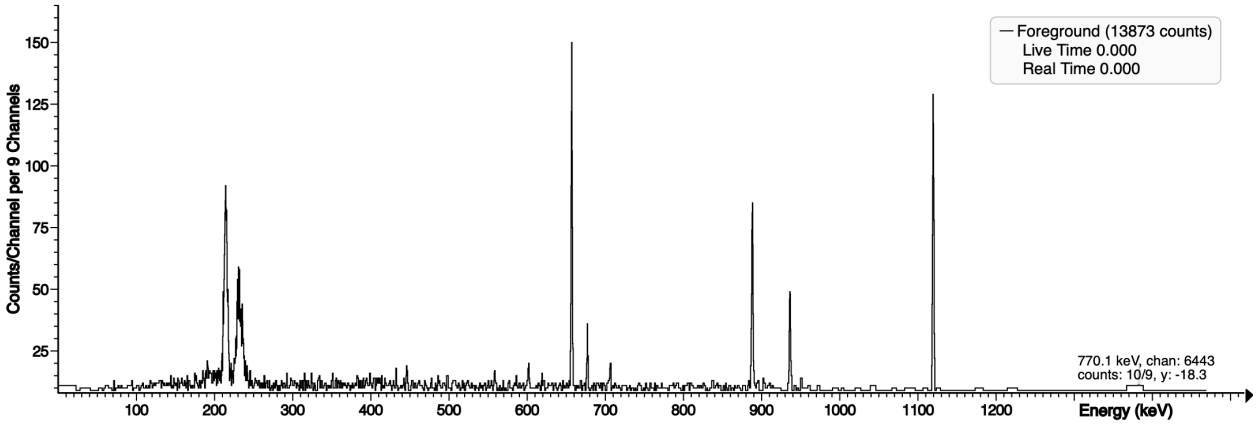

Figure 33: ^{110m}Ag gated at 884 keV, 2710a

For the remainder of the radionuclides, only the energy gated spectrum that is most successful will be presented within the following section. This approach should provide the nest identification of the specific NAA radionuclide of interest.

5.1.1.2 Identification of the remainder of the long-lived NAA products

In standard NAA research, the 604.7 keV gamma way for ^{134}Cs is typically evaluated. However, there is a potential interference due to the 602.7 keV photon gamma ray from ^{124}Sb which has a 60-day half-life. However, ^{134}Cs was positively identified in NIST sample 2710a, which also contains ^{124}Sb, utilizing an energy gate at 795 keV as the 569 keV and 604 keV gamma peaks are visible even with the ^{124}Sb 602.7 keV gamma ray interaction.

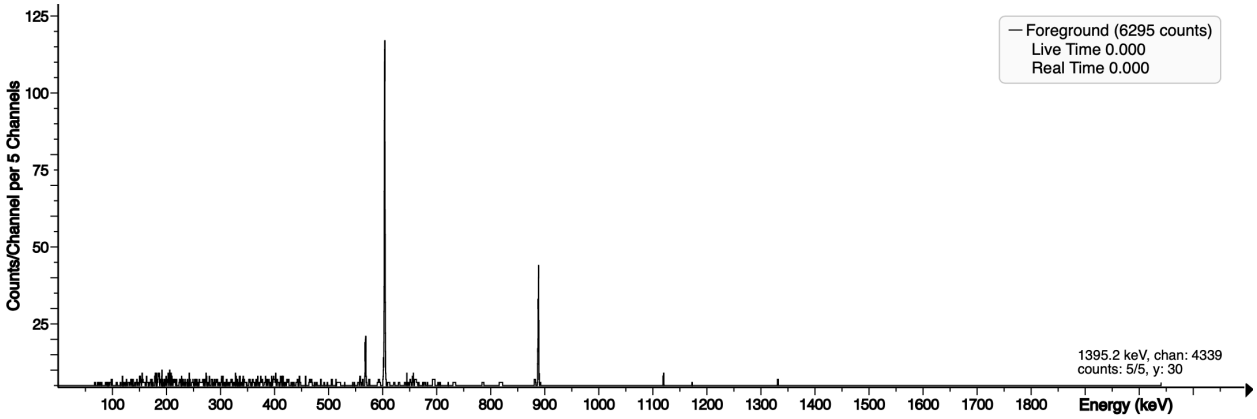

Figure 34: ^{134}Cs gated at 795 keV, NIST 2710a

^{60}Co was identified in NIST sample 1633c and an energy gate at either 1173 keV or 1332 keV was very effective.

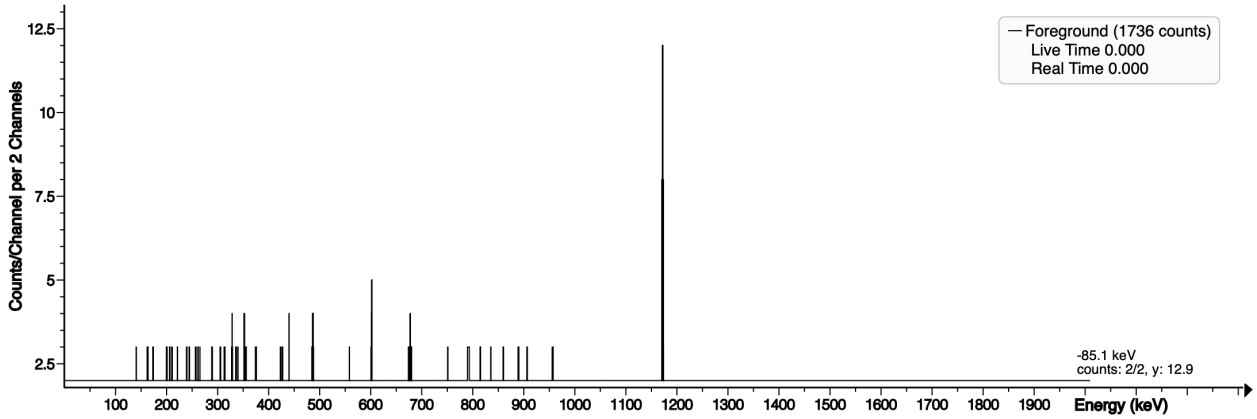

Figure 35: ^{60}Co gated at 1332 keV, NIST 1633c

^{152}Eu was identified in sample 1633c and was gated at 244 keV with a number of coincident gamma rays visible.

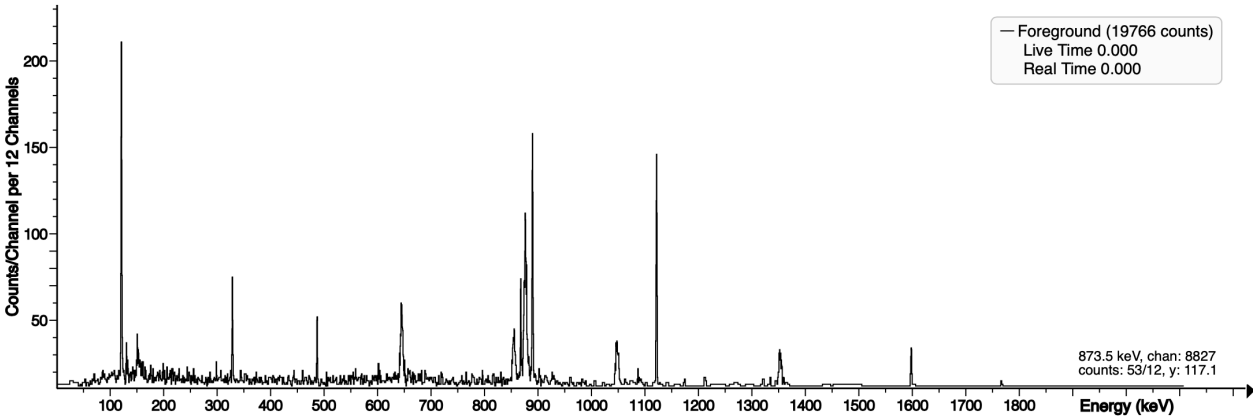

Figure 36: ^{152}Eu gated at 244keV, NIST 1633c

^{59}Fe was identified in both 2710a and 1633c and the most effective energy gate was at 1099 keV as the 192 keV gamma ray is visible.

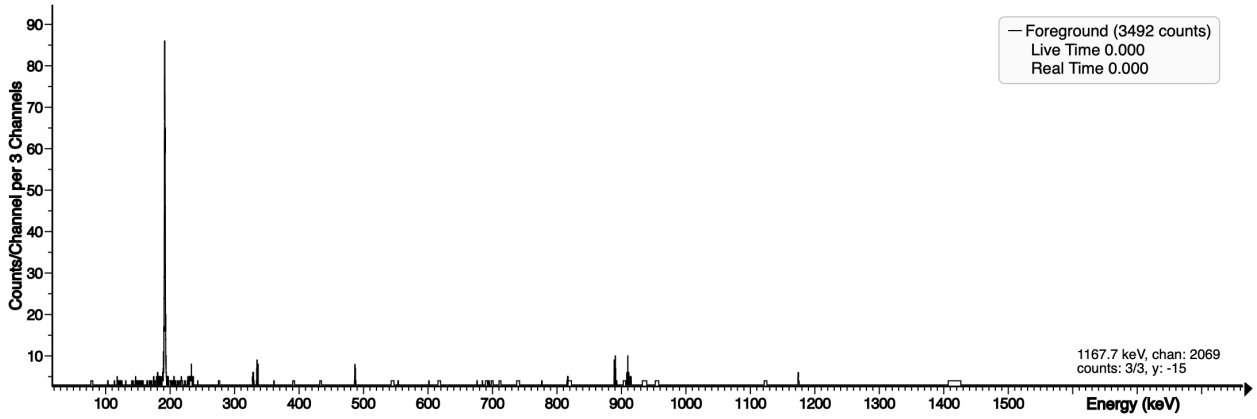

Figure 37: ^{59}Fe gated at 1099 keV, NIST 1633c

Typically for NAA, the 482.2 keV gamma ray for ^{181}Hf is assessed. However, there is a potential spectral interference due to ^{115m}Cd at 484.5 keV. However, ^{181}Hf was identified in NIST samples 2710a and 1633c with the most effective energy gate at 345 keV which makes the 133 keV and 136 keV peaks visible.

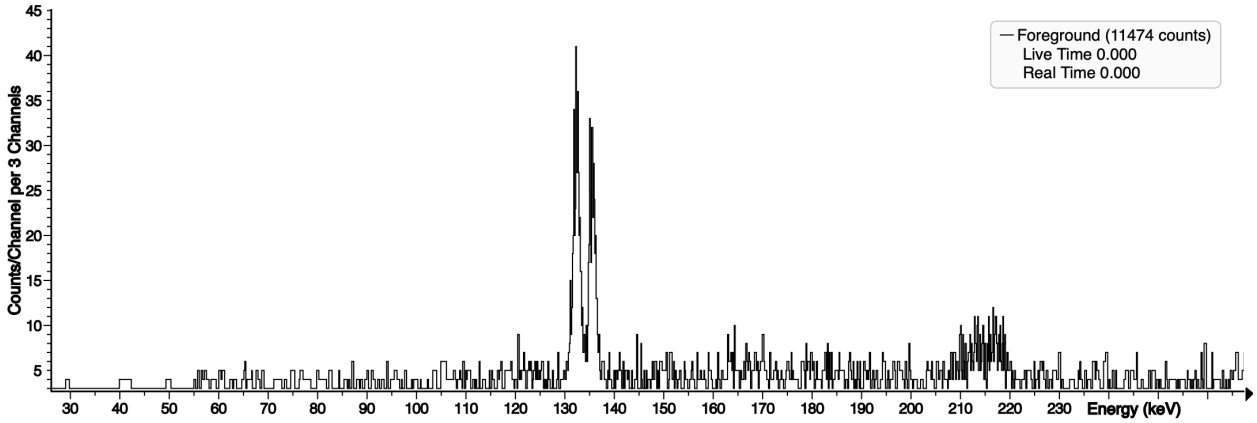

Figure 38: ^{181}Hf gated at 345 keV, NIST 2710a

In 2019, Brennan and Landsberger described some of the spectral and nuclear interferences in the determination of Lutetium. They noted a 209.8 keV emission from ^{239}Np, produced from the neutron absorption of ^{238}U(n,γ)^{239}U($t_{1/2}$ = 25 min) → ^{239}Np($t_{1/2}$ = 2. 35 d) reaction (Brennan & Landsberger, 2019). This potential interference is shown in Figure 39 with the dark gray peak representing the 209.8 keV emission from ^{239}Np and the light gray peak representing the sum of the ^{177}Lu and ^{177m}Lu emissions. However, ^{177m}Lu was successfully identified in NIST samples 2710a and 1633c with effective gating at 112 keV or 208 keV. The coincident peak, 208 keV or 112 keV respectively, was visible in all cases. This is shown in Figure 40.

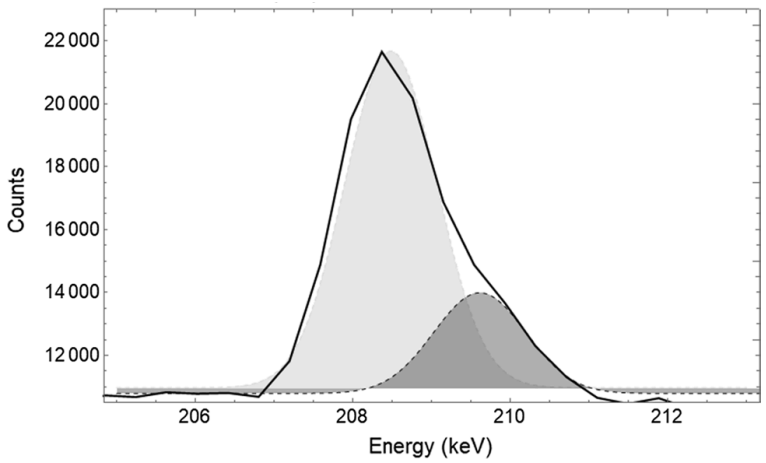

Figure 39: ^{239}Np Spectral Interference with ^{177}Lu

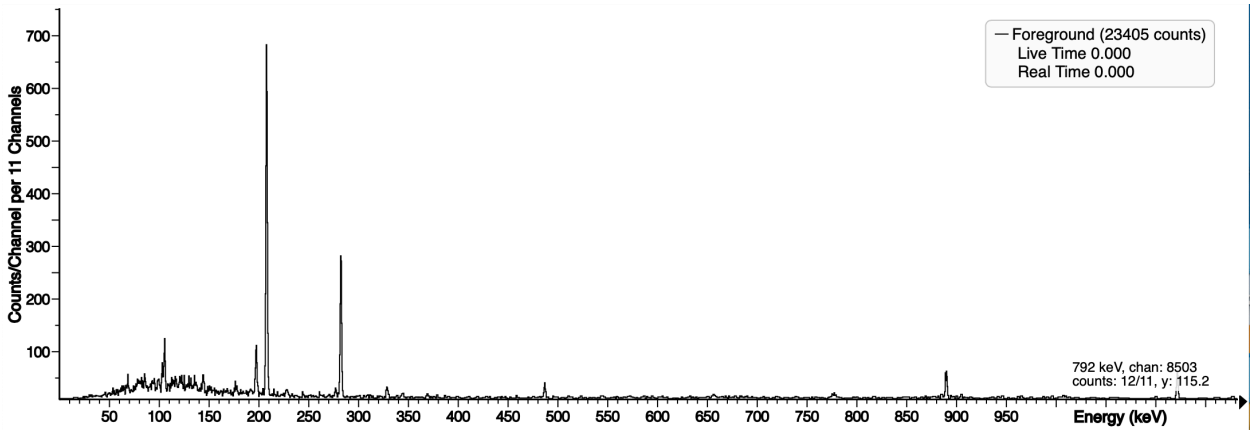

Figure 40: ^{177m}Lu gated at 112 keV, 1633c

^{124}Sb was identified in NIST sample 2710a but required energy gating at 1690 keV. When gated on 1690 keV, the 602 keV peak was visible. Typically, the 602 keV is used in NAA but it has potential interferences from ^{134}Cs at 604.7 keV. However, one can also use the 1690 keV which is interference free, but has a low efficiency. Note that the spectrum was gated on the 1690 and the 602 keV peak is visible.

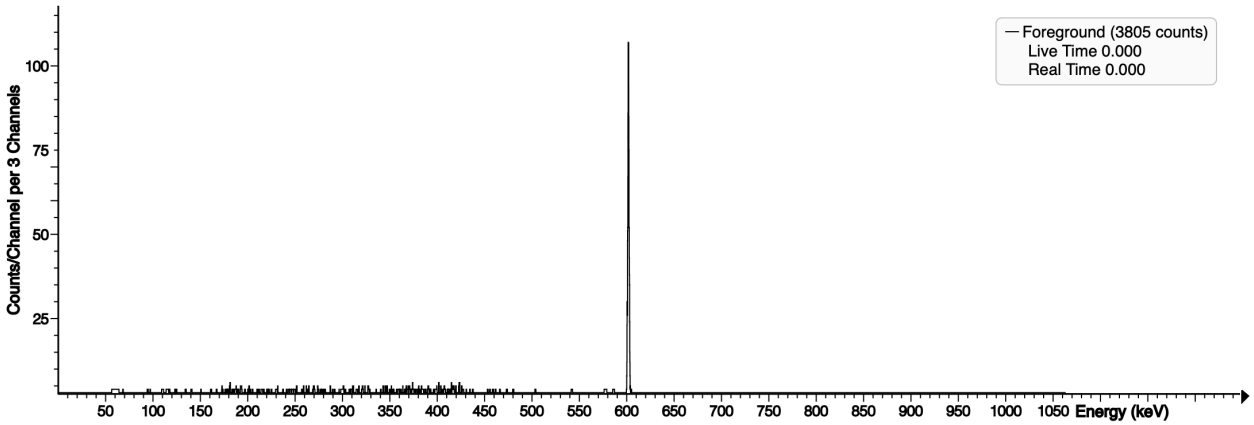

Figure 41: ^{124}Sb gated at 1690 keV, 2710a

^{46}Sc was identified in NIST sample 2710a and 1633c. When an energy gate of either 889 keV or 1120 keV are applied, the corresponding coincidence gamma, 1120 keV or 889 keV respectively, are visible.

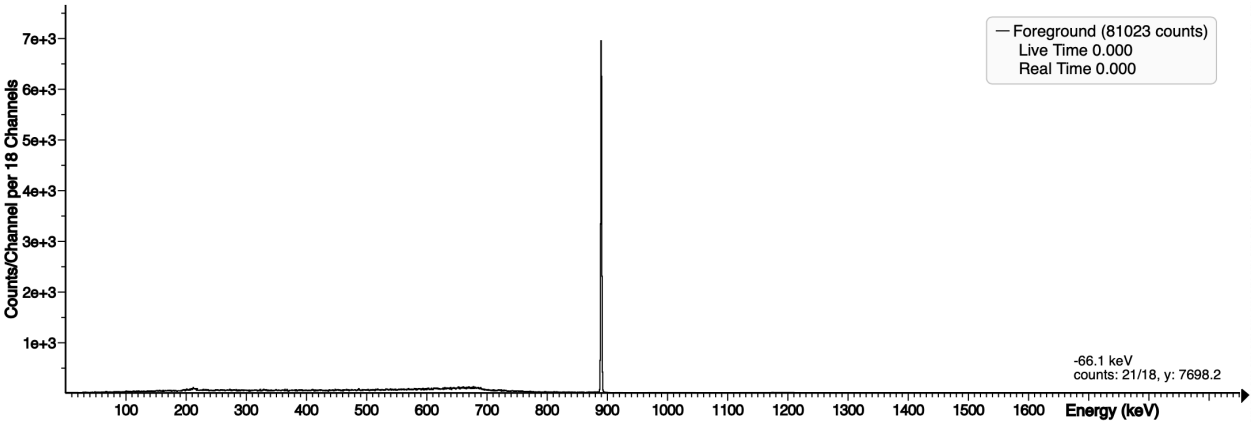

Figure 42: ^{46}Sc gated at 1120 keV, 1633c

^{75}Se has been shown by Yoho and Landsberger to be visible via gamma-gamma coincidence and was validated and identified in NIST sample 1633C for this research (Yoho & Landsberger, 2016). When an energy gate of 136 keV was applied, the coincident 264 keV gamma ray is visible.

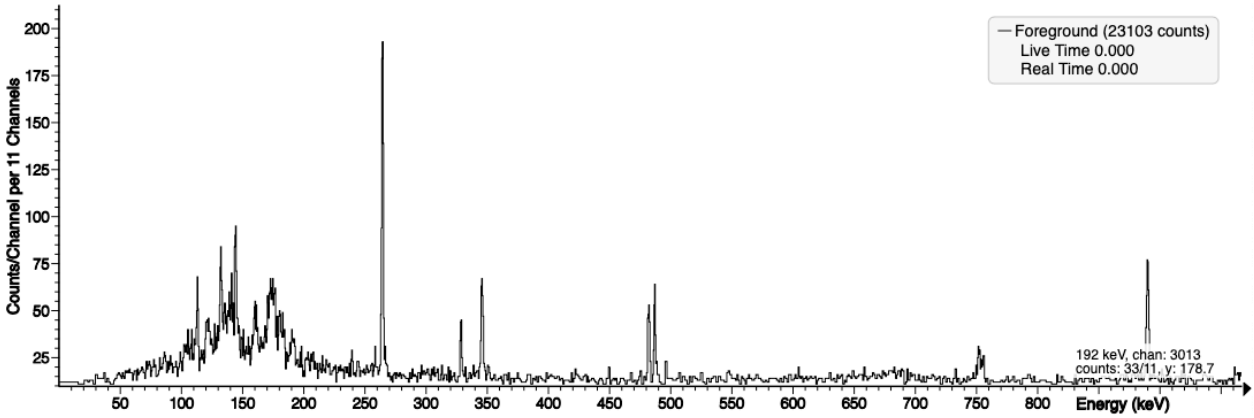

Figure 43: ^{75}Se gated at 136 keV, 1633c

^{160}Tb is normally evaluated via the 879 keV gamma ray peak which can often be buried within the tail of the 889 keV peak from ^{46}Sc, depending on the concentration of Scandium. The singles spectrum for 2710a is shown below to demonstrate this potential interaction, although it does not exist for this specific spectrum that was counted on the Pixie-16.

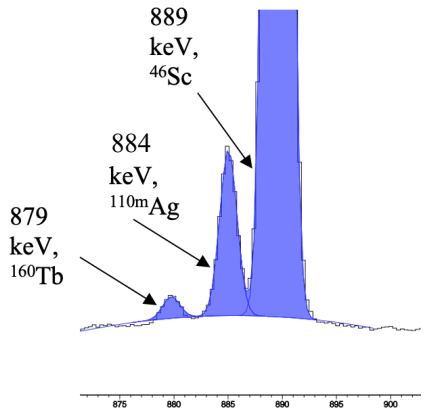

Figure 44: 879 keV gamma peak from ^{160}Tb, with potential interferences

^{160}Tb was identified in NIST sample 1633c. When an energy gate of 879 keV was applied, the coincident 298 keV gamma ray is visible.

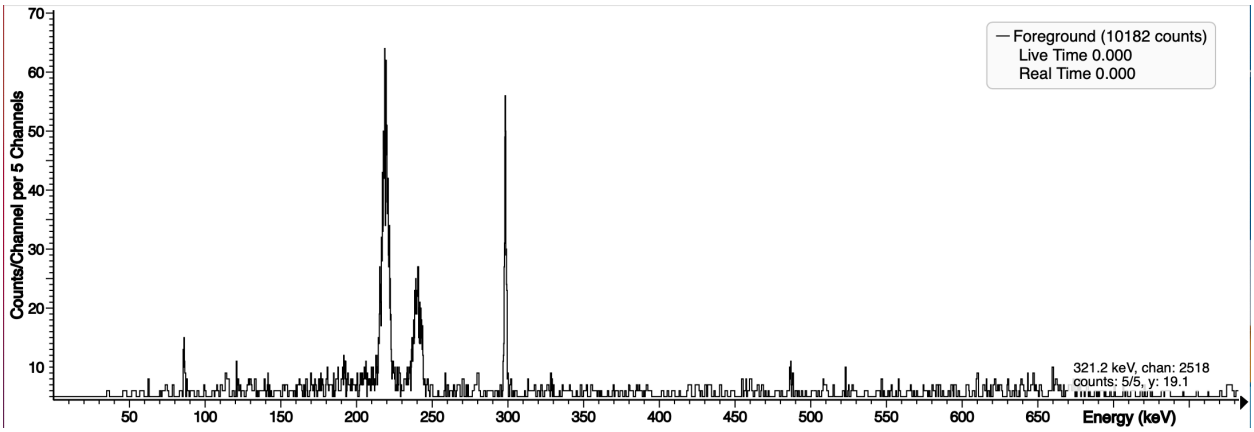

Figure 45: ^{160}Tb gated at 879 keV, 1633c

^{175}Yb is normally identified in NAA via the 396.3 keV gamma ray which has two potential interferences at 398.2 keV and 398.6 keV, ^{147}Nd and ^{233}Pa respectively. The 396.3 keV gamma ray has no coincident gamma rays. However, ^{175}Yb was successfully identified in NIST samples 1633c and 2710a when an energy gate of 282 keV was applied, the coincident 113 keV gamma ray is visible.

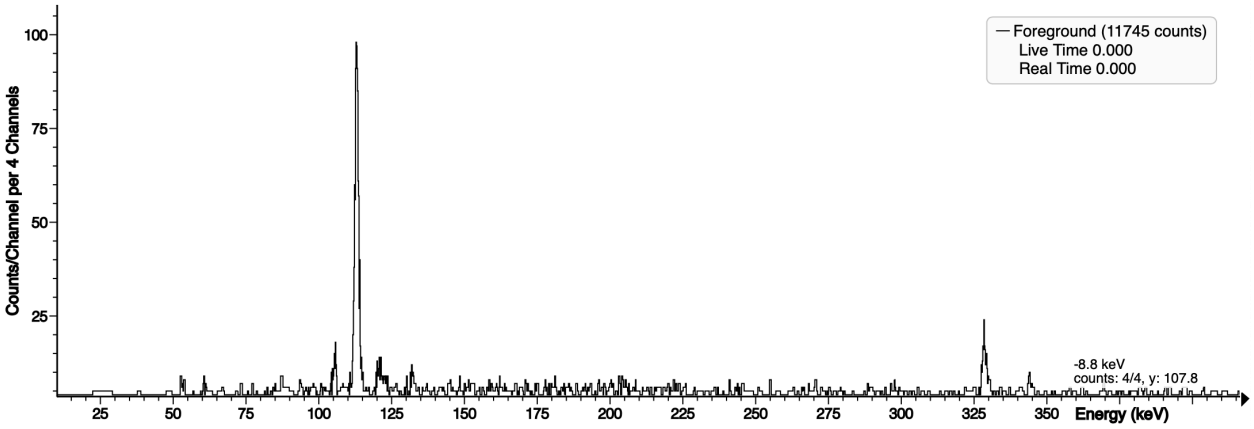

Figure 46: ^{175}Yb gated at 282 keV, 1633c

5.1.2 Medium-lived NAA products

For the medium-lived radionuclides, a number of them were identified in samples that were prepared for short-lived NAA whereas others were measured in samples prepared for long-lived NAA. In conventional NAA, a sample is irradiated for short-lived radionuclides followed by a longer irradiation that is used to determine medium- and long-lived radionuclides. Typically, a sample prepared for short-lived radionuclides cannot be used for medium-lived NAA due to high activity radionuclides, which often are the source of very high Compton background levels (e.g., ^{24}Na and ^{82}Br). However, the Pixie-16 system has demonstrated the capability of being able to identify medium-lived radionuclides in samples prepared for short-lived NAA that contain high activity radionuclides, including both ^{24}Na and ^{82}Br. For the medium-lived NAA, the sample was placed directly against the face of both detectors, in many cases after a 5 min irradiation followed by a 1-hour decay. This greatly increased the counting efficiency when compared to counting of the sample on the conventional Clamshell at a distance of 10 cm which had a high dead time of greater than 40% which deteriorated the FWHM.

Similarly to what was done for the long-lived NAA products, the medium-lived NAA products and a summary of the important information for each radionuclide is found in Table 8. NAA products that are normally difficult to identify has a discussion provided to discuss the process of identification and all other NAA products have been presented with a spectrum that clearly demonstrates their identification.

Table 8: Medium-lived NAA products coincidences

Element	Isotope	Half life	Major Gamma Coincidences	Was γ- γ coincidence successful?
As	As-76	26.3h	YES	YES
Au	Au-198	2.7d	NO	N/A
Br	Br-82	35.3h	YES	YES
Cd	Ina-115m	53.5h	NO	N/A
Ga	Ga-72	14.1h	YES	NO
Ge	Ge-77	11.3h	NO	N/A
Hg	Hg-197	64.1h	NO	N/A
Ho	Ho-166	26.8h	NO	N/A
K	K-42	12.36h	YES	NO
La	La-140	40.23h	YES	YES
Mo	Mo-99	66.02h	YES	NO
Na	Na-24	15.02h	YES	YES
Pd	Pd-109	13.7h	YES	NO
Sb	Sb-122	2.72d	YES	YES
Sm	Sm-153	46.7h	YES	YES
U	Np-239	2.35d	YES	YES
W	W-187	23.9h	YES	YES

5.1.2.1 Identification of ^{153}Sm

One NAA product that can be a challenge to identify is Samarium. This is in part due to the fact that there are spectral interferences from Uranium, Thorium and Gadolinium (Landsberger & Simsons, 1987). The first main interference arises from the characteristic 103.7 keV K X-ray produced in the ^{238}U (n,γ) ^{239}U ($t_{1/2}$ =23.5 min.) -> ^{239}Np ($t_{1/2}$ = 2.35 days) sequence. A second interference comes from the ^{232}Th (n, γ) ^{233}Th ($t_{1/2}$=22.2 min.)->^{233}Pa ($t_{1/2}$=27.0 days) sequence. The ^{233}Pa isotope decays with a plethora of γ-rays, twenty-five in all, including a 103.9-keV γ-ray which has an intensity of ~ 2% relative to the strongest decay line at 311.9 keV. The last interfering reaction is ^{152}Gd (n, γ) ^{153}Gd ($t_{1/2}$=246.1 days). This radioactive isotope decays by β+ emission to ^{152}Eu giving the same 103.2-KeV gamma-ray as in the β- decay of ^{153}Sm.

The 103.2 keV gamma ray belonging to ^{153}Sm is in coincidence with a 69 keV gamma ray whereas ^{238}U, ^{232}Th, and ^{152}Gd do not have any coincident gamma rays with their respective 103 keV gamma rays. Thus, the expectation is that the use of the Pixie-16 system to implement gamma-gamma coincidence to eliminate the interferences that exist from ^{238}U, ^{232}Th, and ^{152}Gd.

An experiment was performed in which NIST Standard 1633c was irradiated with thermal neutrons for 2 hours with the reactor power set at 950 kW. After approximately 2 weeks, the sample was measured on the Pixie-16 system for 18 hours. The resulting coincidence spectrum can be seen in Figure 47. This spectrum includes all coincident gamma rays for all radionuclides that exist in the sample.

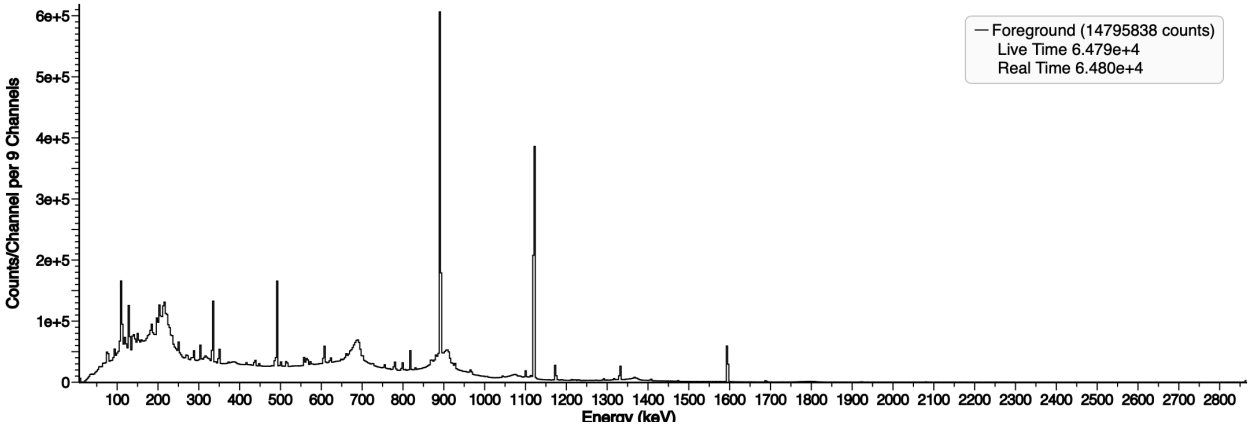

Figure 47: Gamma-gamma coincidence spectrum, NIST 1633c

From the spectrum, it appears that there is a 103 keV gamma peak in the spectrum. However, it is impossible to note which of the 4 radionuclides noted above contributes this 103 keV gamma ray. As the ^{153}Sm has the 103 keV/69 keV gamma ray coincidence, an energy gate was applied at 103 keV to validate that a 103 keV/69 keV gamma ray pair existed. In addition,

an energy gate of 69 keV was applied to the spectrum to determine which of the two energy gates provided better information. The two energy gated spectra can be seen in Figure 48 and

Figure 49. Figure 48 shows the output spectra of the 103 keV gating and Figure 49 shows the output spectra of the 69 keV gating.

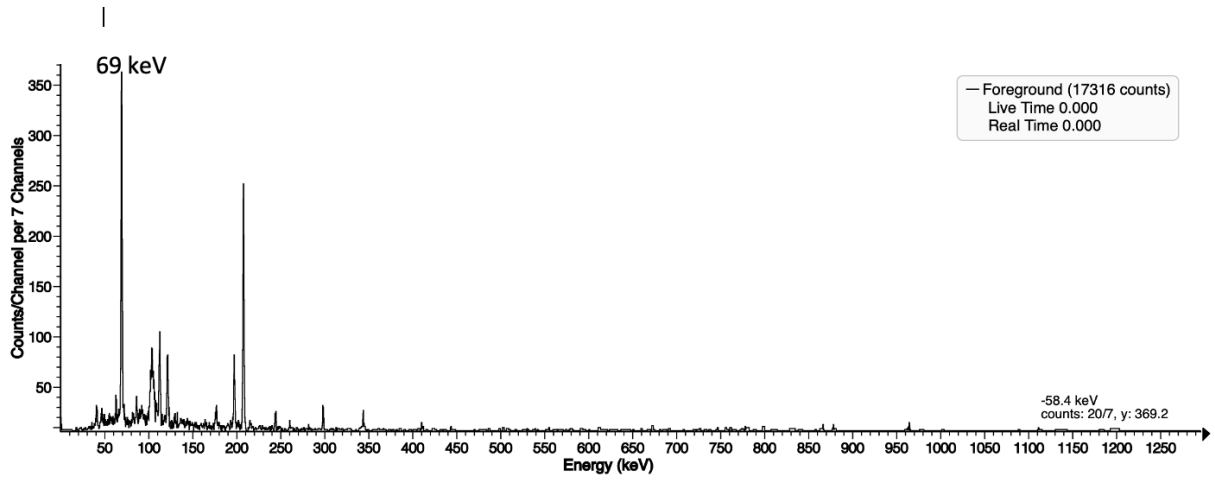

Figure 48: Identification of ^{153}Sm in NIST 1633c, gated at 103 keV

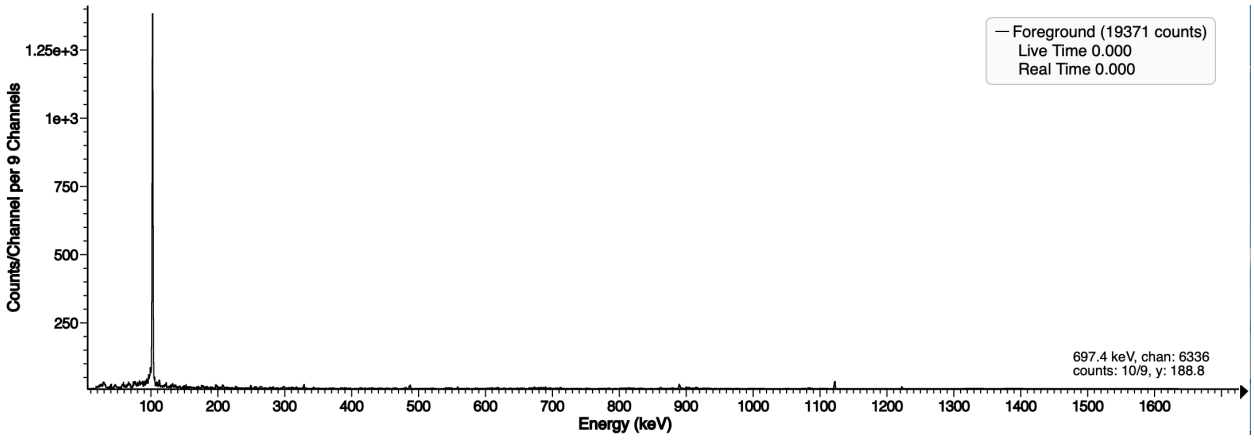

Figure 49: Identification of ^{153}Sm in NIST 1633c, gated at 69 keV

When evaluating the gated spectra, it becomes evident that the gating of the 69 keV gives better counting statistics for the identification of the 103 keV gamma ray, while the gating at the 103 keV gamma ray gave poorer statistics for the 69 keV gamma ray.

For the remainder of the radionuclides, only the energy gated spectrum that is most successful will be presented within the following section.

5.1.2.2 Identification of the remainder of the medium-lived NAA products

As described earlier, the medium-lived NAA products were assessed in samples that were prepared for short- and long-lived NAA product determination.

^{76}As was identified in NIST standard 1632d. When an energy gate of either 657 keV was applied, the coincident 559 keV gamma ray is visible. This sample was counted for 3 hours after allowing it to decay for 1 hour which is typically not possible using conventional analog modules.

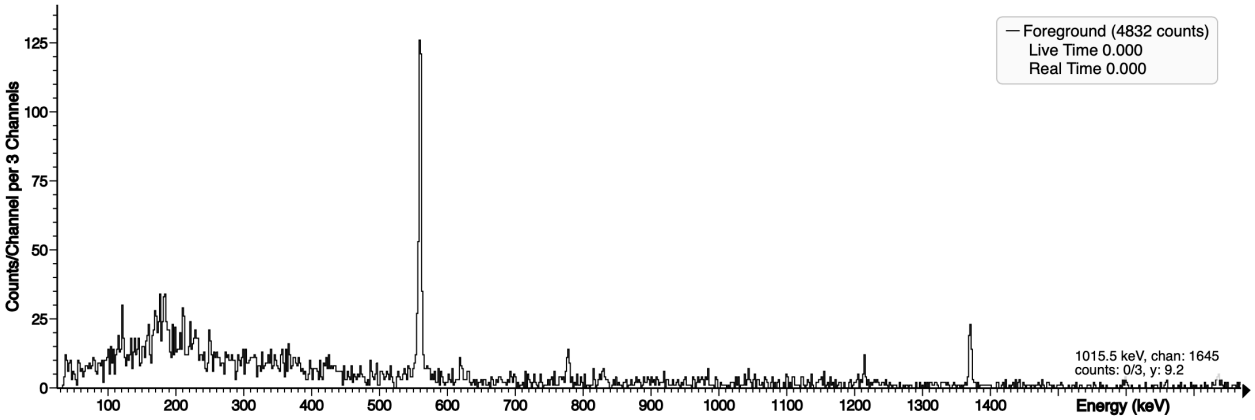

Figure 50: ^{76}As gated at 657 keV, 1632d

^{82}Br was identified in NIST 1632d. When an energy gate of 619 keV was applied, the coincident 554 keV is visible along with other ^{82}Br peaks.

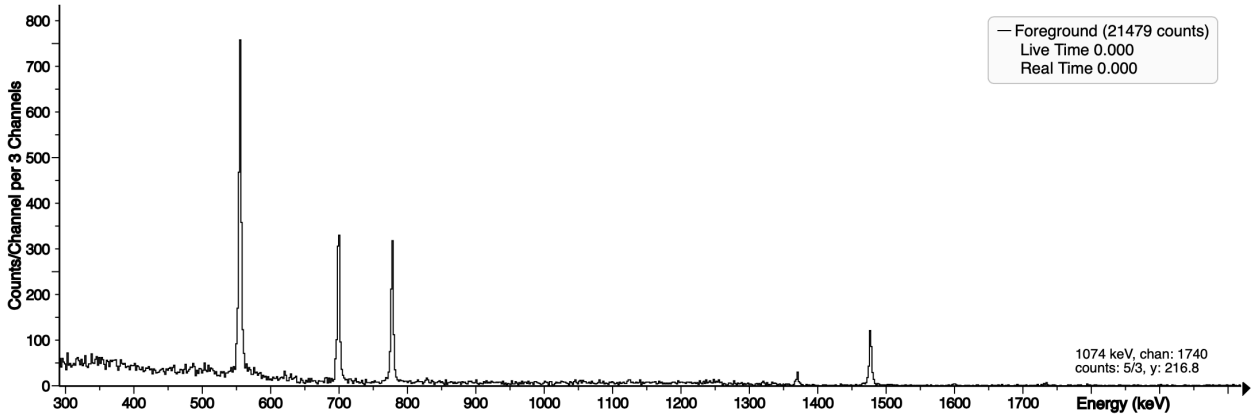

Figure 51: ^{82}Br gated at 619 keV, 1632d

^{140}La was identified in NIST 1632d. When an energy gate of 487 keV was applied, the coincident 328 keV and 1597 keV gamma rays are visible.

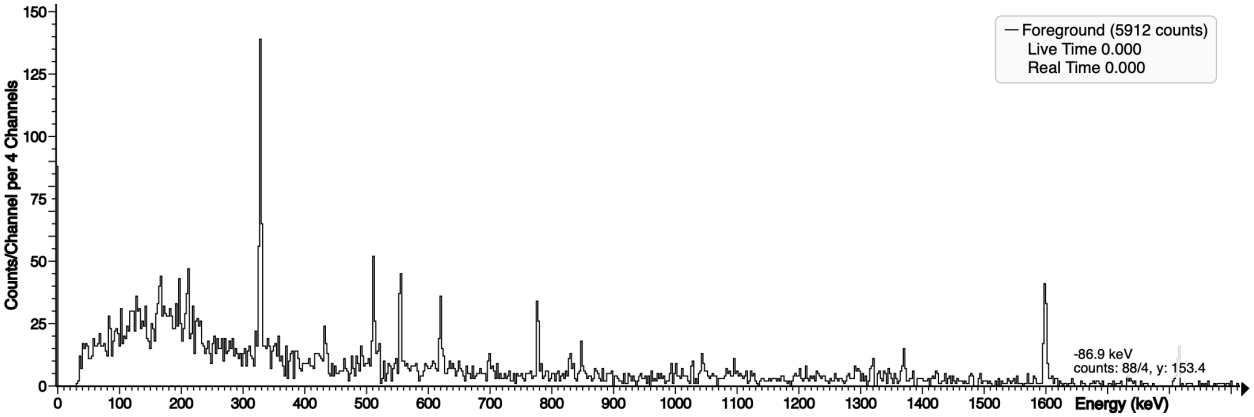

Figure 52: ^{140}La gated at 487 keV, 1632d

^{24}Na was easily identified in a number of different samples. When an energy gate of either 1368 keV or 2754 keV was applied, the coincident 2754 keV or 1368 gamma rays are visible.

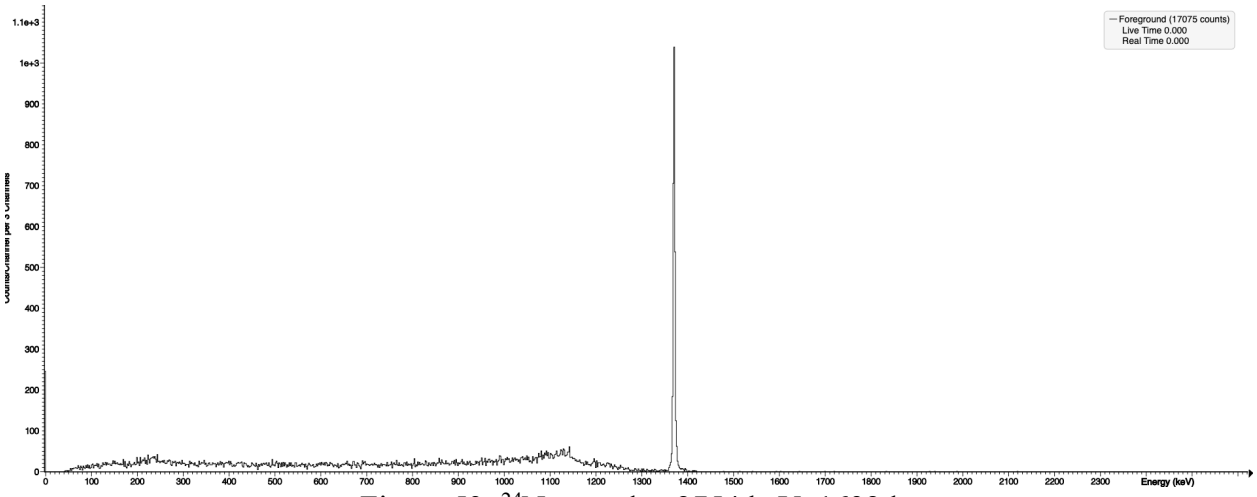

Figure 53: ^{24}Na gated at 2754 keV, 1632d

^{122}Sb was identified in NIST 2710a. When an energy gate of either 564 keV or 692 keV was applied, the coincident 692 keV or 564 keV gamma rays are visible.

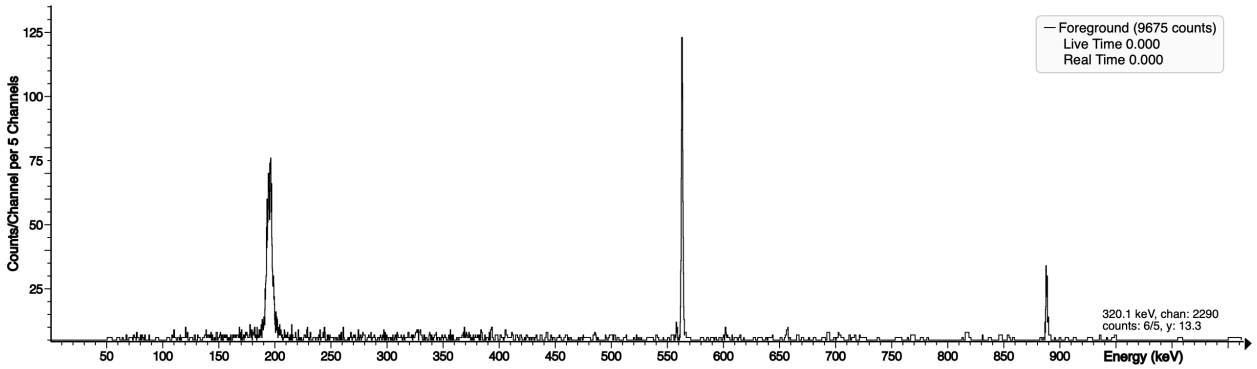

Figure 54: ^{122}Sb gated at 692 keV, 2710a

^{187}W was identified in NIST 2710a. When an energy gate of 72 keV was applied, the coincident 134 keV gamma ray was visible.

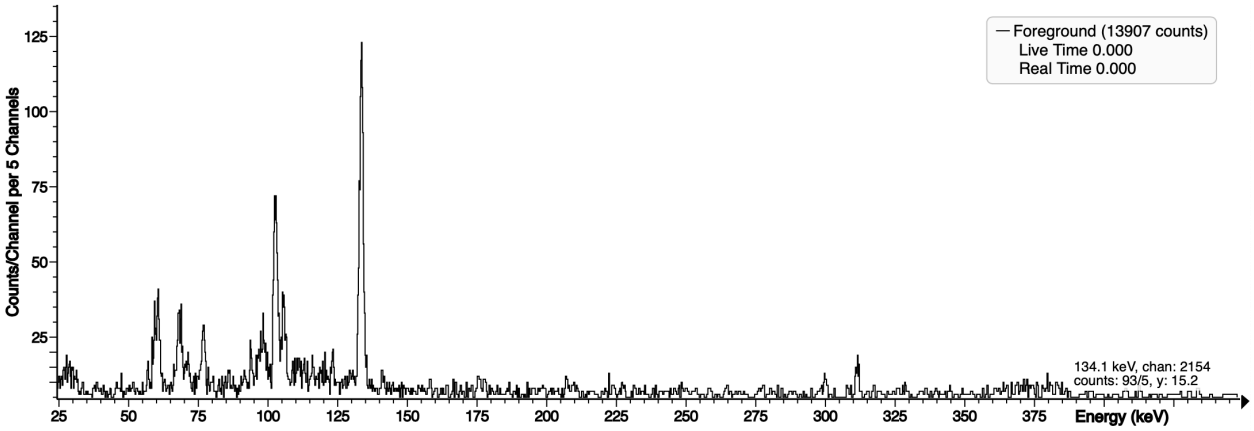

Figure 55: ^{187}W gated at 72 keV, 2710a

^{239}Np can often be challenging to identify due to the overlap of the 103.2 keV peak from ^{153}Sm over 103.7 keV peak from ^{239}Np. ^{239}Np was identified in NIST 2710a. When an energy gate of 277 keV was applied, the coincident 106 keV gamma rays is visible.

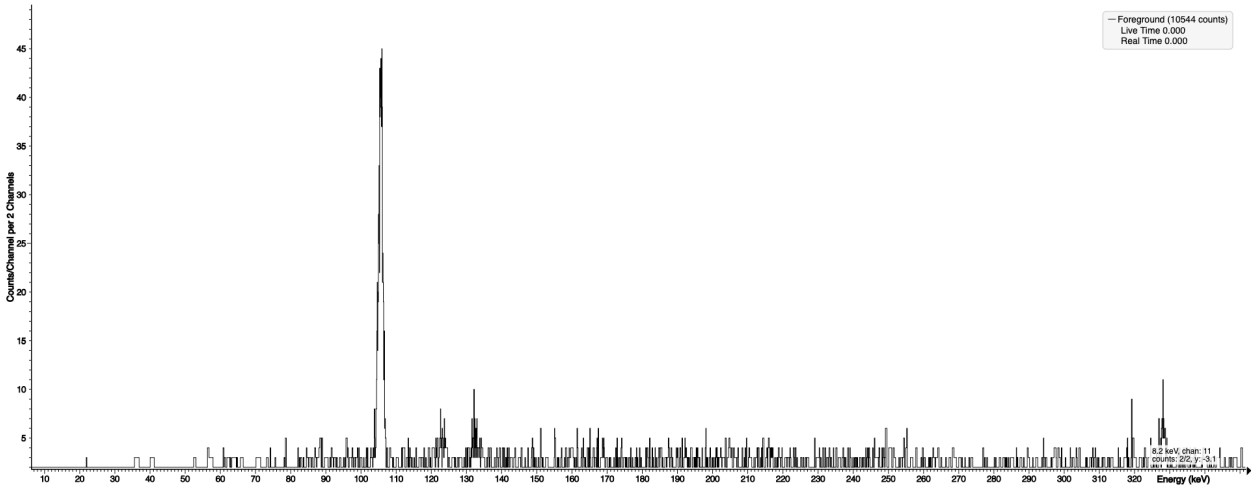

Figure 56: ^{239}Np gated at 206 keV, 2710a

5.1.3 Short-lived NAA products

There are a few unique characteristics to note about short-lived NAA products. First, of the short-lived NAA products, only six of them have major gamma-gamma coincidences. These short-lived NAA products are not typically challenging to identify. However, for completeness of

this research, all short-lived NAA products were evaluated to demonstrate their successful identification.

Table 9: Short-lived NAA products coincidences

Element	Isotope	Half life	Major Gamma Coincidences	Was γ- γ coincidence successful?
Ag	Ag-110	24.6s	NO	N/A
Al	Al-28	2.24m	NO	N/A
Ba	Ba-139	83.2m	NO	N/A
Br	Br-80	17.7m	YES	NO
Br	Br-80m	4.42h	NO	N/A
Ca	Ca-49	8.7m	NO	N/A
Cl	Cl-38	37.3m	YES	YES
Co	Co-60m	10.48m	NO	N/A
Cu	Cu-66	5.1m	NO	N/A
Dy	Dy-165	2.3 hour	YES	YES
F	F-20	11.0s	NO	N/A
I	I-128	25m	NO	N/A
In	In-116m	54.2m	YES	YES
K	K-42	12.36h	NO	N/A
Mg	Mg-27	9.45m	NO	N/A
Mn	Mn-56	2.58h	YES	YES
Na	Na-24	15h	YES	YES

5.1.3.1 Identification of the short-lived NAA products

^{38}Cl was identified in NIST sample 1632d. An energy gate at either 1642 keV or 2167 keV helped clearly identify the coincident gamma ray, 2167 keV and 1642 keV respectively.

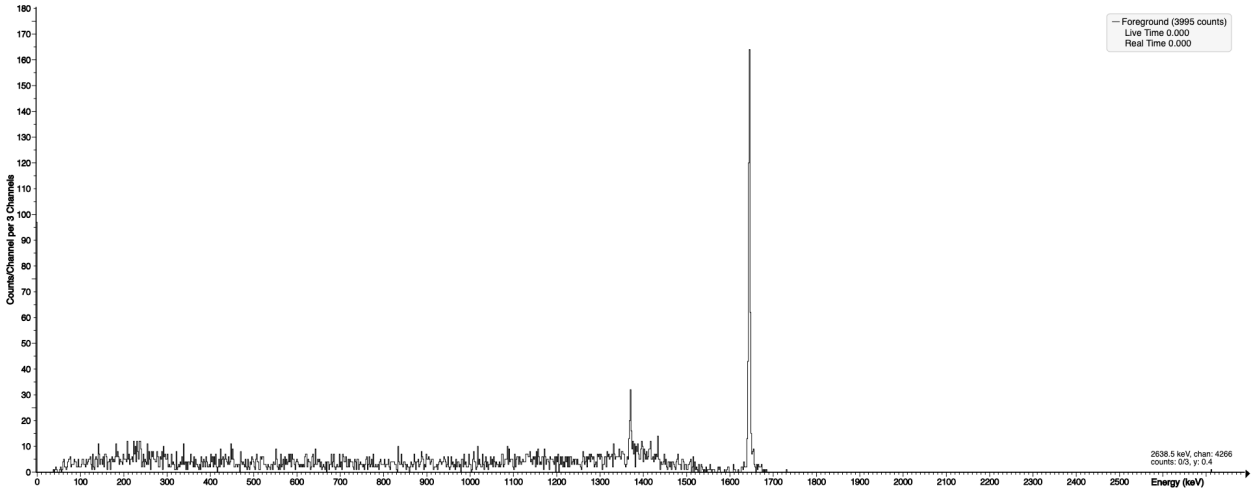

Figure 57: Identification of ^{38}Cl in NIST 1632d, gated at 2167 keV

^{165}Dy was identified in NIST sample 1632d. The most successful energy gate was found at 715 keV which clearly identified the 279 keV coincident gamma ray.

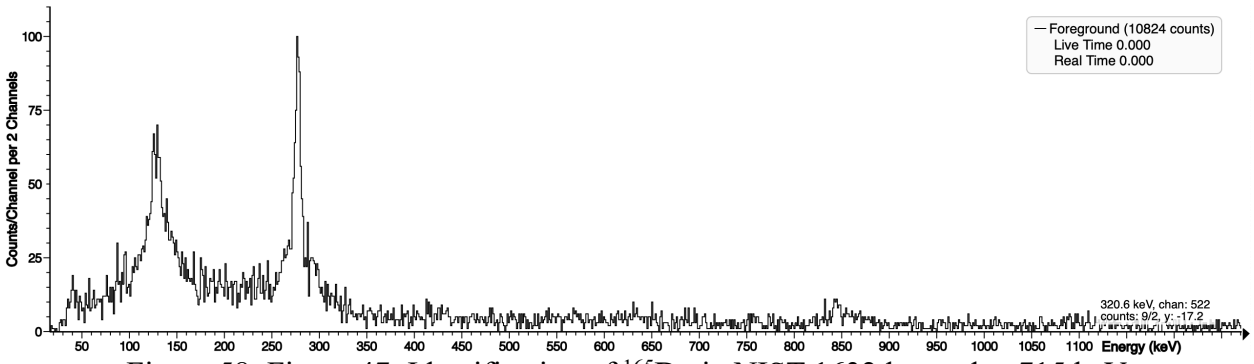

Figure 58: Figure 47: Identification of ^{165}Dy in NIST 1632d, gated at 715 keV

^{116m}In was identified in NIST sample 1632d. The most successful energy gate was found at 1293 keV which clearly identified the 1097 keV coincident gamma ray.

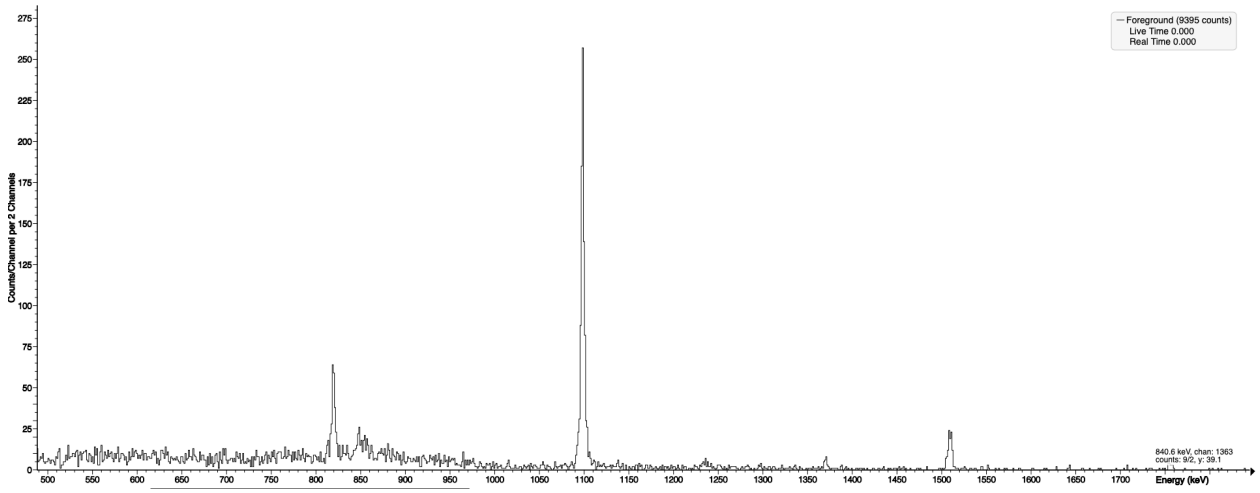

Figure 59: Identification of ^{116m}In in NIST 1632d, gated at 1293 keV

^{56}Mn was identified in NIST sample 1632d. The most successful energy gate was found at 846 keV which clearly identified the 1810 keV and 2113 keV coincident gamma rays; the 2522 keV gamma ray can be identified at a lower level as well.

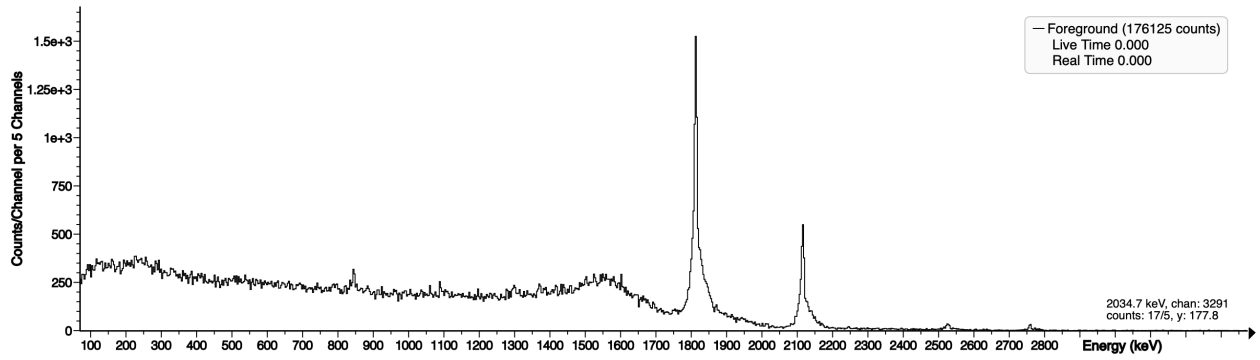

Figure 60: Identification of ^{56}Mn in NIST 1632d, gated at 846 keV

Chapter 6: Additional Analytical evaluation of the Pixie-16

This section in the dissertation will provide a number of additional analytical evaluations with experimental validations to demonstrate the effectiveness of the Pixie-16 system to provide valid, useful data.

6.1 Effect of angular orientation of detectors

During the proposal phase of this PhD, a question was asked regarding how the angle between the detectors was chosen and whether or not the angle of the detectors would affect the number of counts that were measured. The initial assumption was that there would be little or no effect due to this angle based on the cylindrical shape of the samples that were being measured and the isotropic nature of radioactive material. However, after some research, it was found that gamma rays are emitted in an angular distribution that is dependent on the electromagnetic multipoles of the radiation that is involved (Smith et al., 2019). As such, it seemed important to perform a set of experiments to demonstrate how significantly the angular correlation between the two detectors can affect the total number of counts recorded for a specific coincident gamma ray.

One of the experiments that was performed to evaluate the effect of the angular correlation of the detectors utilized a ^{60}Co source. The source was placed between the two detectors, at a distance of 5 inches from the face of each detector, and then data was measured using the Pixie-16 system in gamma-gamma mode. This was repeated for different angles varying, between 70° and 180°. The data was then gated around the 1173 keV gamma ray peak to reduce any background information and then the total counts were evaluated. The data for the ^{60}Co experiment can be seen in Table 10 and Figure 61. In Figure 61, note that the data was normalized for the

total counts where the counts at specific angles were divided by the total counts at the angle that had the highest total counts, 180°.

Table 10: Total counts for 1332 keV gamma ray for ^{60}Co with varying angles

θ	Counts	Normalized
180	407.2	1
165	365.4	0.897348
150	380.5	0.93443
135	321	0.78831
100	350.7	0.861248
90	332.8	0.817289
85	338.6	0.831532
70	328.3	0.806238

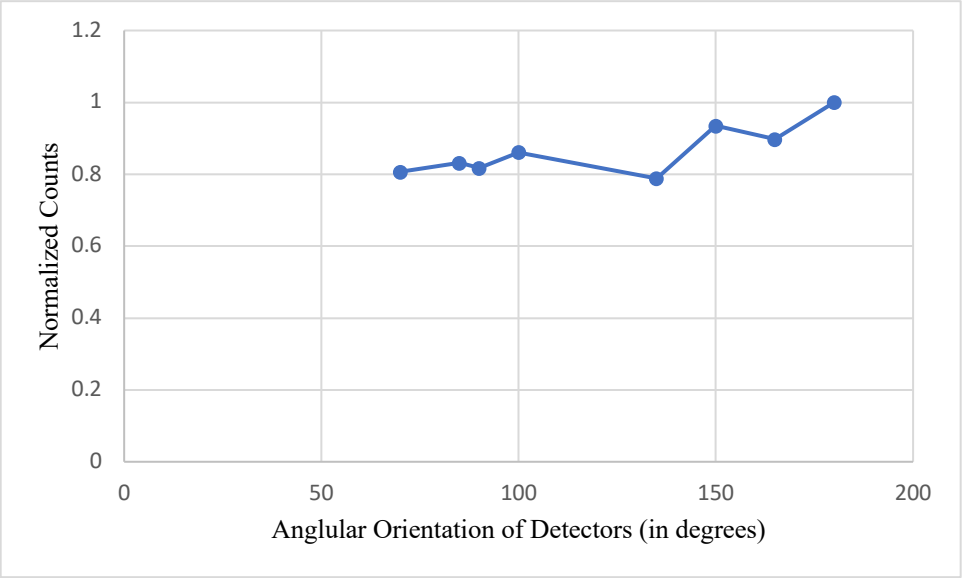

Figure 61: Normalized counts for 1332 keV gamma ray, ^{60}Co, versus detector angular position

Note that there is a difference in total counts when comparing the data from the two configurations. The 180° configuration generated a total of 407 counts whereas the 135° generated a total of 321 counts.

Another experiment was performed to ensure that similar results could be generated for a more complex gamma decay scheme. This experiment utilized a ^{152}Eu source. Due to its more complex decay scheme, it seemed possible that any effect due to angular correction might be amplified. The 121/1408 keV coincident decay scheme was evaluated in this case. The output spectrum was gated on the 1408 keV gamma ray. The data to this experiment can be seen in Table 11 and Figure 62.

Table 11: Total counts for 121 keV gamma ray for ^{152}Eu with varying angles

θ	**Counts**	**Normalized**
180	1053.7	0.996595
165	1005	0.950534
150	1057.3	1
135	807.3	0.763549
100	637.9	0.603329
90	702.9	0.664807
85	682.3	0.645323
70	695.5	0.657808

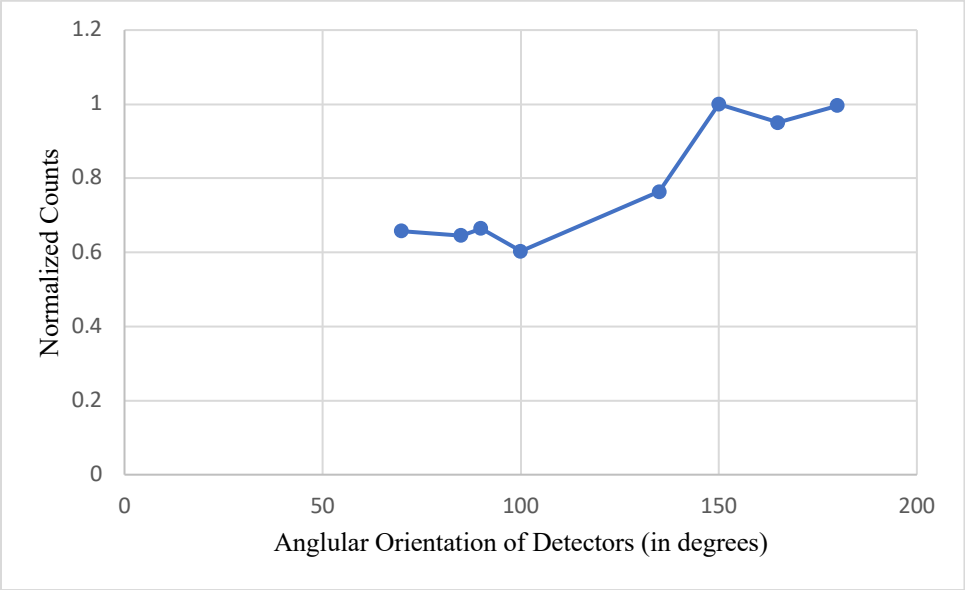

Figure 62: Normalized counts for 121 keV gamma ray, ^{152}Eu, versus detector angular position

When reviewing the data for ^{152}Eu, it becomes evident that there is a significant change in the total counts when the angular positioning between the two detectors is changed. For this experiment, the total number of counts measured for the 85° configuration is 682 counts versus 1083 counts for the 180° configuration.

The data from these two experiments demonstrates that there is an effect due to the angular position of the detectors. For this research, a decision was made to maintain a 180° configuration, since that arrangement provided a higher total number of counts in both experiments. As the intent of the research was to identify radionuclides that might be enhanced by gamma-gamma coincidence, a larger number of counts seemed more practical than optimizing the angular position of the detectors for individual radionuclides.

6.2 Follow-up dead time/FWHM evaluation of Pixie-16

As experiments were being performed on the Pixie-16 system in singles and gamma-gamma mode, it became evident that the FWHM was maintained in higher dead time situations when compared to typical analog systems as exhibited by the "Clamshell" system at NETL. An experiment was developed to quantify these improvements.

Two different certified sources of ^{152}Eu were evaluated with the Pixie-16 system in singles mode. One of the sources had an activity of 98,500 Bq, and the second had a lower activity of 1,700 Bq. Each one of these sources was independently measured with the Pixie-16 and "Clamshell" systems. The source was placed directly against the face of the HPGe detectors of the Pixie-16 system. For the "Clamshell," the source was put on the "A spacer" and the "blue

spacer" which creates a separation between the source and the detector face by approximately 1.9 cm and 10 cm, respectively. Both configurations were set to count for 30 minutes.

The Clamshell only utilized the high activity source while changing the distance between the detector face and the source to reduce dead time. Rather than changing the distance of the detectors in the Pixie-16 configuration, both the higher activity and lower activity sources were measured directly against the detector faces. The resulting FWHM data for these experiments can be found in Table 12.

Table 12: FWHM with increasing dead time, Pixie-16 and Conventional "Clamshell" Gamma Spectroscopy System

Energy	Weak Source - Pixie-16	Strong Source - Pixie-16	Clamshell - Blue Spacer (further)	Clamshell - A Spacer (closer)
121	1.59	1.7	1.07	1.33
244	1.64	1.64	1.2	1.44
344	2.12	2.02	1.28	1.52
411	2.05	2.07	1.32	1.57
444	1.76	1.74	1.33	1.6
778	2.26	2.21	1.61	1.85
867	1.88	1.99	1.67	1.92
964	2	2.01	1.75	2
1112	2.37	2.28	1.8	2.06
1299	2.45	2.32	1.99	2.17
1408	2.46	2.38	2.07	2.26

This data best exhibits one of the important capabilities of the Pixie-16 system, its dead time correction capability. As evident from the data, when a low activity source with lower dead time, versus a higher activity source, with higher dead time, are counted with the Pixie-16, there is no noticeable change to the FHWM. When utilizing a more traditional analog gamma spectroscopy system, as demonstrated with the Clamshell system, there is a degradation of the

FWHM in a higher dead time scenario. This is visually demonstrated in Figure 63. Note that in many cases, there appears to be a single dot representing the FWHM for the Pixie-16 due to the fact that the dots are laying almost directly on top of one another in the plot.

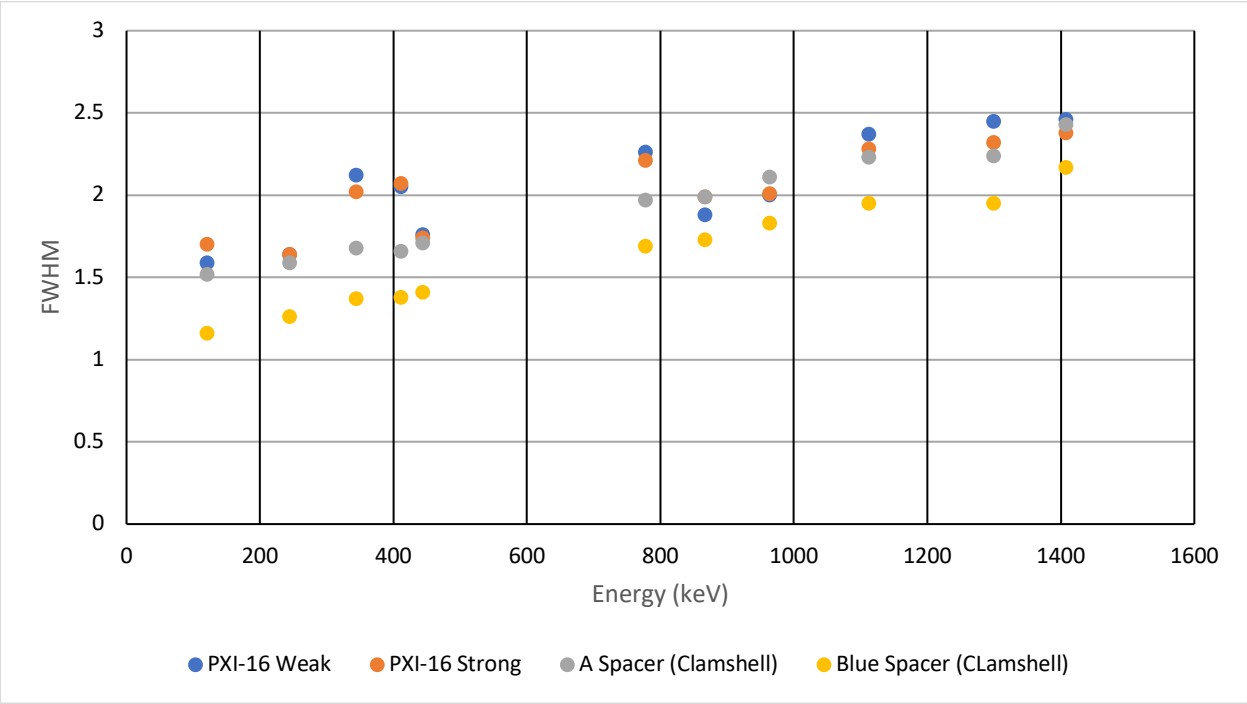

Figure 63: FWHM with increasing dead time, Pixie-16 vs. Clamshell

The data for the Clamshell system shows approximately a 0.25 keV delta between the FWHM values for an increase in dead time. Although the increase in dead time shows a degradation of the FWHM for the Clamshell, the sophisticated dead time correction used in the Pixie-16 allows for the quality of the data to be maintained even in high dead time scenarios as demonstrated by the negligible change in FWHM. There is likely a point at which the dead time correction capability of the Pixie-16 is unable to function effectively (not pursued here). For those situations, it is important to optimize the distance to the detectors and also to couple that with an

optimization of the angular placement of the detectors to ensure a high-quality count of the any potential NAA radionuclides of interest.

6.3 Detection limit evaluation

One of the common questions that arises with regards to NAA is what the detection limit of a specific radionuclide is. As this research was not intended to provide a quantifiable limit of NAA products but rather a qualitative limit of whether or not NAA products could be identified, a review of the data from a specific experiment was performed to attempt to quantify this. The data captured for NIST standard 2670 for a 1-hour post irradiation measurement and a 25-hour post irradiation measurement was evaluated and can be seen in Table 13. This is a valuable assessment due to the existence of ^{24}Na in the sample which has a 15-hour half-life.

Table 13: Detection Limits

	1-hour post irradiation	25-hour post irradiation
Singles Data Detection Limit	.034 ppm	.026 ppm
Coincidence Data Detection Limit	.350 ppm	.245 ppm

Note the detection limits are effectively unaffected by the decay time but are lowered approximately one order of magnitude when implementing gamma-gamma coincidence.

Chapter 7: Additional Implementation of gamma-gamma coincidence for NAA and non-NAA applications

This section discusses a number of additional experiments that were performed utilizing the Pixie-16 system. Although the focus of this PhD work was on the use of gamma-gamma coincidence in NAA, a number of questions arose from the committee members due to the demonstrated success of the implementation of the XIA Pixie-16. A few experiments were performed related to some of these questions to determine if there was benefit to using the Pixie-16 gamma-gamma coincidence capability for these applications. These experiments are discussed below.

7.1 Gamma-gamma coincidence use for identification of ^{239}Pu[1]

At present, gamma-ray spectroscopy is used for determination of plutonium isotopic measurements (Sampson, 1991). However, it may be possible to utilize gamma-gamma coincidence to determine the plutonium isotopic composition more effectively, even in samples with high americium content.

The value in using ^{239}Pu with the Pixie-16 gamma-gamma coincidence system can be determined from its decay scheme. A simplified version of the decay scheme of ^{239}Pu is shown in Figure 64, with only the usual major gamma rays displayed (Egozi et al., 2020).

[1] Egozi, C., Martinez, F., Luna, B. de, Terry, J., & Landsberger, S. (2020). A PRELIMINARY INVESTIGATION FOR THE USE OF DIGITAL GAMMA-GAMMA COINCIDENCE SPECTROMETRY TO DETERMINE ^{239}Pu. *4*, 1–4. https://doi.org/10.21175/RadProc.2020.00; Martinez led many of the experiments and the data analysis and co-authored the article.

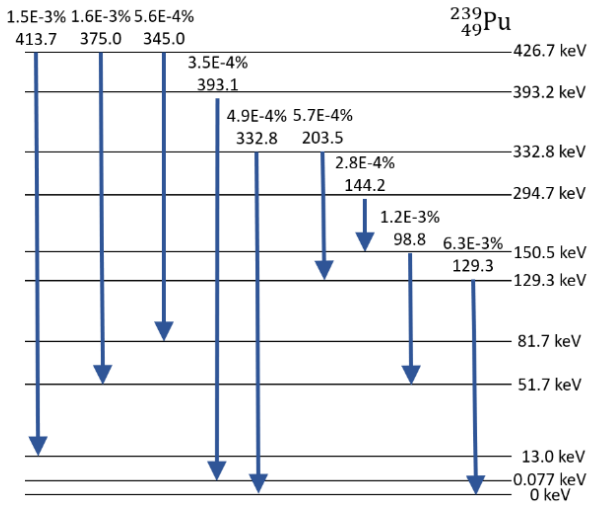

Figure 64: Major Gammas Belong to the ^{239}Pu Decay Scheme

In the decay scheme, there are multiple gamma rays that are in coincidence with each other, including the 144 keV and 98.8 keV gamma rays, and the 203 keV and 129.3 keV gamma rays. Therefore, the use of gamma-gamma coincidence on ^{239}Pu would be effective due to the isotope's gamma rays that are in coincidence.

7.1.1 Coincidence Gating of ^{239}Pu

Once determining that the decay scheme for ^{239}Pu has gamma rays in coincidence, experimental data was evaluated to observe the coincidences.

Figure 65 includes an overlay of singles and coincidence spectra of a ^{239}Pu foil electrodeposited on nickel with an activity of 1.81E6 Bq.

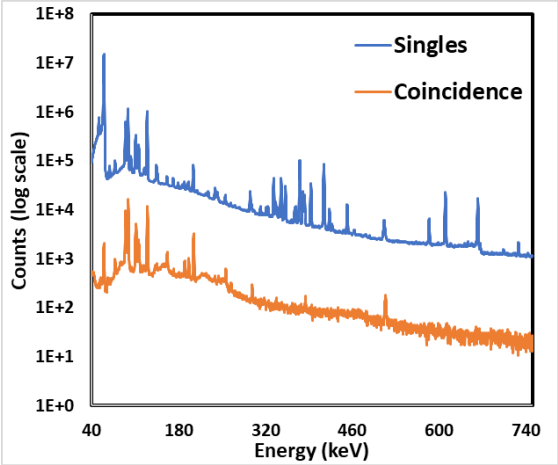

Figure 65: ^{239}Pu Foil Singles and Coincidence with 97-hour Live Time Count

The comparison of the singles and coincidence data was then used to evaluate the gamma rays in coincidence. From Figure 65 it can be seen that the most gammas in coincidence are in the range of 94 keV to 129 keV, with almost no gammas in coincidence above that range. Therefore, several gammas within the range were analyzed further by energy gating.

The gating was done by the use of the UT-written energy gating software, in which the energy of interest at detector 1 was specified by the user after performing a run with the two detectors touching the ^{239}Pu source. The software then found all energy peaks in detector 2 that were in coincidence with the specified energy. This process was performed on the 94 keV, 103 keV, 111 keV, and the 129 keV energy peaks. The energy gated spectrum for 129 keV is shown below in Figure 66. The coincidence spectrum is overlaid on the energy gated spectra for reference.

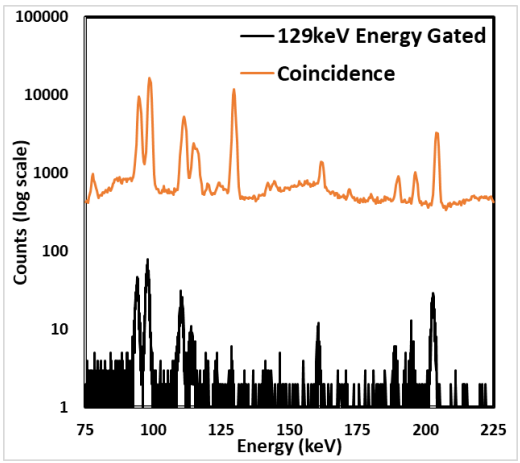

Figure 66: 129 keV Energy Gated and Coincidence Spectra Overlay of ^{239}Pu

The gated spectrum demonstrates experimentally that gamma rays 94, 98, 111, 114, and 203 keV are in coincidence with the 129 keV gamma ray. In addition, the gated spectrum has a background count reduction of 3 orders of magnitude relative to the coincidence data, and 5 orders of magnitude reduction relative to the singles data.

To quantify the background reduction, a comparison of the net counts of the 203 keV peak in the singles, coincidence, and gated spectra was done. The 203 keV peak is indicated by the red box in Figure 67 below, and the net counts are shown in Table 14.

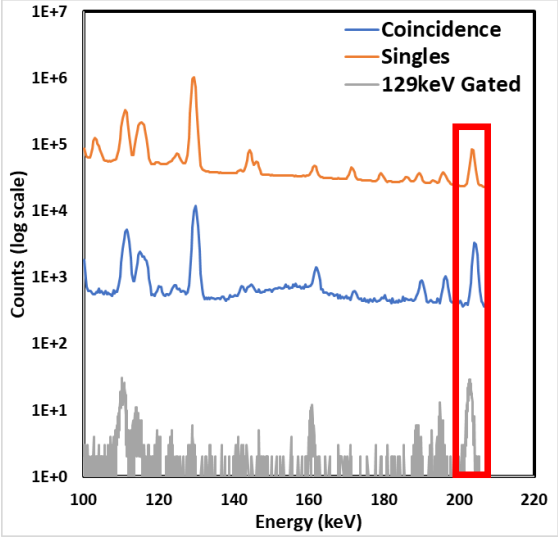

Figure 67: Singles, Coincidence, and 129 keV Gated Spectra Comparison of 203 keV Peak

The ratio of net counts of the singles to the energy gated data at 203 keV is 364. This reduction of greater than two orders of magnitude of the net counts indicates that gamma-gamma coincidence can be used with the absence of shielding.

Table 14: Net counts in 203 keV peak for ^{239}Pu in singles, coincidence, and gated spectra

203 keV Peak	Net Area	Ratio of Net Area to 129 keV Gated Net Area
Singles	258419±790	364
Coincidence	12727±137	18
129 keV Gated	710±29	1

7.1.2 Discussion of results for application of gamma-gamma coincidence for ^{239}Pu

The use of gamma-gamma coincidence, without any shielding, reduces background counts by two orders of magnitude for this application. Gamma-gamma coincidence can be used for ^{239}Pu, as the isotope has several gamma rays in coincidence, including the 94, 98, 115, and 129keV

gammas. The use of energy gating in addition to coincidence further reduces the background by 3 more orders of magnitude and is an efficient method to experimentally determine the gamma rays in coincidence with a particular gamma ray. The lack of shielding required for background reduction, in addition to the numerous gamma rays of the isotope in coincidence, make this method ideal for verification purposes of ^{239}Pu.

7.2 Gamma-gamma coincidence use for identification of ^{235}U

One question that arose during the dissertation proposal for this research was whether or not this system might be successful for the identification of the 185.72 keV gamma ray that is in the decay of ^{235}U as there is a spectral interference due to a 186.21 keV gamma ray contribution from ^{226}Ra. In ^{226}Ra, the 186.21 keV gamma ray does not have a coincident decay; however, the 185.72 keV gamma ray in ^{235}U is in coincidence with a 202 keV gamma ray.

7.2.1 Discussion of results for application of gamma-gamma coincidence for ^{235}U in ore

For this experiment, a certified uranium ore sample standard from Canada Centre for Mineral and Energy Technology was evaluated. The sample, BL-4a was certified at 0.12 % uranium. For this source, a 20-gram sample was counted for 6 hours in singles and gamma-gamma coincidence mode on the Pixie-16 system.

When reviewing the coincidence spectrum, it can be seen that the 185 keV gamma ray is not visible. Unfortunately, the intensity of this gamma ray and its coincident gamma rays are very low, as are all the other gamma rays from ^{235}U. The singles spectrum for the sample can be seen in Figure 68 and the coincident spectrum can be seen in Figure 69. Note that the 185.72/186.21 keV gamma ray is visible in the singles spectrum; however, the coincident 202

keV gamma ray for ^{235}U is not visible in this spectrum. Due to the lack of the 202 keV, the coincident spectrum does not show either the 185.72 keV or the 202 keV gamma rays. This experiment demonstrates that this technique is not feasible for this application as it did not improve the ability to identify the 185.72 keV gamma ray for ^{235}U at the concentration level of .12%. This may potentially work at higher concentration levels in uranium ore.

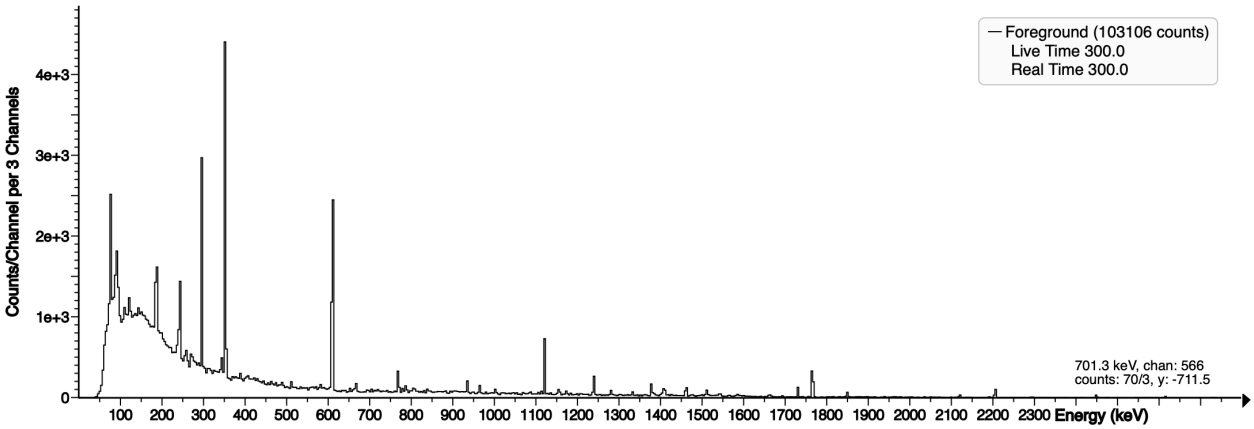

Figure 68: ^{235}U, .12% sample, singles spectrum

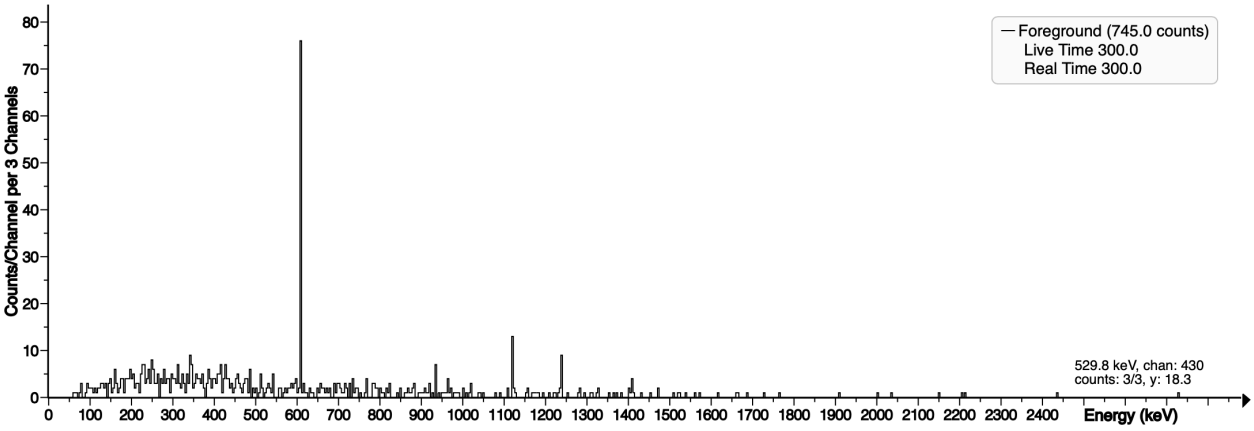

Figure 69: ^{235}U, .12% sample, coincidence spectrum

7.3 Gamma-gamma coincidence use for identification of Arsenic in a biological sample

One NAA product that continues to be a challenge is the identification of arsenic at natural levels in biological materials (Zeisler et al., 2006). This is in part due to the high activities that occur from ^{24}Na, ^{82}Br and ^{32}P (Bremsstrahlung radiation) when performing NAA on the sample. Because of the high activity of ^{24}Na, an irradiated sample is usually allowed to decay 2 to 4 days to allow for a reduction in the contribution to the high Compton background from ^{24}Na. The ability to identify arsenic in a sample within a short time of it being irradiated would be a significant improvement. As such, the Pixie-16 system was utilized to determine if it was capable of identifying arsenic in a diet reference material, NIST 1548a, and in a freeze-dried urine reference material, NIST 2670. The mass fraction value of arsenic in NIST 1548a is 0.20 ± .1 ppm and is 0.48 ± .1 ppm for an elevated level in NIST 2670.

7.3.1 Discussion of results for identification of Arsenic in Diet sample, NIST 1548a

The sample was irradiated in the NETL TRIGA reactor with a power of 500kW for 30 minutes. The sample was then allowed to decay for approximately 1 hour prior to being counted. The dead time correction of the Pixie-16 makes this possible. The sample was then counted using the Pixie-16 system for a period of 3 hours. The data was evaluated in singles mode, coincidence mode and then an energy gate was applied to determine if it was possible to identify ^{75}As in the sample.

Figure 70 is the output singles spectrum. A few of the major gamma peaks that are visible in the spectrum are the 1368 keV and 2754 keV peaks from ^{24}Na. As the major gamma peaks that exist for ^{75}As occur at 559 keV and 657 keV, Figure 71 shows an adjusted spectrum to allow for

a better visualization of the spectrum within the energy range where these gamma peaks exist. Neither the 559 keV or 657 keV peak are visible in this spectrum. However, it is notable that the peak that occurs at approximately 554 keV can be attributed to ^{82}Br; a close inspection shows that this peak appears to be wide. This may be due to spectral interferences between the 554 keV peak from ^{82}Br and the 559 keV peak from ^{75}As but could also be due to peak tailing due to the less-than-optimal resolution of the detectors.

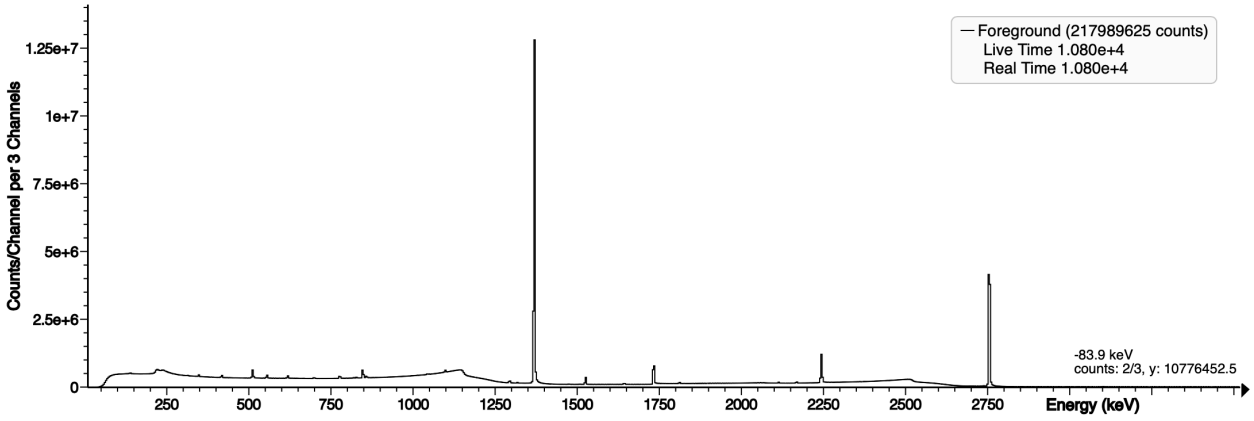

Figure 70: Singles spectrum for diet sample, 1548a

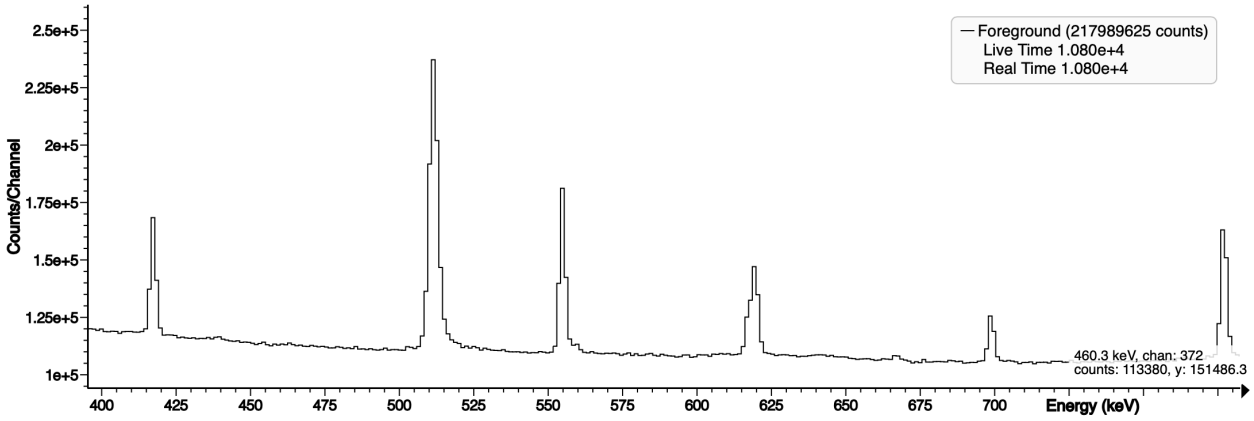

Figure 71: Singles spectrum, 400-800 keV, for diet sample, 1548a

The next figures, Figure 72 and Figure 73, provide the output gamma-gamma coincidence spectrum. Figure 72 is provided as a reference to help the reader evaluate the difference between

the singles data and the coincidence data. Figure 73 is again focused on the 400-800 keV range to try to identify the 559 keV and 657 keV peaks for ^{75}As.

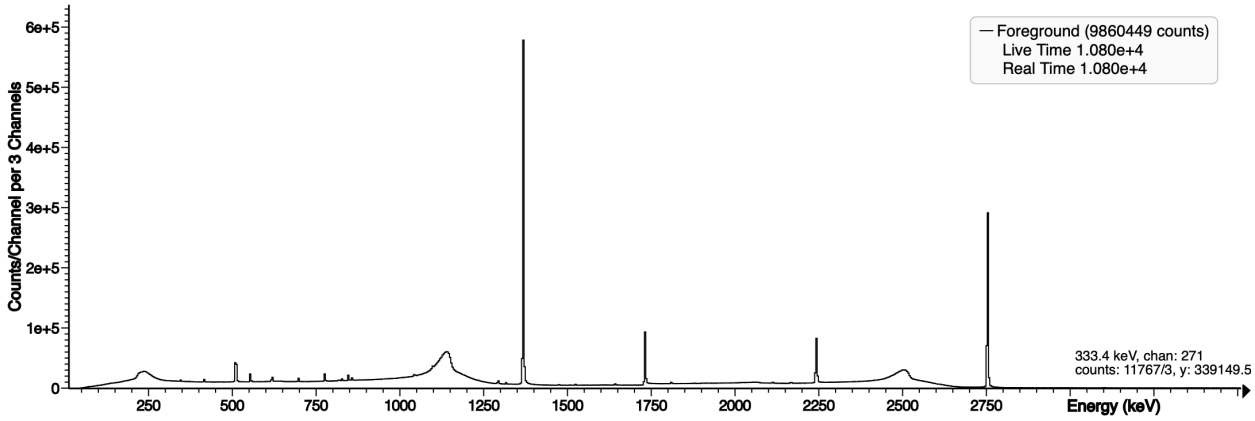

Figure 72: Coincidence spectrum for diet sample, 1548a

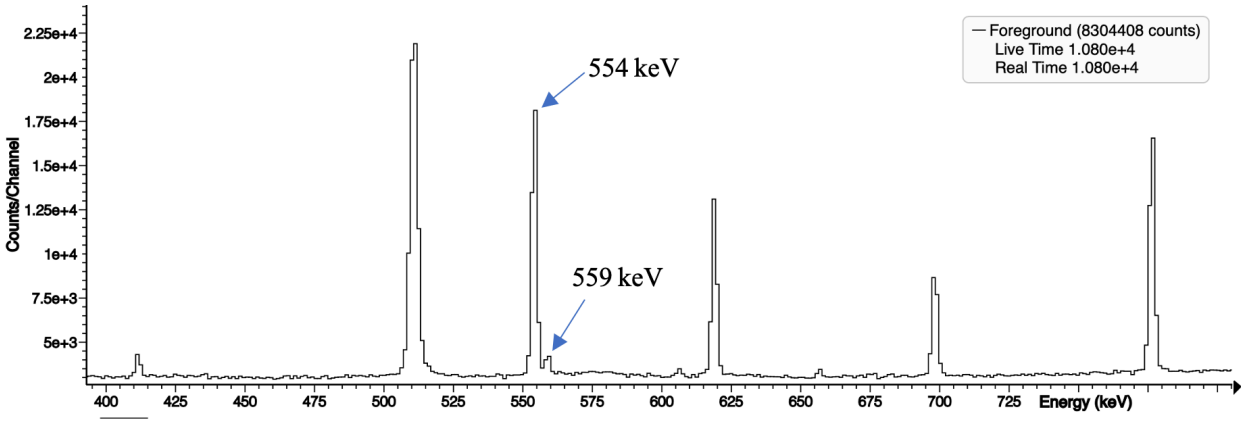

Figure 73: Coincidence spectrum, 400-800 keV, for diet sample, 1548a

The coincidence spectrum shown in Figure 73 begins to illustrate what might be a small spectral interference between the 554 keV gamma ray from ^{80}Br and the 559 keV gamma ray from ^{75}As. From this data it is possible to infer that there is arsenic in the sample. However, to ensure an accurate assessment, the ability to identify another gamma ray energy that exists within the ^{75}As decay scheme is important. It is important to note that the potential evidence of the existence of arsenic was not possible from the singles data, but only from the gamma-gamma coincidence data.

To confirm that ^{75}As exists in the sample, an energy gate was applied on the 559 keV gamma ray to determine if the 657 keV, 2096 keV or 2110 keV coincident gamma rays are visible. The output spectrum from this energy gate can be seen in Figure 74. In addition, an energy gate was applied at 657 keV to determine if the 559 keV gamma ray was visible when the opposite gating was applied. This spectrum is found in

Figure 75.

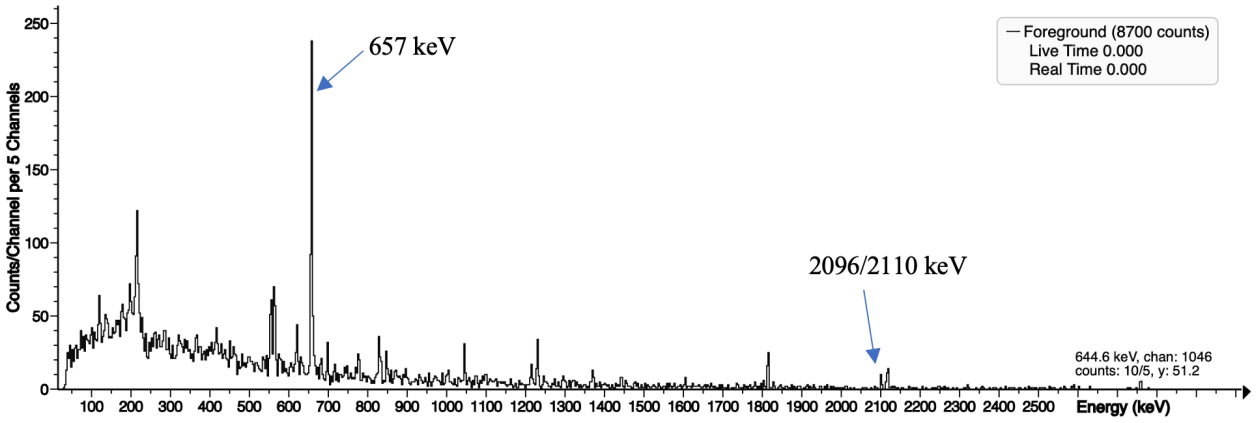

Figure 74: Coincidence spectrum, gated at 559 keV, for diet sample, 1548a

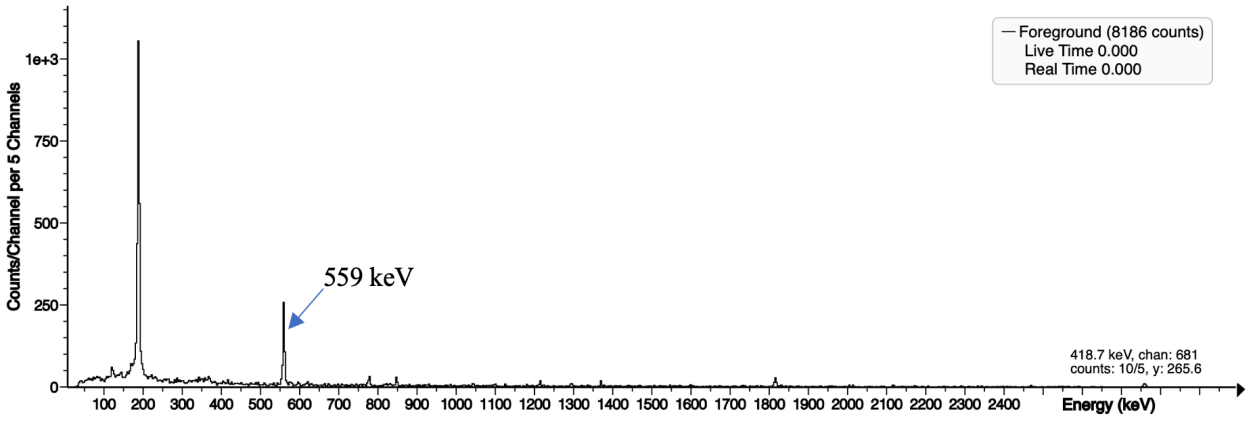

Figure 75: Coincidence spectrum, gated at 657 keV, for diet sample, 1548a

These two spectra clearly show that ^{75}As is identified within the sample. As noted earlier, a number of energy gates may be required to definitely identify that a specific radionuclide is in the sample. Utilizing either of the two energy gates proves to be very effective.

7.3.2 Discussion of results for identification of arsenic in freeze-dried urine, NIST 2670

Similar to the diet reference material, NIST 2670 was irradiated in the TRIGA reactor with a power of 500kW for 30 minutes, allowed to sit for approximately 1 hour prior to being counted and then counted using the Pixie-16 system for a period of 3 hours. The data was evaluated in singles mode, coincidence mode, and then an energy gate was applied to determine if it was possible to identify ^{75}As in the sample.

Rather than presenting the same set of spectra that was presented for the diet sample, different spectra will be presented as there is a unique feature that is worth noting.
Figure 76 shows the singles spectrum for the freeze-dried urine sample. Figure 77 shows a portion of the spectrum focused around the 559 keV gamma ray from ^{75}As. Note that the 554 keV gamma ray from ^{82}Br is visible and that the 559 keV gamma ray due to ^{75}As is also visible.

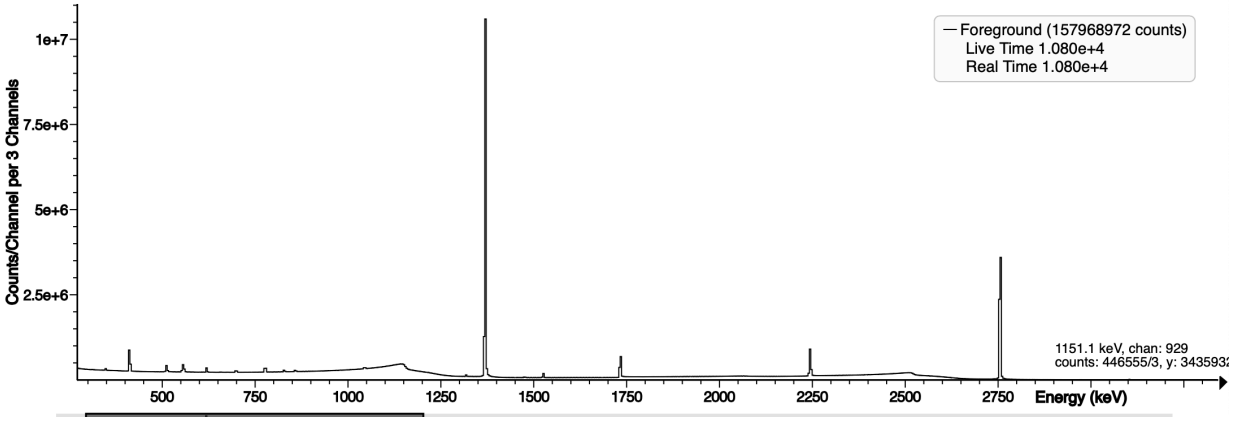

Figure 76: Singles spectrum for freeze-dried urine, 2670

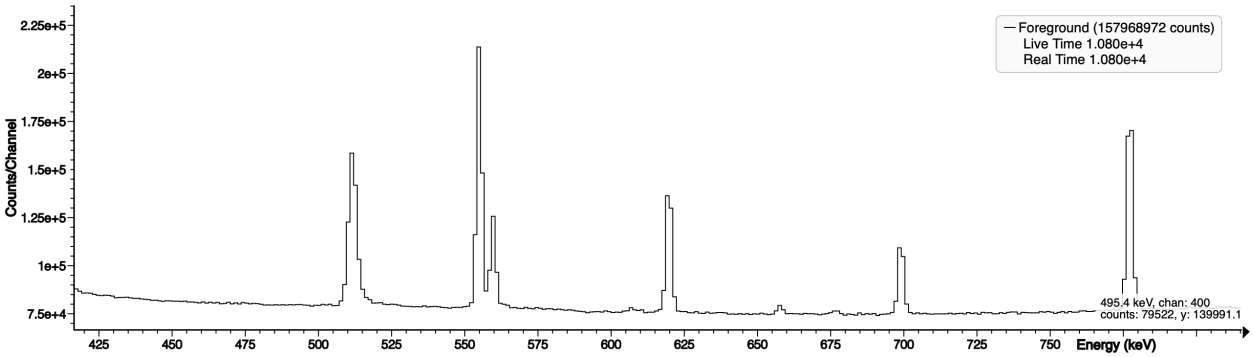

Figure 77: Singles spectrum, 400-800 keV, for freeze-dried urine, 2670

For the coincidence spectrum, there is very little change between it and what is visible in the singles spectrum as the 554 keV and 559 keV peaks are distinctly visible. One aspect that can be noted is a reduction of approximately 1 order of magnitude in the background counts and peak counts with respect to the same counts for the singles data. The coincidence spectrum for freeze-dried urine for a range of 400 keV to 800 keV is found in Figure 78.

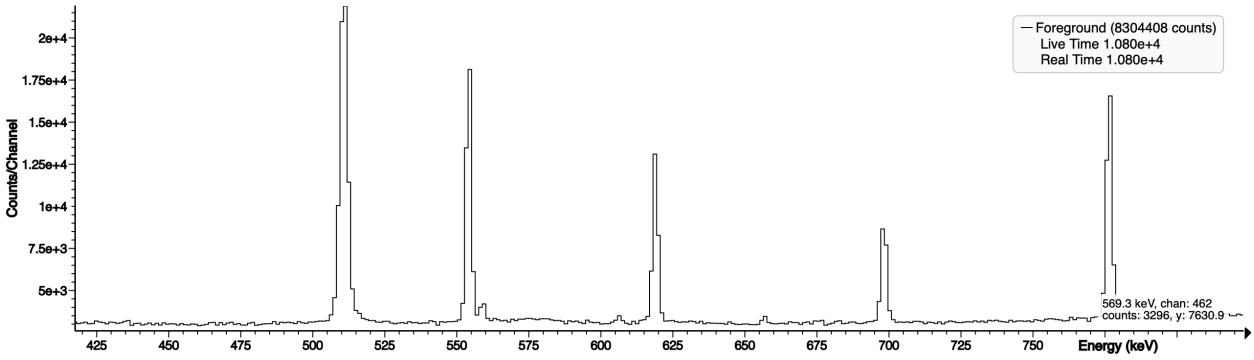

Figure 78: Coincidence spectrum, 400-800 keV, for freeze-dried urine, 2670

In this case, not only is there not necessarily a need to perform the coincidence mode, there is also no need to perform an energy gate to determine that ^{75}As is found in the sample. When evaluating the coincidence data, and even the singles data in this instance, the 559 keV gamma ray is easily visible. Upon closer inspection, the coincident 657 keV gamma ray is also visible within

the spectrum. Although it was noted earlier, it is worth mentioning again that this data was collected 1 hour after a 30-minute irradiation with the reactor set at 500 kW. This is something that is not ever possible with standard NAA techniques utilizing more conventional gamma spectroscopy systems. As a reference, the same irradiated sample was put in the Clamshell system and was measured to have greater than 45 % dead time at a distance of 10 cm. However, due to its dead time correction, the Pixie-16 system was capable of performing this measurement and has shown to have provided data that is of high enough quality to identify ^{75}As.

Chapter 8: Discussion of Results and Conclusion

8.1 Conclusions

At the start of this research, it was anticipated that the implementation of gamma-gamma coincidence would significantly reduce the background levels. While this was true, the reduction of the background and the implementation of two detectors in coincidence with each other, the uncertainties and detection limits did not dramatically improve as expected. As such, the focus of this research was primarily to evaluate the Pixie-16 system and secondly, to give a detailed analysis of a high percentage of the NAA products that could be used in gamma-gamma coincidence. However, gamma-gamma coincidence was shown, in several cases, to eliminate spectral interferences, e.g., in the analysis of ^{153}Sm, ^{175}Yb and ^{76}As.

During the course of this research, it became evident how effective the XIA Pixie-16 system is for the use in identification of gamma ray peaks at high dead time scenarios. This system has proven to maintain spectral resolution across all energies in the singles data and gamma-gamma coincidence modes. These advantages, coupled with the use of the custom written software to implement energy gating for further reduction of background levels or to validate specific gamma ray coincidences, demonstrates it to be a successful tool for use with neutron activation analysis.

The advanced digital electronics-based architecture of the XIA Pixie-16 system contribute to its successful implementation for this research. Its sophisticated electronics were crucial in its maintaining of the spectral resolution (FWHM) which allowed the identification of NAA products at significantly less decay times. Many of the NAA products that were identified are typically difficult, and in some cases impossible, to identify in high dead time situations via traditional

analog gamma spectroscopy systems or less advanced digital systems. The capability to implement the coincidence function assisted with reduction of background levels which further improved the capability of identification of gamma peaks within a sample. The coincidence counting configuration also rejected all gamma ray peaks that did not have a coincident gamma ray which eliminated peaks that were not of interest.

An important parameter worth noting is that all of the experiments that were performed on the Pixie-16 system were executed in an unshielded gamma-spectroscopy laboratory. Although no additional sources were near the experimental setup, there are a number of other sources within the laboratory. The Pixie-16 system effectively reduced background levels in spite of being unshielded. All comparisons between singles data to the NETL Clamshell system is comparing the unshielded Pixie-16 system to a shielded system.

Something else worth noting is that the two detectors used in this research were older HPGe ones and as previously noted, one stopped working midway through the research and was replaced with a detector with a poorer resolution. However, due to the resolution of the better of the two detectors in coincidence mode and the advanced digital electronics within the Pixie-16 hardware, it proved to be successful.

The system was able to identify a number of different NAA products that are typically a challenge to identify. The ability to correctly evaluate for ^{153}Sm is difficult in geological samples due to the spectral interferences arising from the neutron activation of uranium, thorium and gadolinium. These spectral interferences completely eliminated due to the implementation of gamma-gamma coincidence and energy gating. The ability to identify ^{76}As in biological samples, including human urine, was also important as the strong energy peaks from ^{24}Na typically make this challenging. Not only did the Pixie-16 prove to identify ^{76}As in biological samples, it was

able to do it after a 1-hour decay. This is something that has not been not possible without radiochemistry. The Pixie-16 system also proved to be successful in the identification of ^{239}Pu even in a sample with high ^{241}Am content via the implementation of gamma-gamma coincidence. This should prove to be an extremely beneficial technique for researchers who are specifically looking to identify ^{239}Pu.

Lastly, although the primary focus of this research was to demonstrate the ability of the Pixie-16 system to identify NAA products through the use of gamma-gamma coincidence, the system has demonstrated that even in singles mode it can be a very helpful NAA tool. This research has demonstrated that the Pixie-16 system is very successful for use in NAA and likely could become the system of choice, especially to reduce decay times. This has the ability to greatly reduce human and equipment resources, and make NAA more cost competitive with faster turnaround times.

A standard gamma spectroscopy system would require the sample to be moved away from the detector which would lower the efficiency of the count rate or would require the system to be counted for a much longer time. The longer count time, coupled with the degraded FWHM alone, makes a strong case for using the Pixie-16 rather than a conventional gamma spectroscopy system. The only limitation that was identified with this system was the loss of data when implementing coincidence and energy gating. This lowered the detection limits but helped with spectral interferences.

The high-quality singles data, gamma-gamma coincidence implementation, dead-time correction of the XIA Pixie-16 system and its successful identification of a number of challenging NAA products even in high-dead time scenarios demonstrates that the Pixie-16 system can successfully be utilized for NAA and likely could become a powerful tool to compliment routine

and Compton suppression NAA. An ideal system would couple gamma-gamma coincidence with Compton suppression in a Pixie-16 system.

8.2 Future work and recommendations

One potential implementation for future work for this research would be to further explore the implementation of the system with identification of different isotopes of plutonium. ^{239}Pu proved to be successful; the ability to help identify different isotopes of plutonium could prove to be beneficial.

Secondly, this research was not optimized for any specific NAA product but rather was configured for the identification of all potential NAA products. The following recommendations can be implemented to optimize the system for identification of specific NAA radionuclides of interest.

- The angular position of the detectors can be optimized for specific NAA radionuclides of interest, e.g., the fission product ^{134}Cs.
- The distance between the sample being measured and the detectors can be adjusted to optimize the efficiency of total counts for a specific radionuclide.
- The efficiency of the detectors can be optimized with a larger number of detectors or detectors with larger measurement areas (detector faces).
- An efficiency database can be developed for specific radionuclides of interest as required to optimize identification of these radionuclides (K-zero method).

Another focus of future research would be to repeat many of these measurements with higher quality HPGe detectors. The system was successful in the identification of NAA products in spite of using older HPGe detectors, with one having a relatively poor resolution. The

implementation of newer, higher resolution detectors should improve the capability of this system even further by an improved FWHM which will, in turn, improve the energy gating.

Appendix

A.1 Short-lived NAA products decay schemes

Page -224-

GAMMA-RAY ENERGIES AND INTENSITIES

Nuclide: ^{80m}Br* – ^{80}Br Half Life: 4.4205(8) hr.*- 17.68(2) min.
Detector: 50 cm^3 coaxial Ge (Li) Method of Production: ^{79}Br(n,γ)

	E_γ (keV)	σ E_γ	I_γ (rel)	I_γ (%)	σ I_γ	S
*	37.052	0.002		39.1	0.8	1
*	48.85	0.03		0.317	0.009	3
Ann.	511.006		100	4.4	0.4	1
	616.3	0.5	93.45	6.7	0.6	1
	639.4	0.2	3.23	0.26	0.04	2
	665.8	0.2	15.41	1.08	0.12	1
	677.0	1.0		0.008	0.003	4
	687.4	1.0		0.012	0.004	4
	703.8	0.2	2.64	0.19	0.04	1
	788.	3.		0.0134	0.0012	4
	812.2	1.5	0.58	0.041	0.014	2
	1256.2	0.4	1.25	0.073	0.010	1
	1338.5	0.8				4

E_γ, σE_γ, I_γ, σI_γ - 1998 ENSDF Data

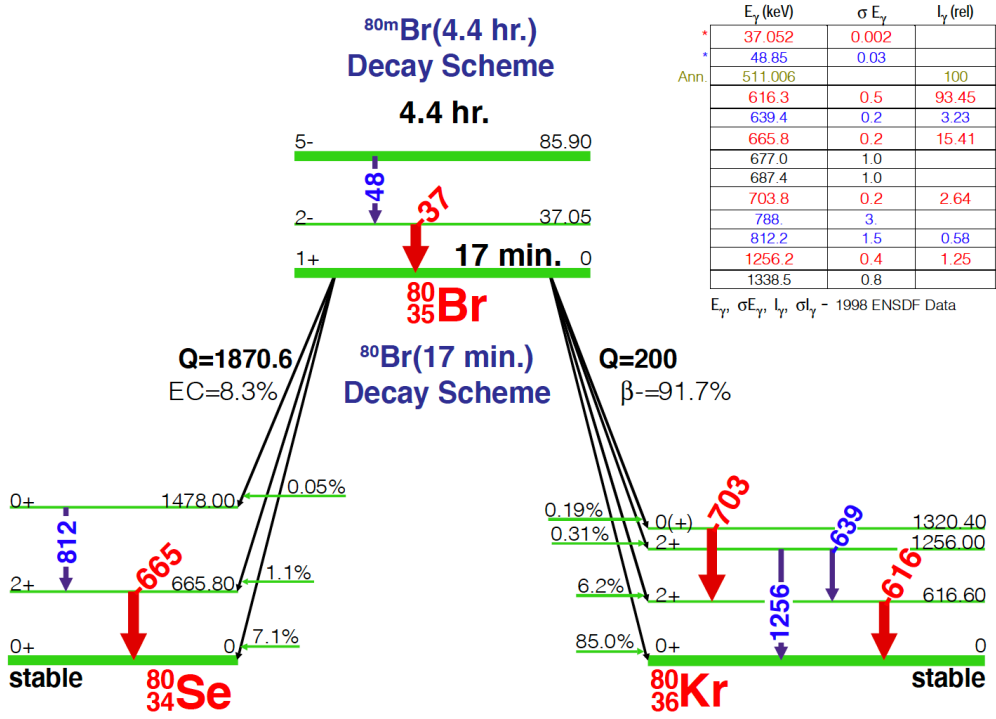

Figure 79: ^{80}Br Decay Scheme

Page -58-

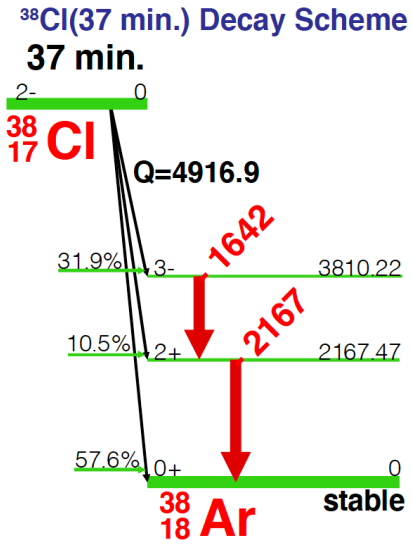

GAMMA-RAY ENERGIES AND INTENSITIES

Nuclide: ^{38}Cl — Half Life: 37.24(5) min.
Detector: 65 cm^3 coaxial Ge (Li) — Method of Production: ^{38}Cl(n,γ)

E_γ (keV)	σ E_γ	I_γ (rel)	I_γ (%)	σ I_γ	S
1642.714		76	31.9	1.0	1
2167.405		100	42.4	1.1	1

E_γ, σE_γ, I_γ, σI_γ - 1998 ENSDF Data

Figure 80: ^{38}Cl Decay Scheme

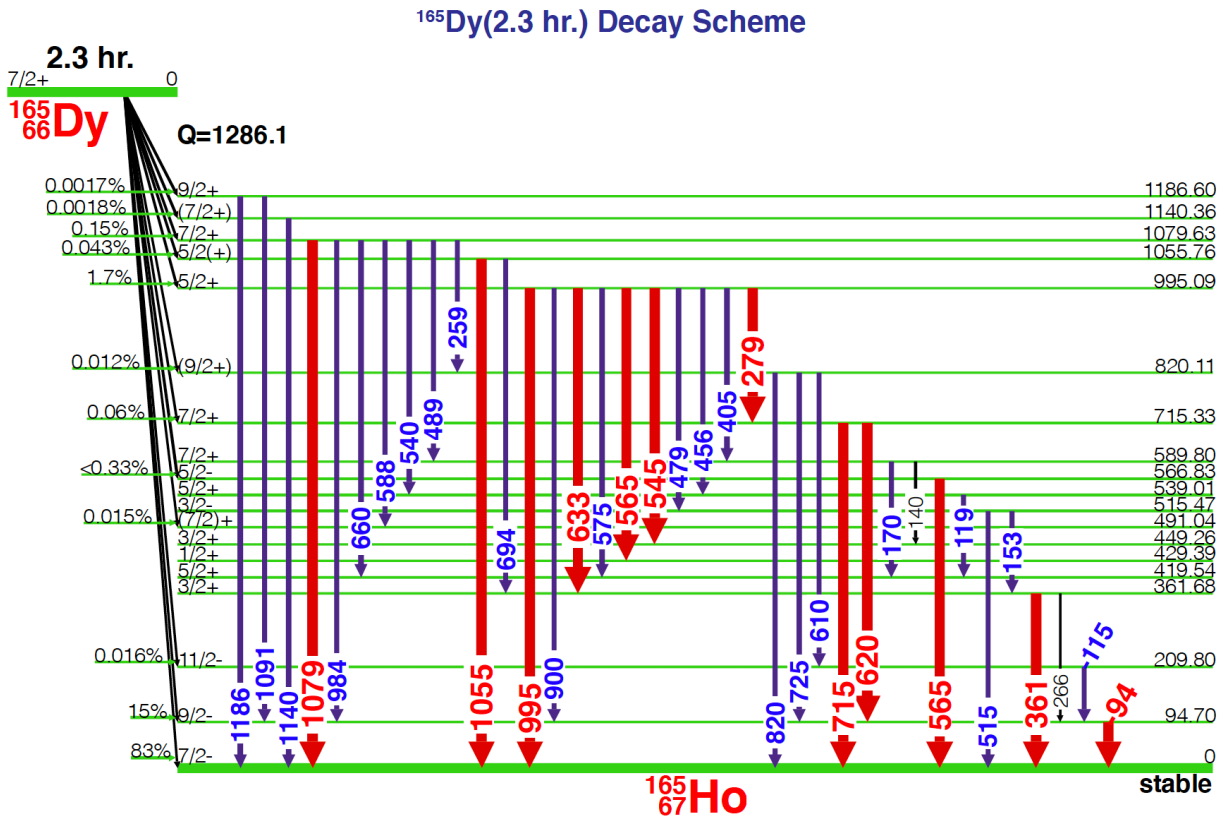

Figure 81: ^{165}Dy Decay Scheme

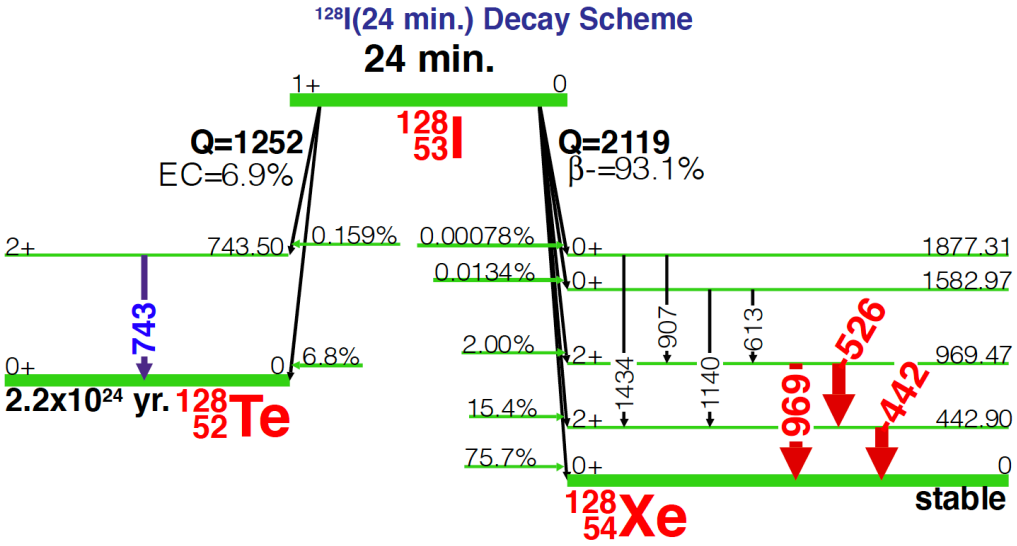

GAMMA-RAY ENERGIES AND INTENSITIES

Nuclide: ^{128}I — Half Life: 24.99(2) min.
Detector: 4.55 cm² x 8mm Ge (Li) — Method of Production: ^{127}I(n,γ)

	E_γ (keV)	σ E_γ	I_γ (rel)	I_γ (%)	σ I_γ	S
	442.901	0.010	100.	18.1	1.8	1
Ann.	511.006			0.006		4
	526.557	0.014	9.89	1.70	0.18	1
	613.493	0.013		0.0033	0.0004	4
	743.50	0.10	1.03	0.16	0.03	2
	907.84	0.05		0.0001	0.0001	4
	969.458	0.020	2.74	0.43	0.05	1
	1140.079	0.023		0.0110	0.0012	4
	1434.40	0.08		0.0007	0.0001	4

E_γ, σE_γ, I_γ, σI_γ - 1998 ENSDF Data

Figure 82: ^{128}I Decay Scheme

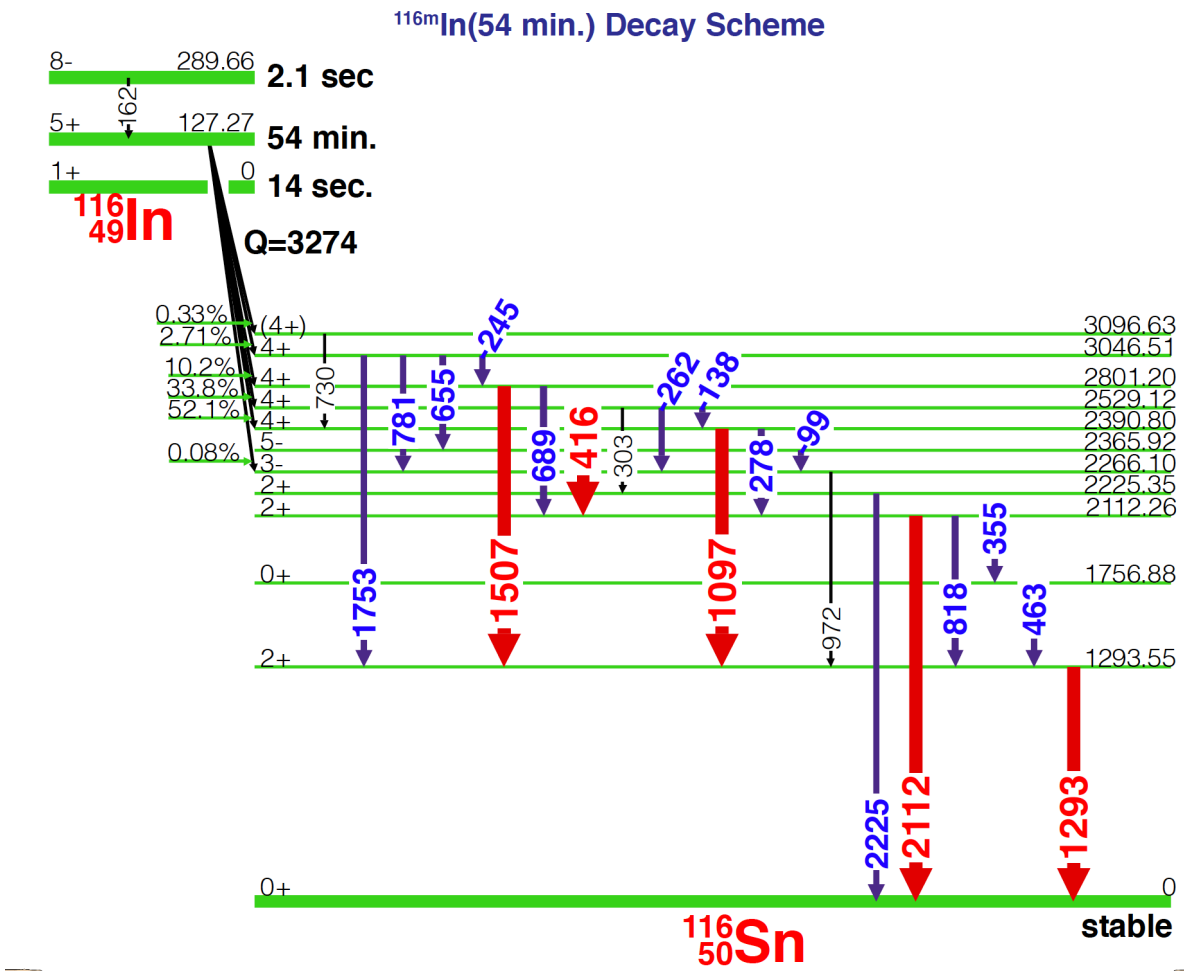

Figure 83: ^{116}In Decay Scheme

Page -66-

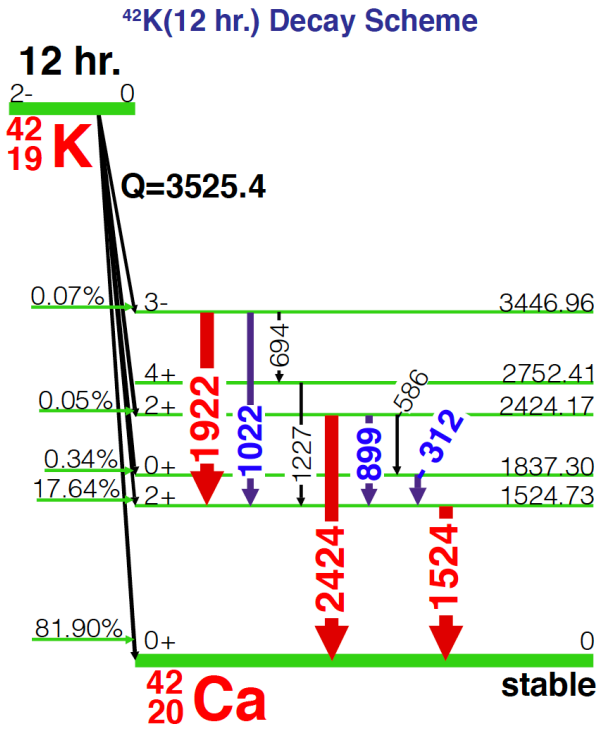

GAMMA-RAY ENERGIES AND INTENSITIES

Nuclide: ^{42}K — Half Life: 12.360(3) hr.
Detector: 55 cm^3 coaxial Ge (Li) — Method of Production: ^{41}K(n,γ)

E_γ (keV)	σ E_γ	I_γ (rel)	I_γ (%)	σ I_γ	S
312.6		1.68	0.336	0.020	2
586.87			0.0004		4
694.54			0.0033	0.0007	4
899.43		0.304	0.0515	0.0025	3
1022.78		0.162	0.0201	0.0014	4
1227.66			0.0024	0.0011	4
1524.7		100	18.08	0.09	1
1922.18		0.232	0.041	0.004	1
2424.09		0.122	0.0199	0.0029	1

E_γ, σE_γ, I_γ, σI_γ - 1998 ENSDF Data

Figure 84: ^{42}K Decay Scheme

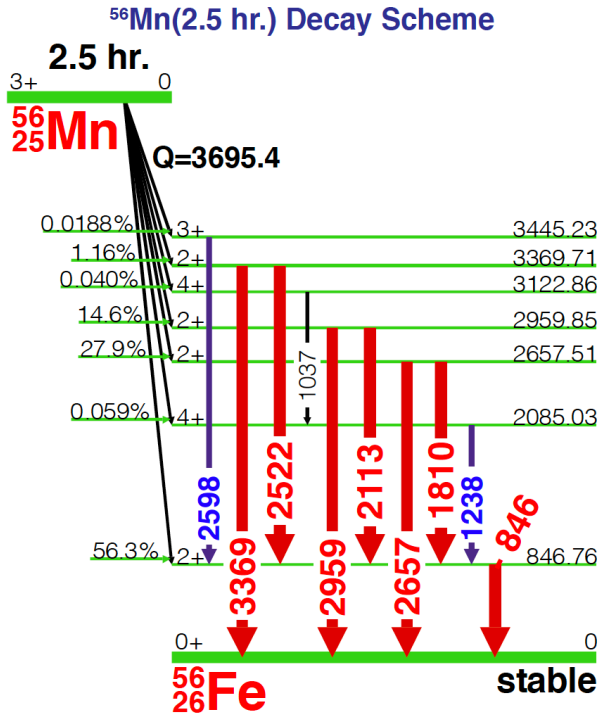

GAMMA-RAY ENERGIES AND INTENSITIES

Nuclide: ^{56}Mn — Half Life: 2.5785(2) hr.
Detector: 35 cm^3 coaxial Ge (Li) — Method of Production: ^{55}Mn(n,γ)

E_γ (keV)	σ E_γ	I_γ (rel)	I_γ (%)	σ I_γ	S
846.7638	0.0019	100	98.9	0.3	1
1037.8333	0.0024		0.040	0.005	4
1238.2736	0.0022	0.09	0.099	0.010	4
1810.726	0.004	28.7	27.2	0.8	1
2113.092	0.006	15.4	14.3	0.4	1
2522.88	0.06	1.15	0.99	0.03	1
2598.438	0.004		0.0188	0.0020	4
2657.45	0.05	0.76	0.652	0.020	1
2959.77	0.06	0.33	0.306	0.010	1
3369.60	0.07	0.184	0.168	0.010	1

E_γ, σE_γ, I_γ, σI_γ - 1998 ENSDF Data

Figure 85: ^{56}Mn Decay Scheme

Page -46-

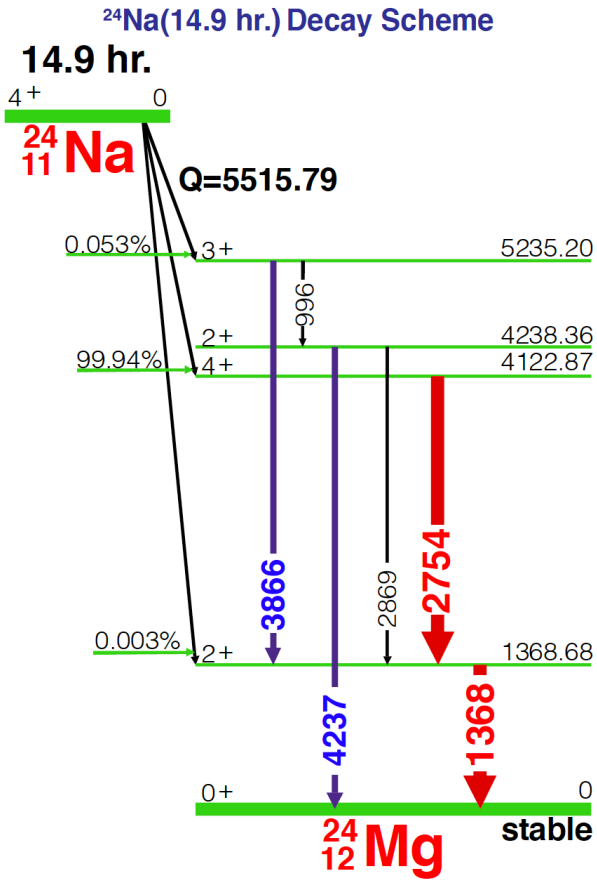

GAMMA-RAY ENERGIES AND INTENSITIES

Nuclide: ^{24}Na — Half Life: 14.9590(12) hr.
Detector: 65 cm ^{3} coaxial Ge (Li) — Method of Production: ^{23}Na (n,γ)

E_γ (keV)	σ E_γ	I_γ (rel)	I_γ (%)	σ I_γ	S
996.82			0.0014	0.0002	4
1368.633		100	100.0		1
2754.028		98.6	99.944	0.004	1
2869.5			0.0003	0.0001	4
3866.19		0.076	0.052	0.004	2
4237.96			0.0011	0.0002	4

E_γ, σE_γ, I_γ, σI_γ - 1998 ENSDF Data

Figure 86: ^{24}Na Decay Scheme

A.2 Medium-lived NAA products decay schemes

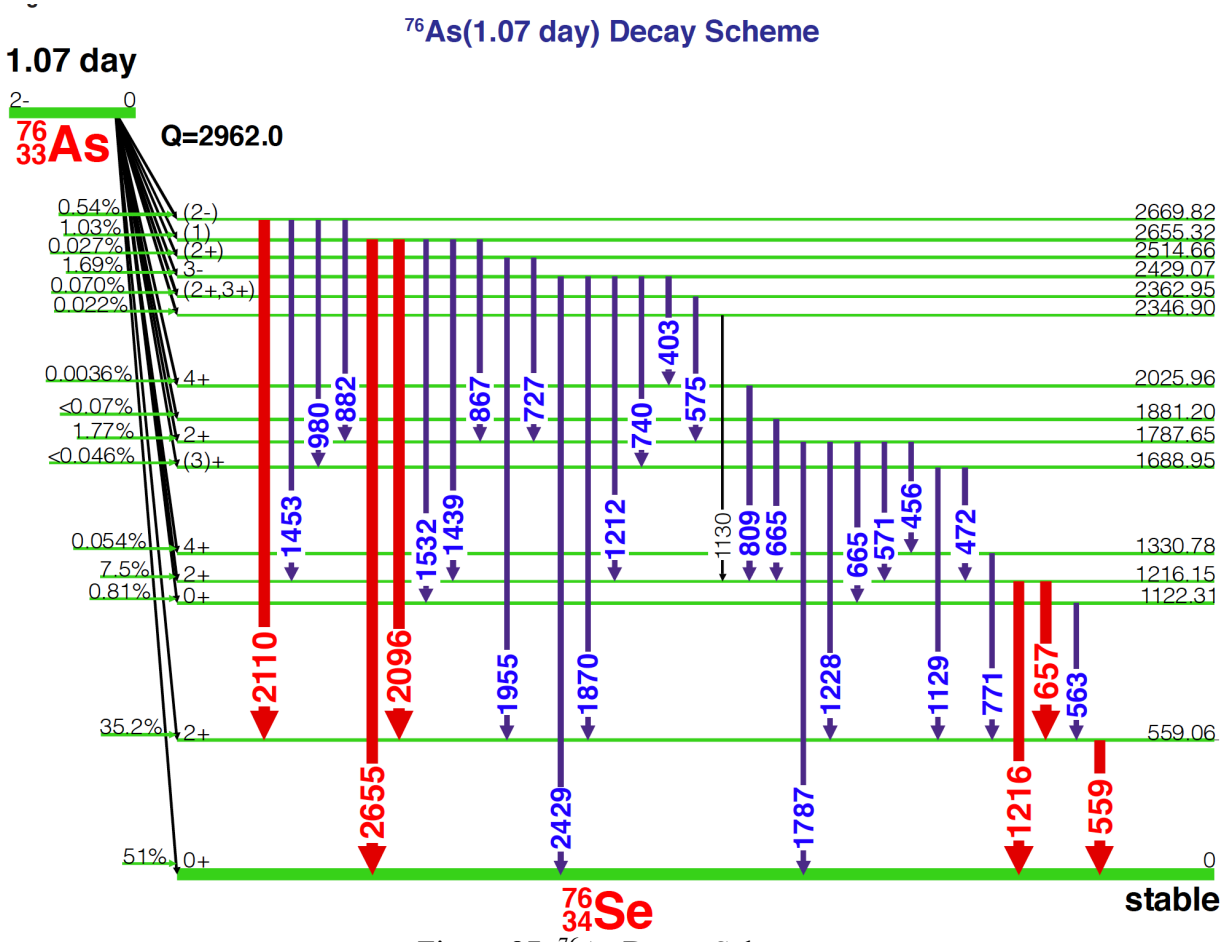

Figure 87: ^{76}As Decay Scheme

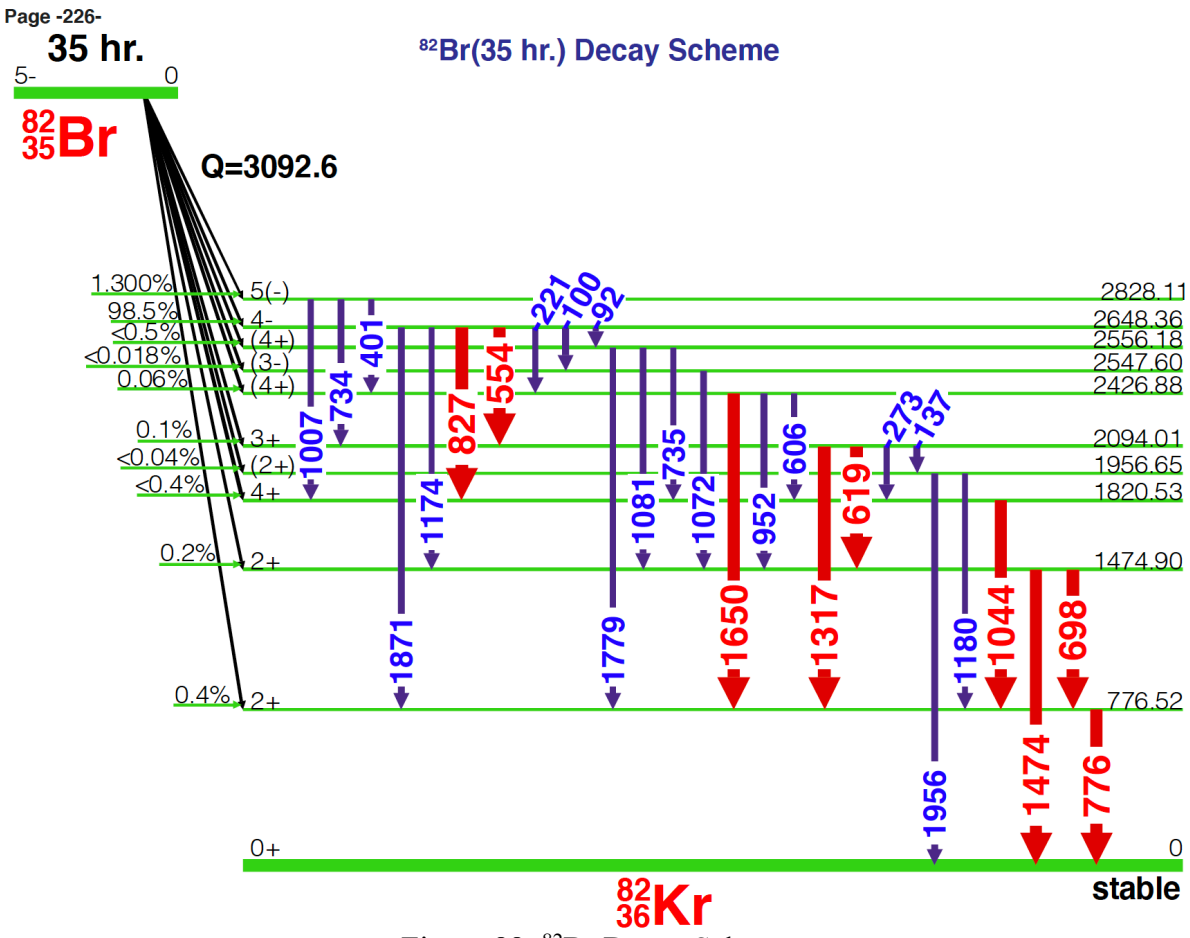

Figure 88: ^{82}Br Decay Scheme

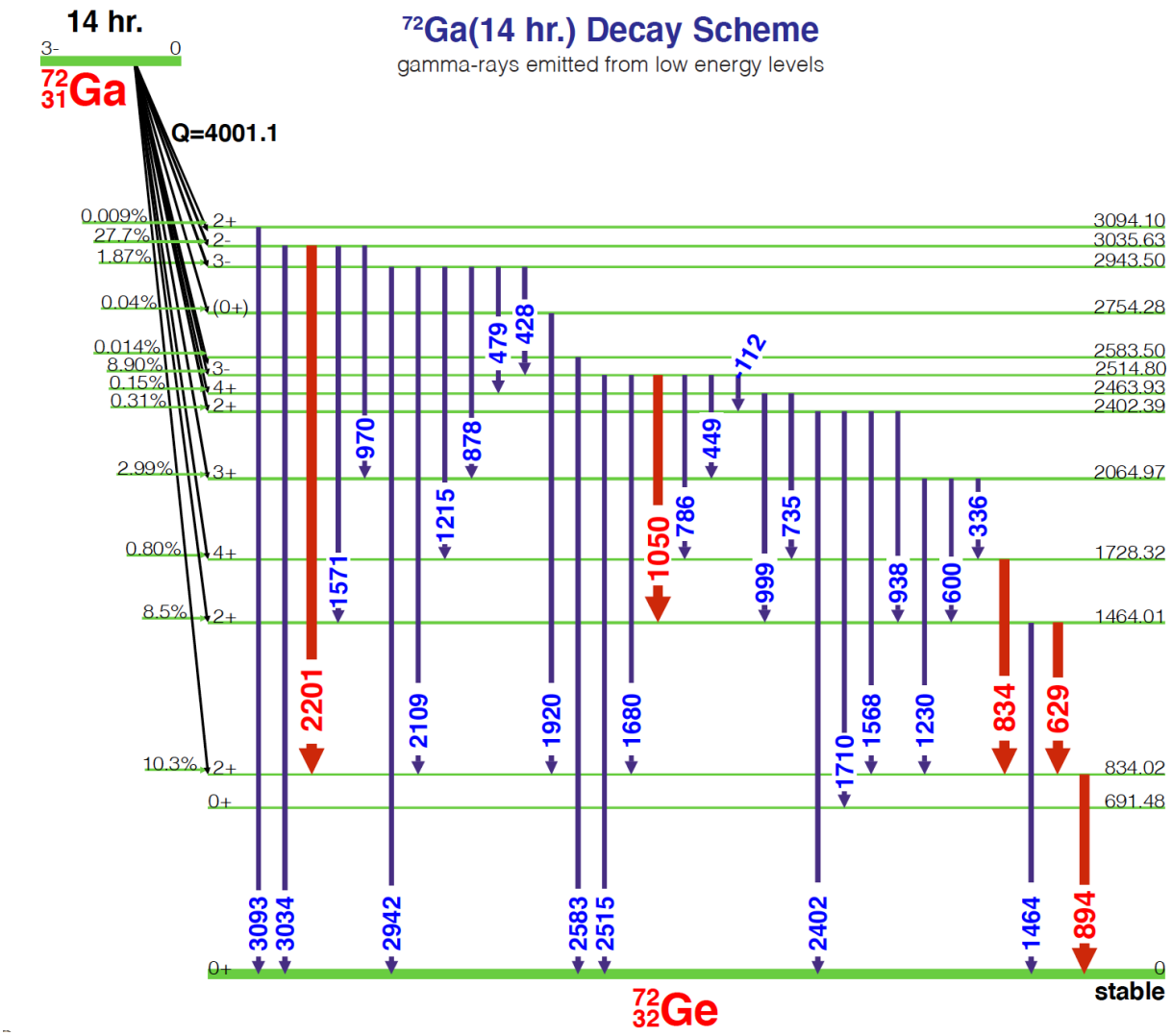

Figure 89: ^{72}Ga Decay Scheme

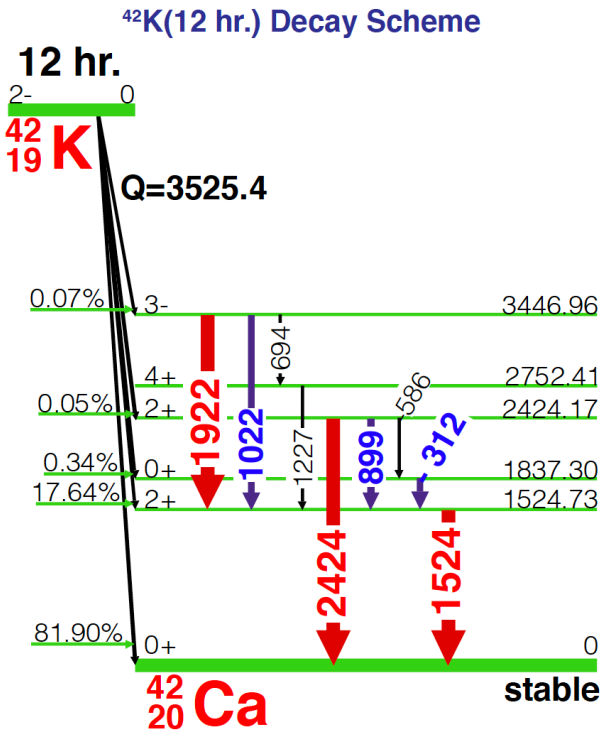

GAMMA-RAY ENERGIES AND INTENSITIES

Nuclide: ^{42}K — Half Life: 12.360(3) hr.
Detector: 55 cm^3 coaxial Ge (Li) — Method of Production: ^{41}K(n,γ)

E_γ (keV)	σ E_γ	I_γ (rel)	I_γ (%)	σ I_γ	S
312.6		1.68	0.336	0.020	2
586.87			0.0004		4
694.54			0.0033	0.0007	4
899.43		0.304	0.0515	0.0025	3
1022.78		0.162	0.0201	0.0014	4
1227.66			0.0024	0.0011	4
1524.7		100	18.08	0.09	1
1922.18		0.232	0.041	0.004	1
2424.09		0.122	0.0199	0.0029	1

E_γ, σE_γ, I_γ, σI_γ - 1998 ENSDF Data

Figure 90: ^{42}K Decay Scheme

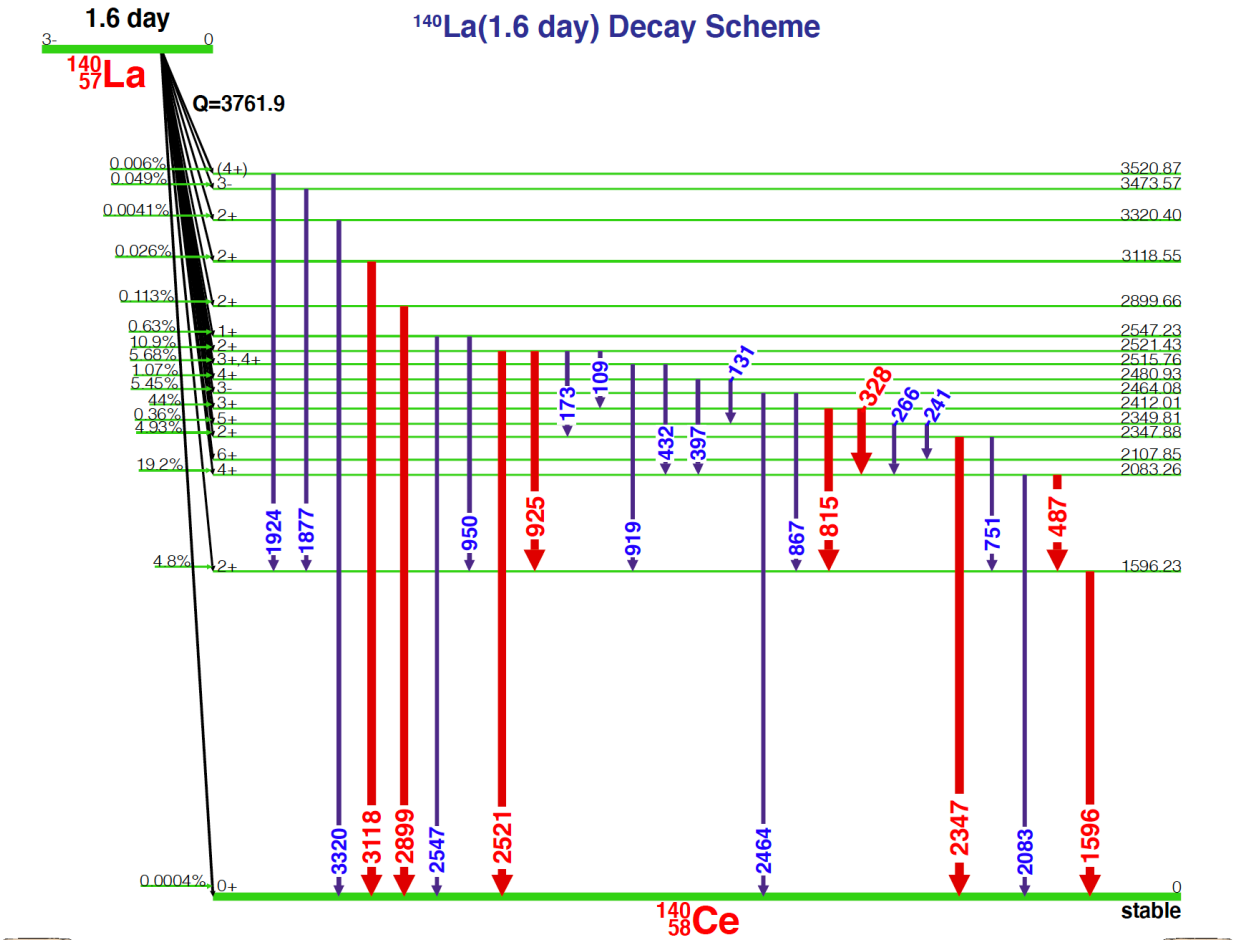

Figure 91: ^{140}La Decay Scheme

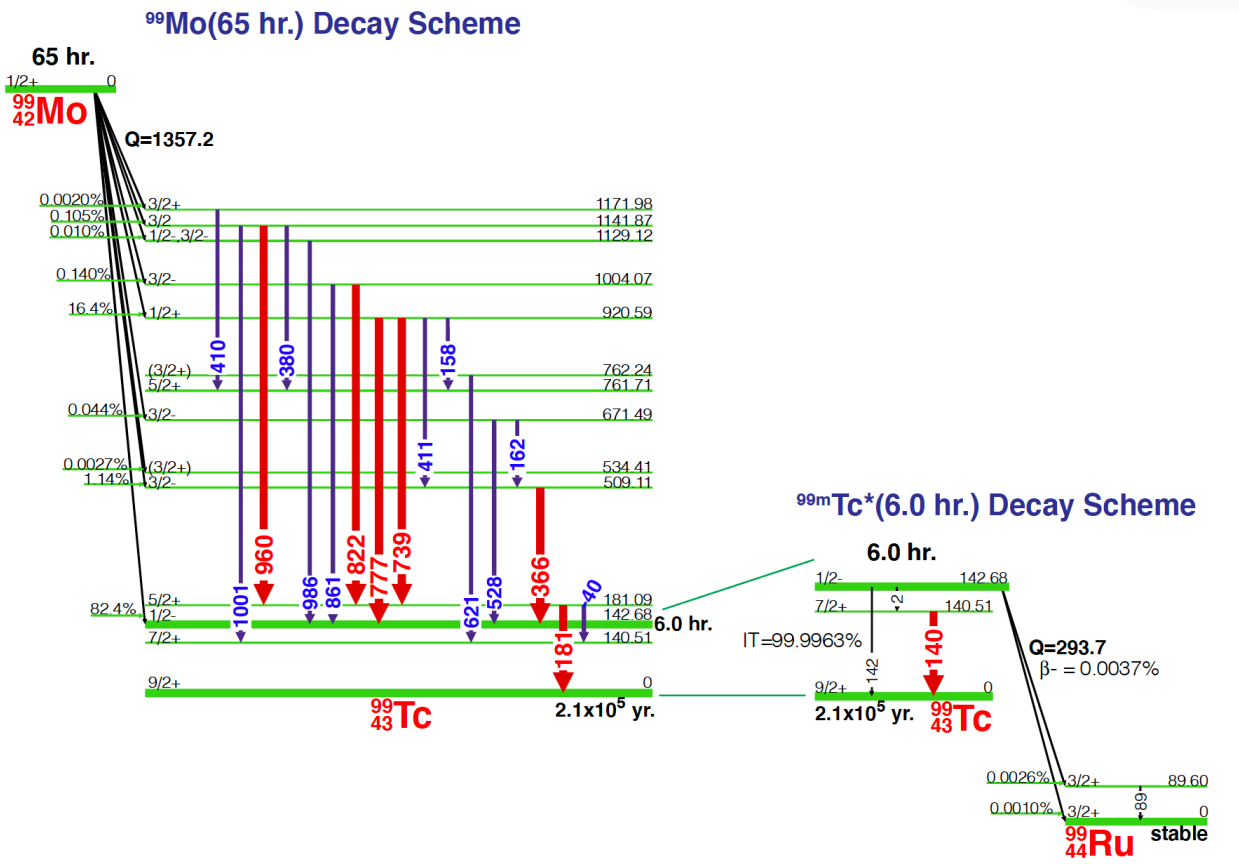

Figure 92: ^{99}Mo Decay Scheme

Decay Scheme

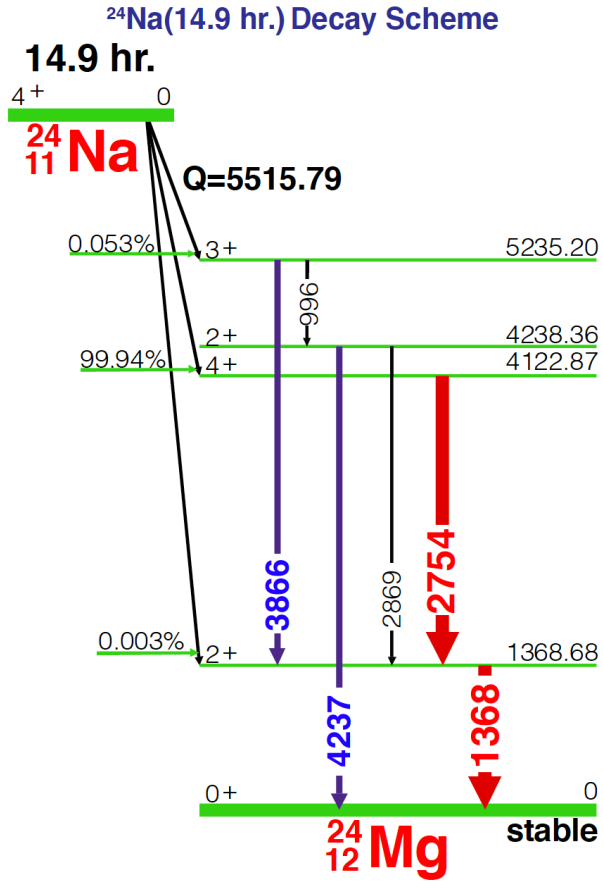

GAMMA-RAY ENERGIES AND INTENSITIES

Nuclide: ^{24}Na — Half Life: 14.9590(12) hr.
Detector: 65 cm ^{3} coaxial Ge (Li) — Method of Production: ^{23}Na (n,γ)

E_γ (keV)	σ E_γ	I_γ (rel)	I_γ (%)	σ I_γ	S
996.82			0.0014	0.0002	4
1368.633		100	100.0		1
2754.028		98.6	99.944	0.004	1
2869.5			0.0003	0.0001	4
3866.19		0.076	0.052	0.004	2
4237.96			0.0011	0.0002	4

E_γ, σE_γ, I_γ, σI_γ - 1998 ENSDF Data

Figure 93: ^{24}Na Decay Scheme

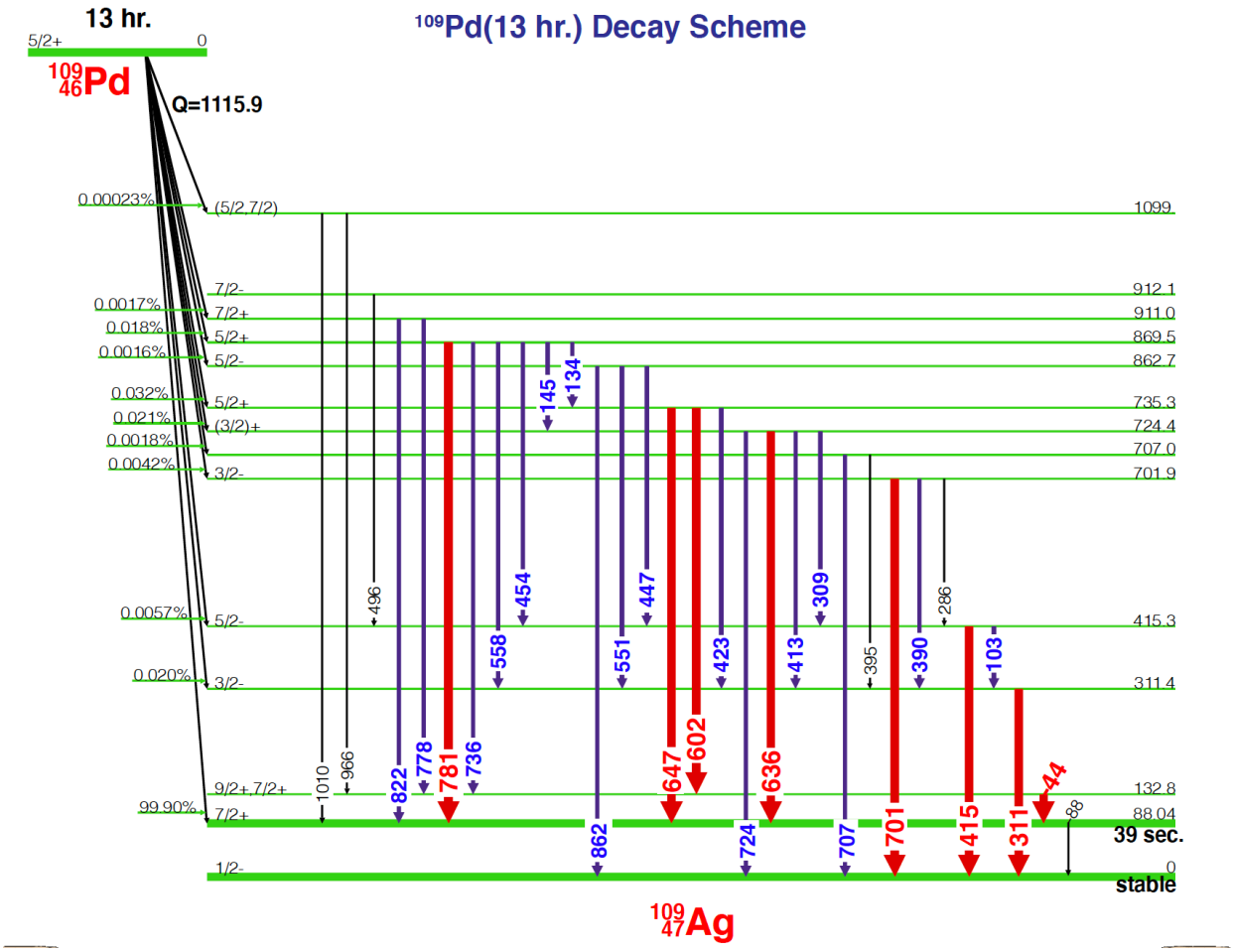

Figure 94: ^{109}Pd Decay Scheme

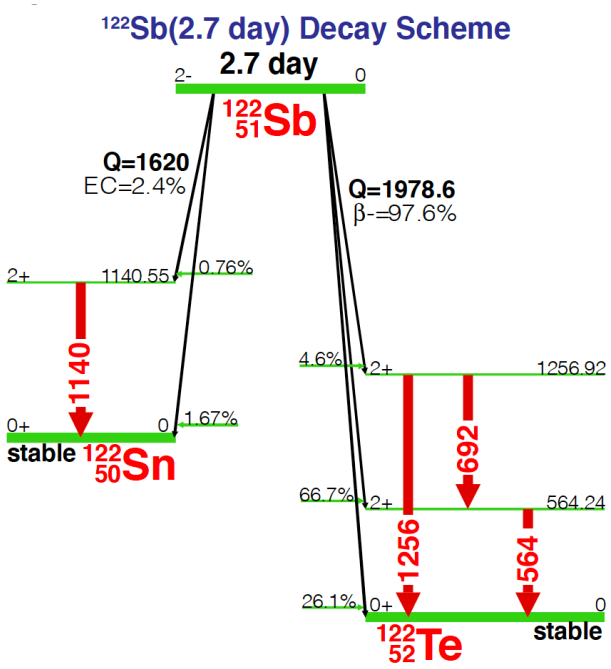

GAMMA-RAY ENERGIES AND INTENSITIES

Nuclide: ^{122}Sb — Half Life: 2.7238(2) day

Detector: 4.55 cm^2 x 8mm Ge (Li) — Method of Production: ^{121}Sb(γ,n)

	E_γ (keV)	σ E_γ	I_γ (rel)	I_γ (%)	σ I_γ	S
Ann.	511.006			0.0125		4
	564.24	0.04	100	72.42	0.16	1
	615.0	0.4		0.012	0.004	4
	692.65	0.04	5.6	3.95	0.13	1
	793.3	0.4		0.017	0.004	4
	1140.46	0.10	1.2			1
	1188.0	1.0		0.0043	0.0007	4
	1256.93	0.04	1.0	0.83	0.04	1
	1752.4	1.5		0.0094	0.0014	4

E_γ, σE_γ, I_γ, σI_γ - 1998 ENSDF Data

Figure 95: ^{122}Sb Decay Scheme

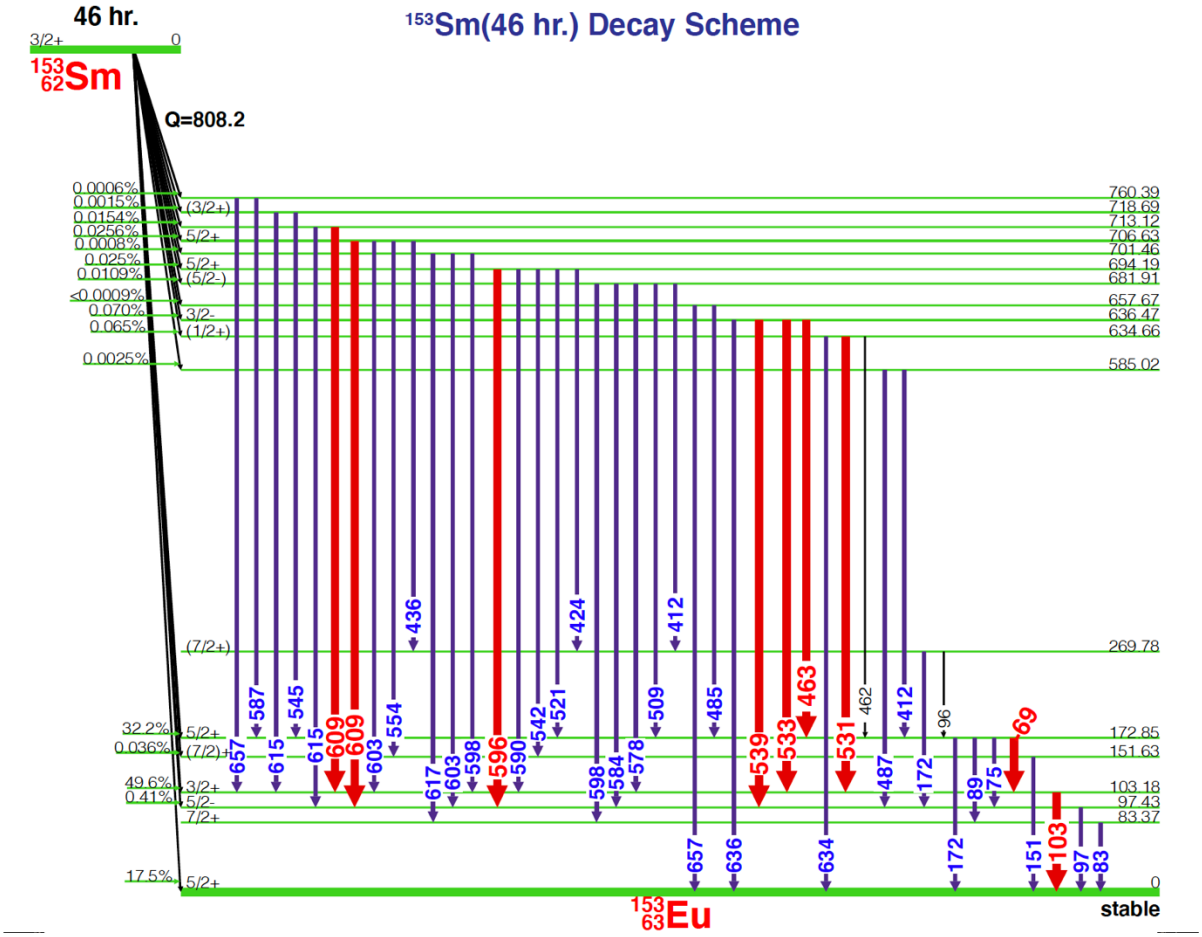

Figure 96: ^{153}Sm Decay Scheme

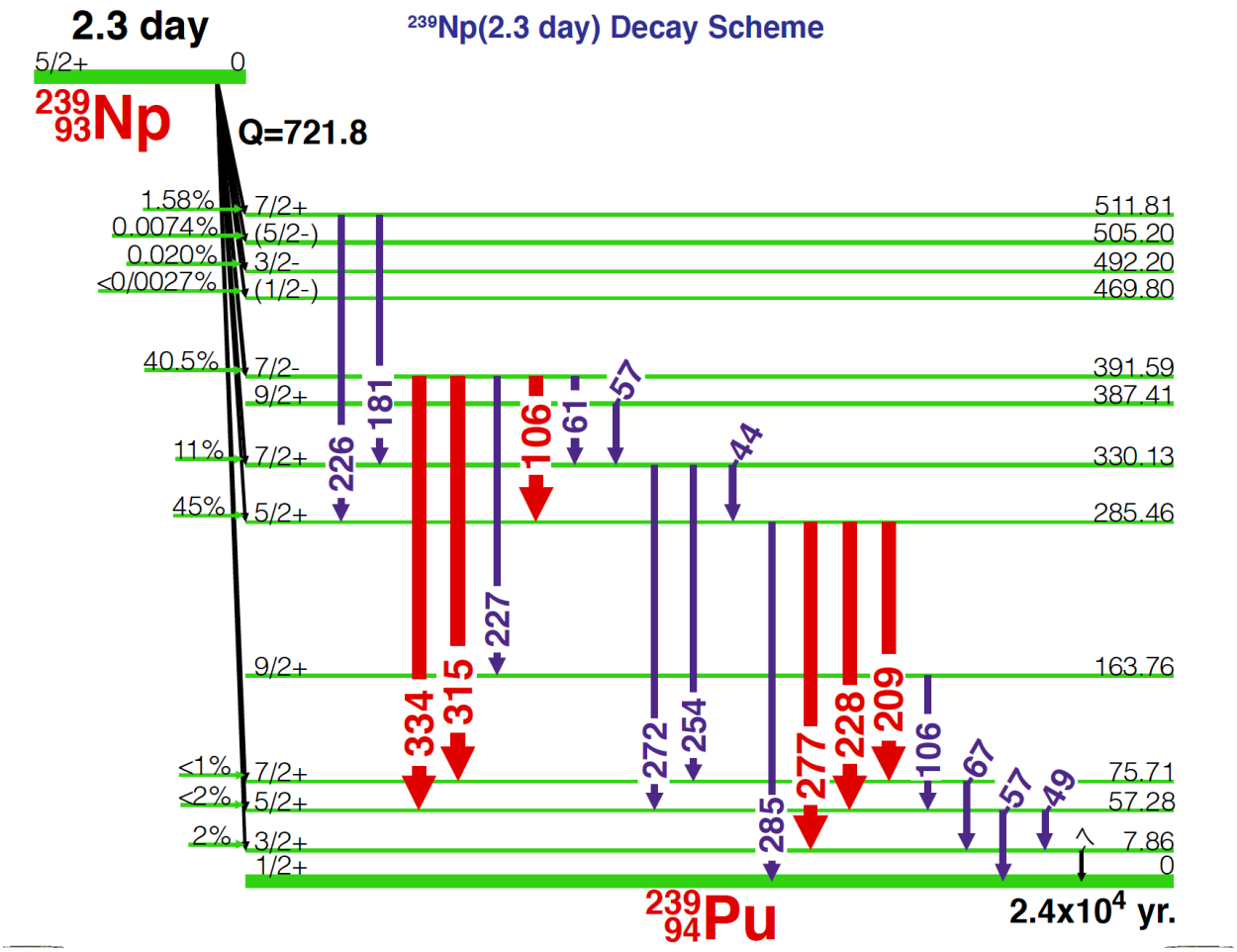

Figure 97: ^{239}Np Decay Scheme

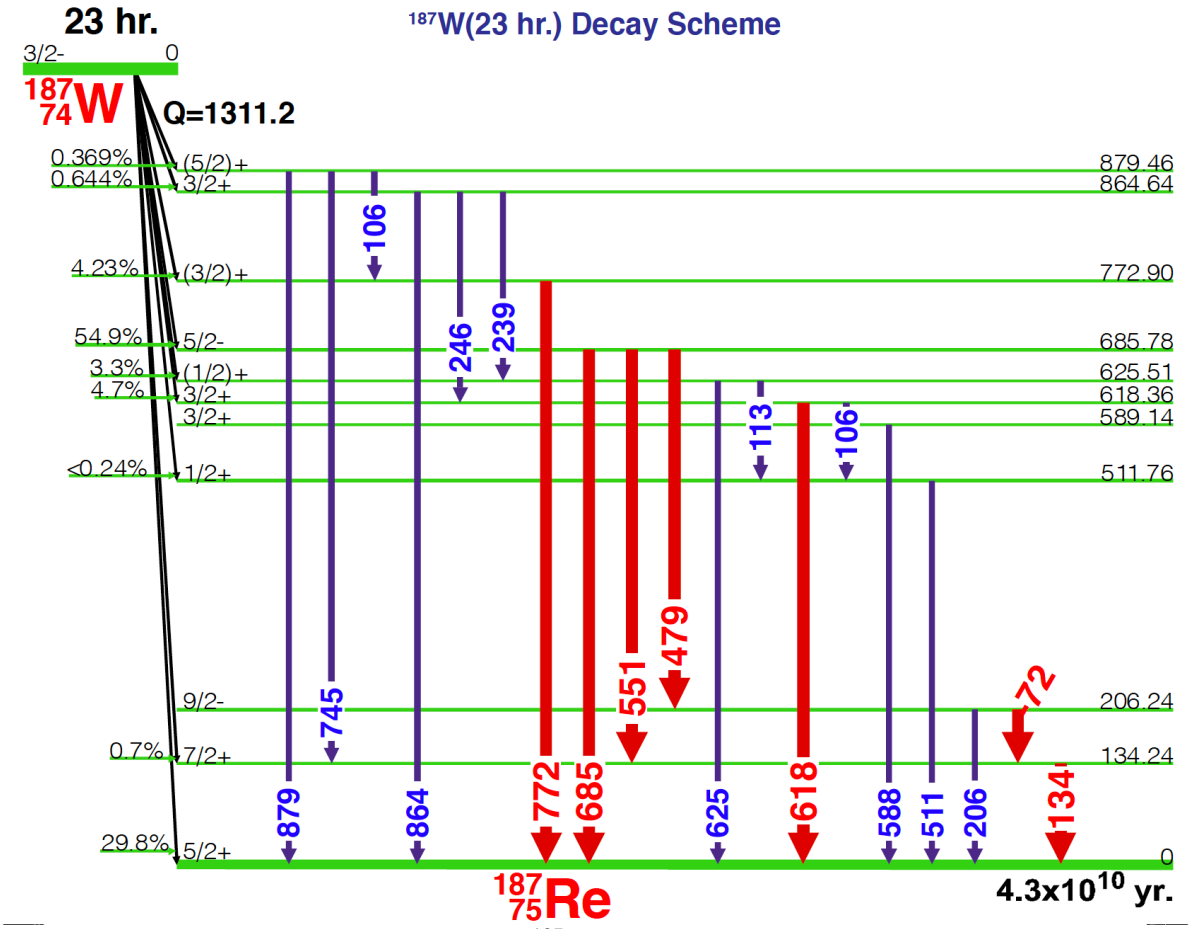

Figure 98: ^{187}W Decay Scheme

A.3 Long-lived NAA products decay schemes

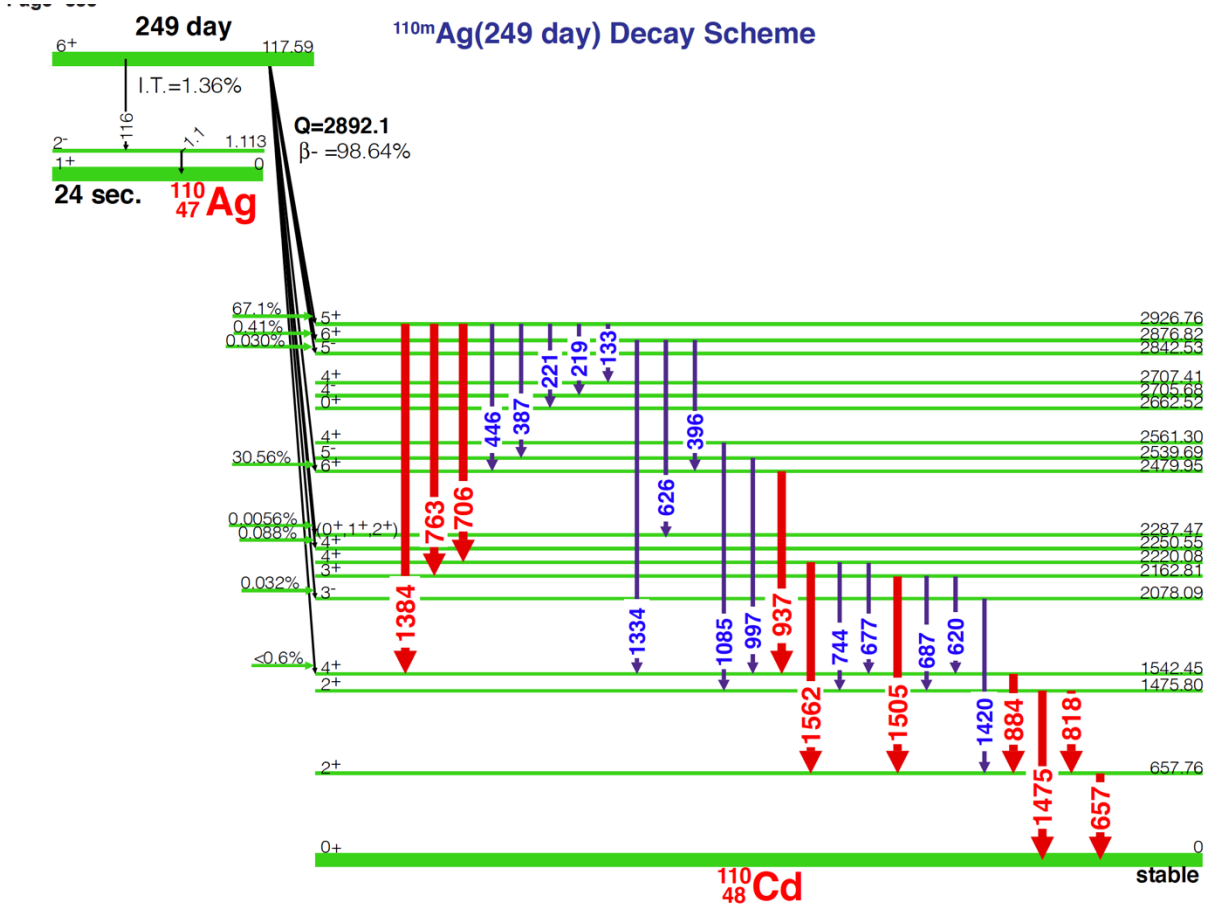

Figure 99: ^{110m}Ag Decay Scheme

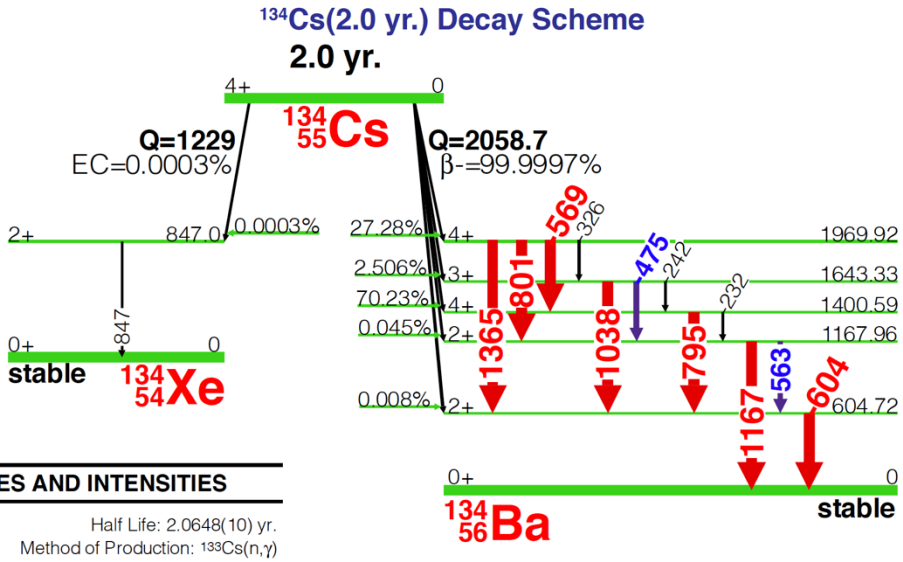

GAMMA-RAY ENERGIES AND INTENSITIES

Nuclide: ^{134}Cs — Half Life: 2.0648(10) yr.
Detector: 55 cm³ coaxial Ge (Li) — Method of Production: ^{133}Cs(n,γ)

E_γ (keV)	σ E_γ	I_γ (rel)	I_γ (%)	σ I_γ	S
232.6			0.0011		4
242.738	0.008		0.027	0.003	4
326.589	0.013		0.0162	0.0010	4
475.365	0.002	1.86	1.486	0.010	3
563.246	0.005	8.0	8.35	0.04	2
569.331	0.003	15.3	15.38	0.06	1
604.721	0.002	100.	97.62	0.03	1
795.864	0.004	87.0	85.53	0.04	1
801.953	0.004	8.8	8.69	0.04	1
847.00	0.20		0.0003	0.0001	4
1038.610	0.007	1.05	0.988	0.004	1
1167.968	0.005	1.96	1.789	0.007	1
1365.185	0.007	3.26	3.014	0.012	1

E_γ, σE_γ, I_γ, σI_γ - 1998 ENSDF Data

Figure 100: ^{134}Cs Decay Scheme

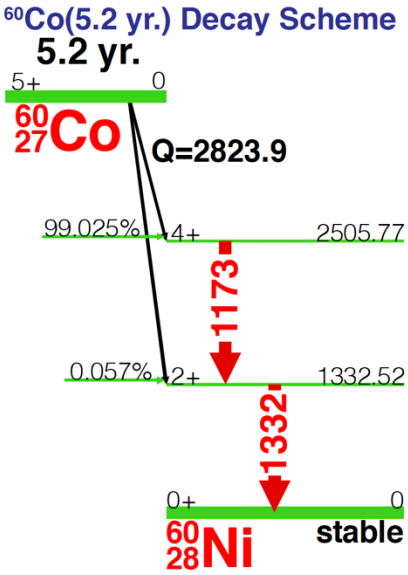

GAMMA-RAY ENERGIES AND INTENSITIES

Nuclide: ^{60}Co — Half Life: 5.2714(5) yr.
Detector: 55 cm³ coaxial Ge (Li) — Method of Production: ^{59}Co(n,γ)

E_γ (keV)	σ E_γ	I_γ (rel)	I_γ (%)	σ I_γ	S
346.93	0.07		0.0076	0.0005	4
826.28	0.09		0.0076	0.0008	4
1173.237	0.004	100	99.9736	0.0007	1
1332.501	0.005	100	99.9856	0.0004	1
2158.77	0.09		0.0011	0.0002	4
2505.					4

E_γ, σE_γ, I_γ, σI_γ - 1998 ENSDF Data

Figure 101: ^{60}Co Decay Scheme

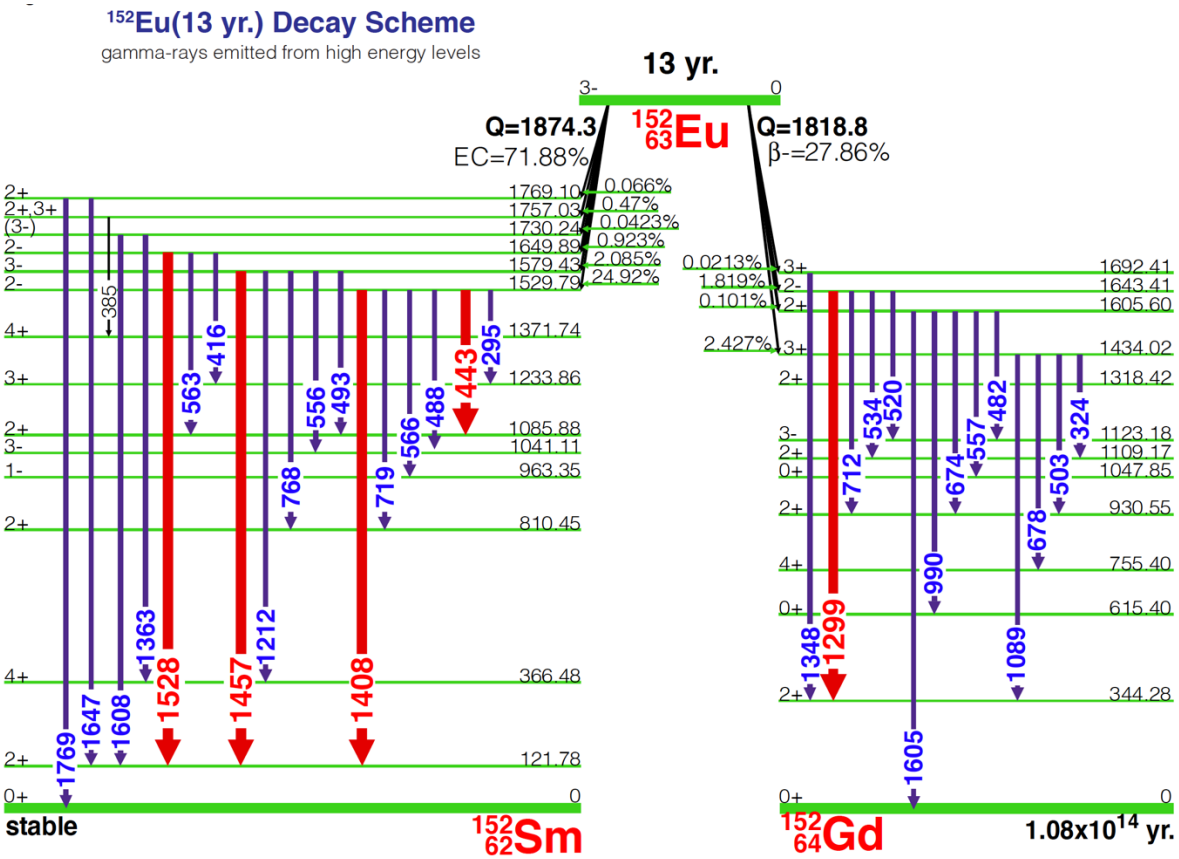

Figure 102: ^{152}Eu Decay Scheme

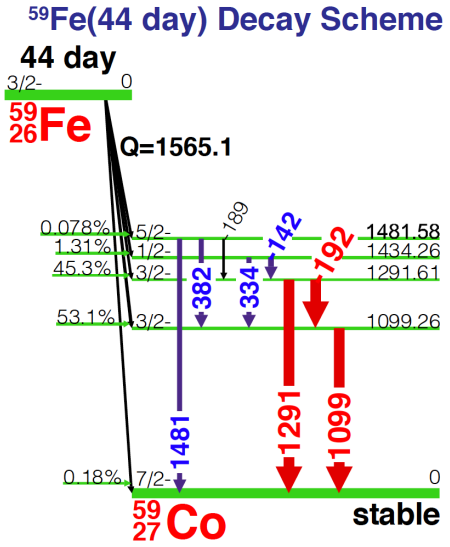

GAMMA-RAY ENERGIES AND INTENSITIES

Nuclide: ^{59}Fe — Half Life: 44.503(6) day
Detector: 65 cm³ coaxial Ge (Li) — Method of Production: ^{58}Fe(n,γ)

E_γ (keV)	σ E_γ	I_γ (rel)	I_γ (%)	σ I_γ	S
142.651	0.002	1.54	1.02	0.04	2
189.			0.0009	0.0009	4
192.349	0.005	4.7	3.08	0.12	1
334.8	0.2	0.47	0.270	0.011	3
382.0	0.4	0.05	0.018	0.003	4
1099.251	0.004	100	56.5	1.8	1
1291.596	0.007	77	43.2	1.4	1
1481.7	0.2	0.11	0.059	0.006	3

E_γ, σE_γ, I_γ, σI_γ - 1998 ENSDF Data

Figure 103: ^{59}Fe Decay Scheme

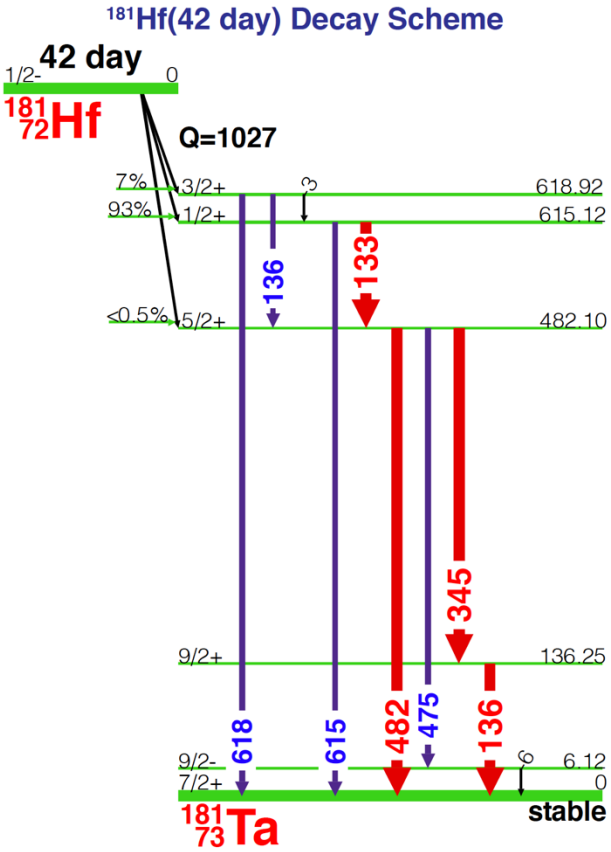

GAMMA-RAY ENERGIES AND INTENSITIES

Nuclide: ^{181}Hf — Half Life: 42.39(6) day
Detector: 65 cm³ coaxial Ge (Li) — Method of Production: ^{180}Hf(n,γ)

	E_γ (keV)	σ E_γ	I_γ (rel)	I_γ (%)	σ I_γ	S
	3.90	0.10				4
	6.3	0.3		0.0115	0.0004	4
	133.021	0.019	44.51	43.3	0.5	1
D	136.260	0.018	7.24	5.85	0.19	1
	136.86	0.04		0.86	0.19	
	345.93	0.06	18.71	15.12	0.12	1
	475.99	0.09	1.45	0.703	0.007	3
	482.18	0.09	100.	80.5	0.4	1
	615.17	0.11	0.32	0.234	0.018	2
	618.66	0.08	0.05	0.0250	0.0012	3

E_γ, σE_γ, I_γ, σI_γ - 1998 ENSDF Data

Figure 104: ^{181}Hf Decay Scheme

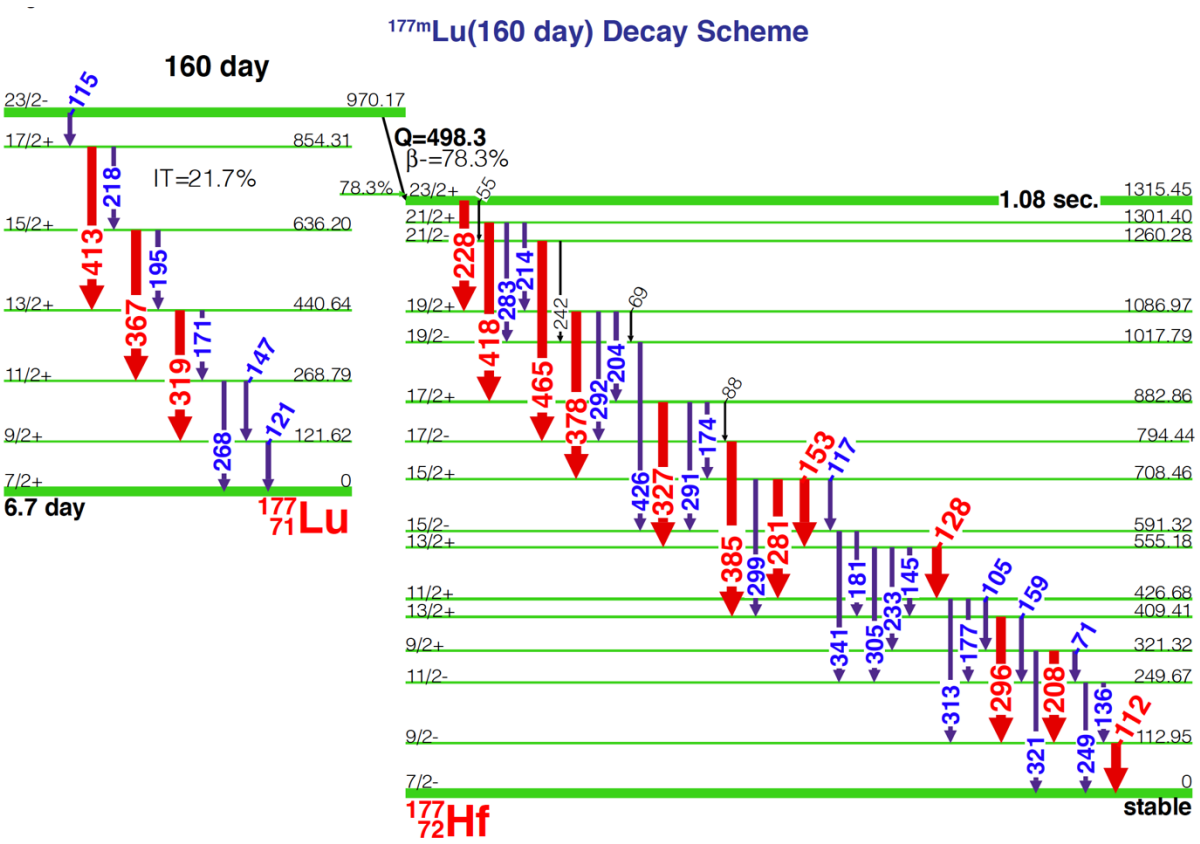

Figure 105: ^{177m}Lu Decay Scheme

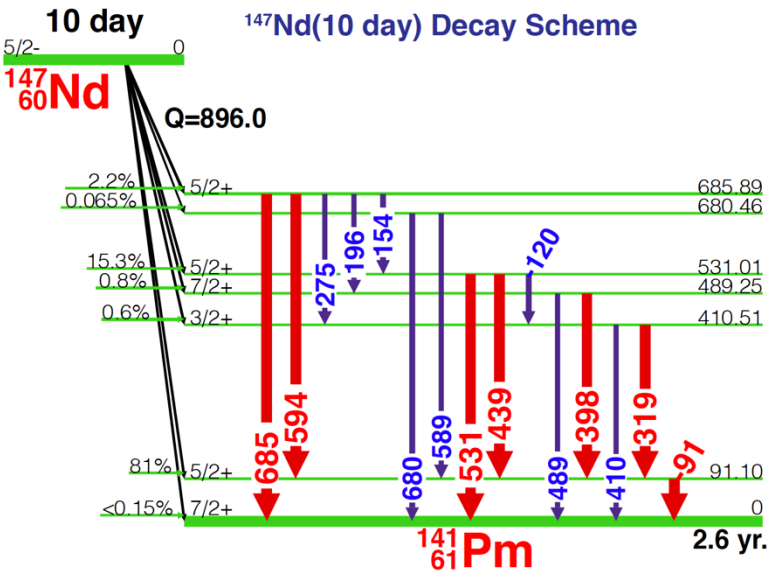

GAMMA-RAY ENERGIES AND INTENSITIES

Nuclide: ^{147}Nd
Detector: 65 cm^3 coaxial Ge (Li)

E_γ, σE_γ, I_γ, σI_γ - 1998 ENSDF Data

Half Life: 10.98(1) day
Method of Production: ^{146}Nd(n,γ)

E_γ (keV)	σE_γ	I_γ (rel)	I_γ (%)	σI_γ	S
91.105	0.002	100.	27.9	1.1	1
120.48	0.05	1.42	0.40	0.04	2
154.0	1.0		0.0558	0.0022	4
196.64	0.04	0.73	0.204	0.019	3
275.374	0.015	2.87	0.80	0.06	2
319.411	0.018	7.0	1.95	0.14	1
398.155	0.020	3.12	0.87	0.07	1
410.48	0.03	0.50	0.140	0.010	3

E_γ (keV)	σE_γ	I_γ (rel)	I_γ (%)	σI_γ	S
439.895	0.022	4.3	1.20	0.10	1
489.24	0.03	0.55	0.154	0.010	3
531.016	0.022	46.9	13.1	0.9	1
589.35	0.04	0.164	0.046	0.005	2
594.80	0.03	0.95	0.265	0.020	1
680.52	0.15	0.070	0.020	0.004	4
685.90	0.04	2.91	0.81	0.06	1

Figure 106: ^{147}Nd Decay Scheme

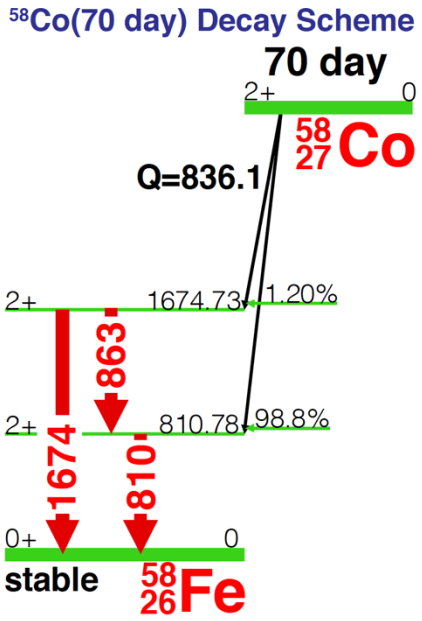

GAMMA-RAY ENERGIES AND INTENSITIES

Nuclide: ^{58}Co — Half Life: 70.86(7) day
Detector: 55 cm³ coaxial Ge (Li) — Method of Production: ^{58}Ni(n,p)

	E_γ (keV)	σE_γ	I_γ (rel)	I_γ (%)	σI_γ	S
Ann.	511.006			29.5	0.3	1
	810.775	0.009	100	99.450	0.010	1
	863.959	0.009	0.74	0.683	0.011	1
	1674.730	0.010	0.54	0.518	0.008	1

E_γ, σE_γ, I_γ, σI_γ - 1998 ENSDF Data

Figure 107: ^{58}Co Decay Scheme

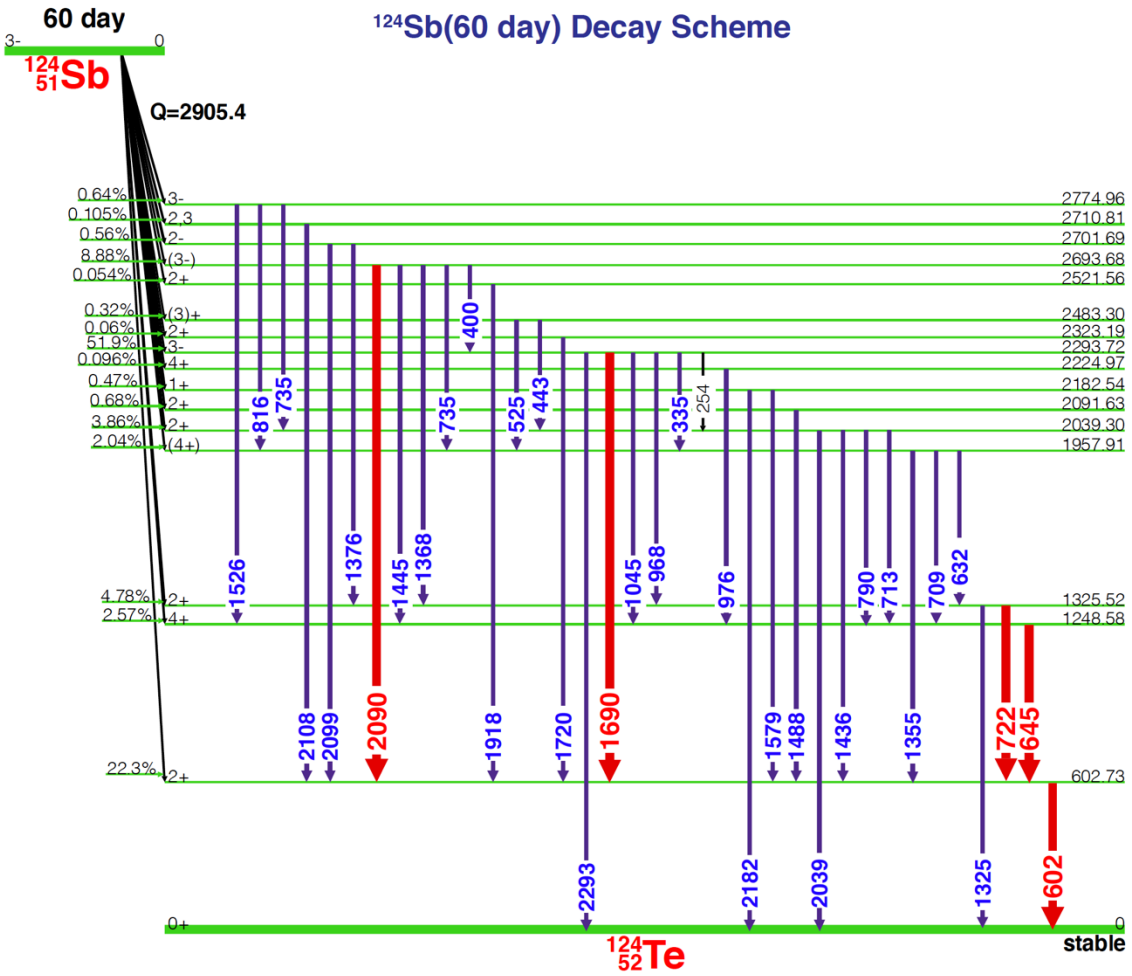

Figure 108: ^{124}Sb Decay Scheme

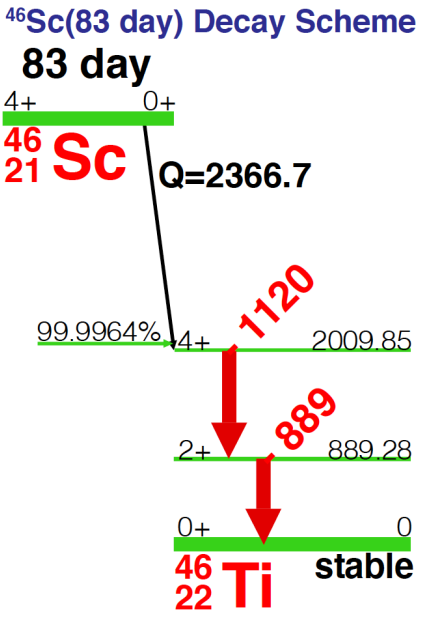

GAMMA-RAY ENERGIES AND INTENSITIES

Nuclide: ^{46}Sc — Half Life: 83.79(4) day

Detector: 65 cm^3 coaxial Ge (Li) — Method of Production: ^{45}Sc(n,γ)

E_γ (keV)	σ E_γ	I_γ (rel)	I_γ (%)	σ I_γ	S
889.277	0.003	100	99.984	0.0010	1
1120.545	0.004	100	99.9870	0.0010	1
2010.					

E_γ, σE_γ, I_γ, σI_γ - 1998 ENSDF Data

Figure 109: ^{46}Sc Decay Scheme

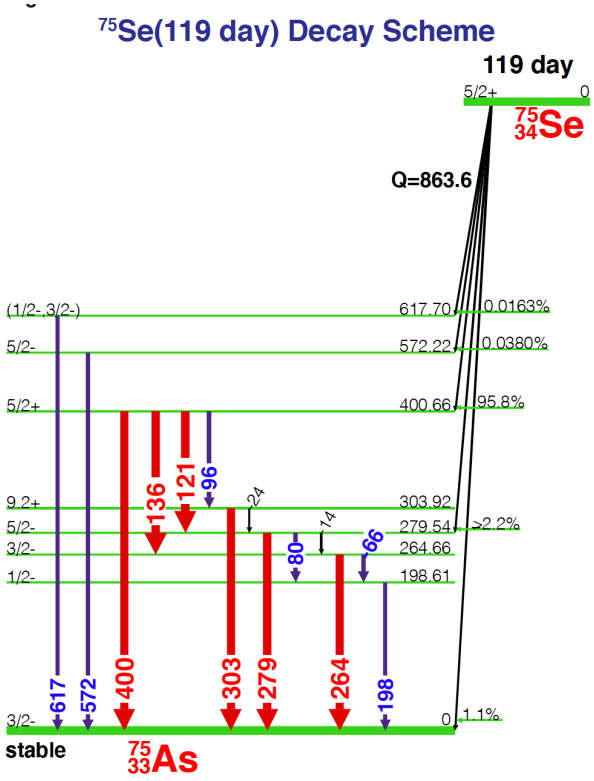

GAMMA-RAY ENERGIES AND INTENSITIES

Nuclide: ^{75}Se — Half Life: 119.79(4) day.
Detector: 65 cm^3 coaxial Ge (Li) — Method of Production: ^{74}Se(n,γ)

E_γ (keV)	σ E_γ	I_γ (rel)	I_γ (%)	σ I_γ	S
14.8846	0.0012		0.0012	0.0006	4
24.3815	0.0014		0.0270	0.0012	4
66.0518	0.0008	1.9	1.112	0.012	4
80.9364	0.0015		0.0077	0.0024	4
96.7340	0.0010	5.4	3.42	0.03	3
121.1155	0.0011	27.4	17.2	0.4	1
136.0001	0.0006	93.1	58.3	0.8	1
198.6060	0.0012	2.44	1.48	0.05	2
249.3	0.3		0.0001		4
264.6576	0.0009	100	58.9	0.4	1
279.5422	0.0010	42.88	24.99	0.14	1
303.9236	0.0010	2.27	1.316	0.009	1
373.61	0.24		0.0024		4
400.6572	0.0008	19.95	11.47	0.09	1
419.1	0.3		0.0118	0.0003	4
468.6	0.4		0.0003	0.0001	4
542.02	0.17		0.0001		4
556.90	0.17				4
572.22	0.24	0.65	0.0356	0.0005	3
617.8	0.3		0.0044		4
821.56	0.17		0.0001		4

E_γ, σE_γ, I_γ, σI_γ - 1998 ENSDF Data

Figure 110: ^{75}Se Decay Scheme

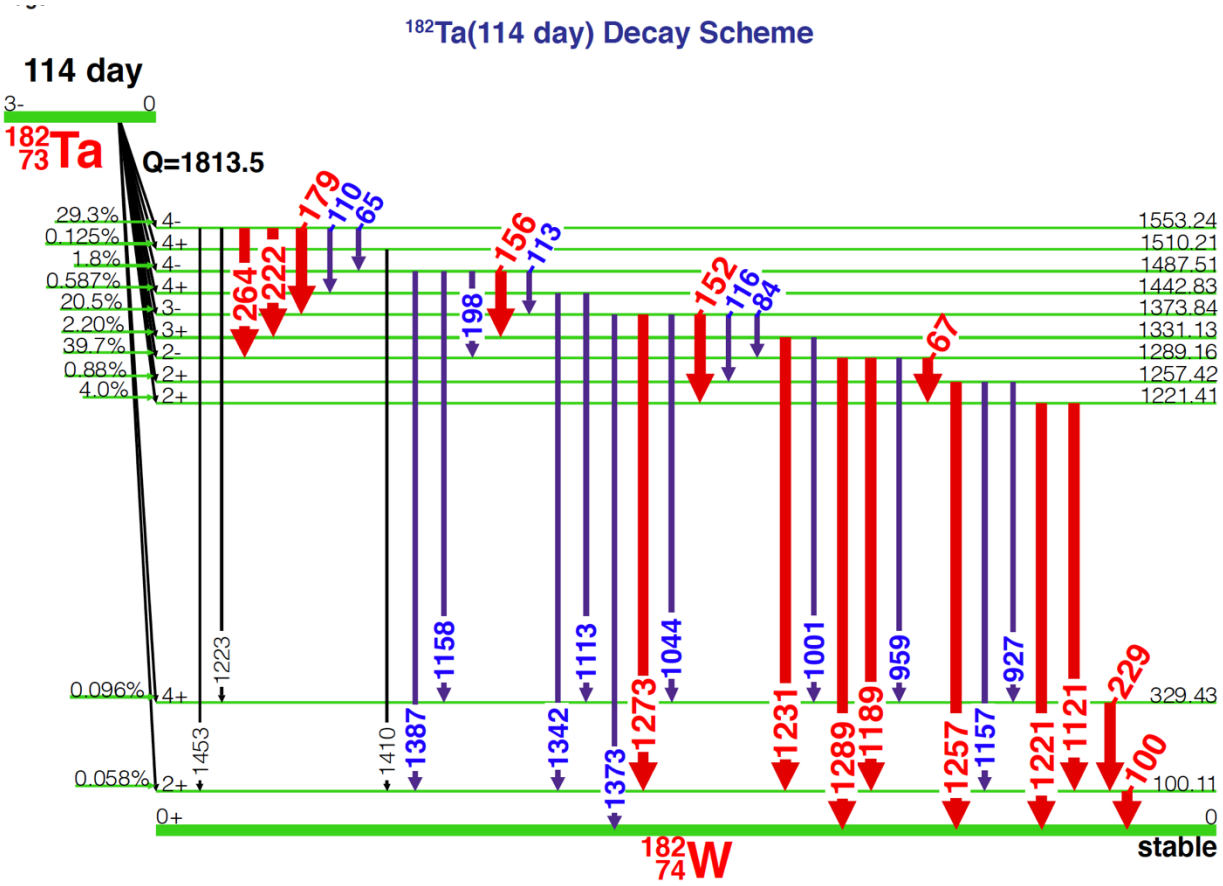

Figure 111: ^{182}Ta Decay Scheme

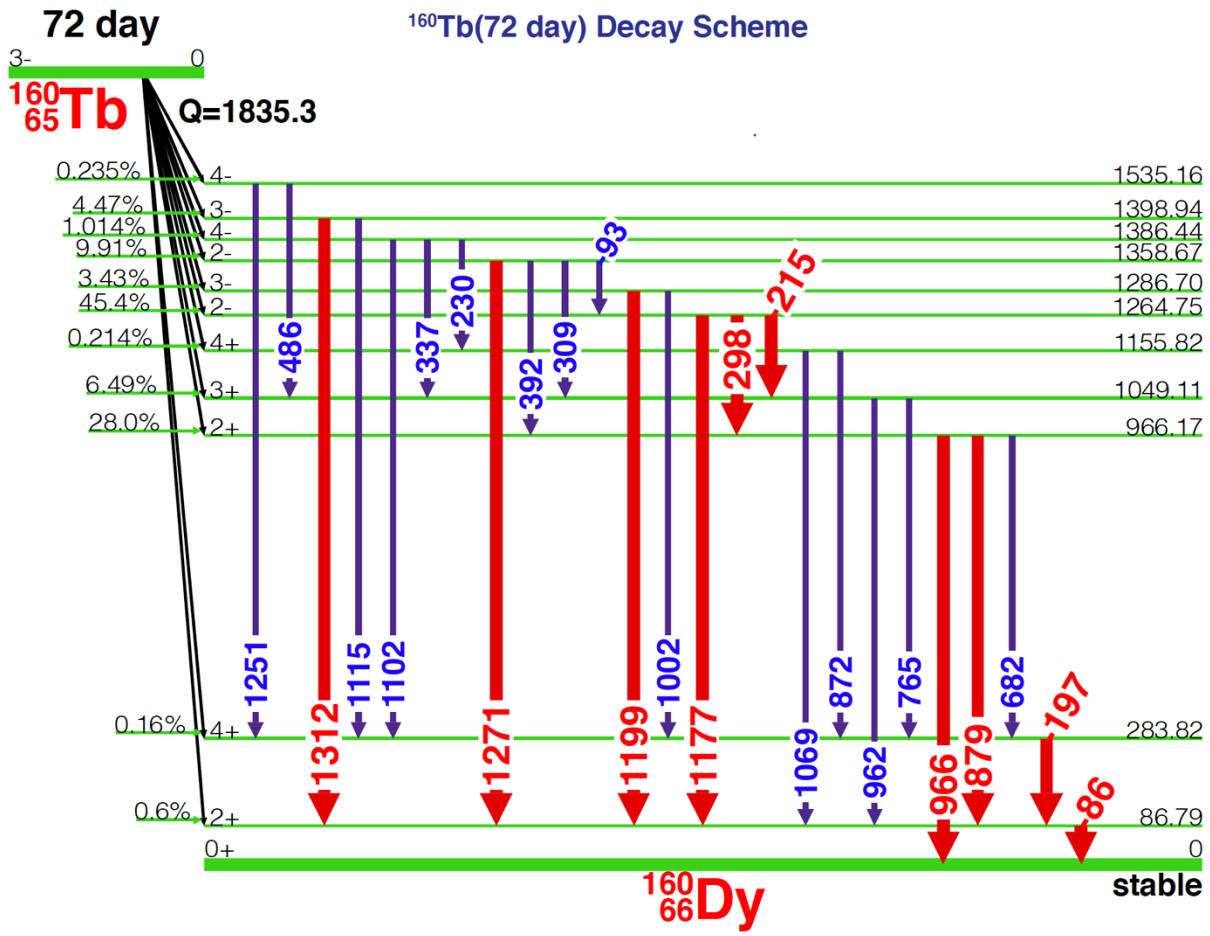

Figure 112: ^{160}Tb Decay Scheme

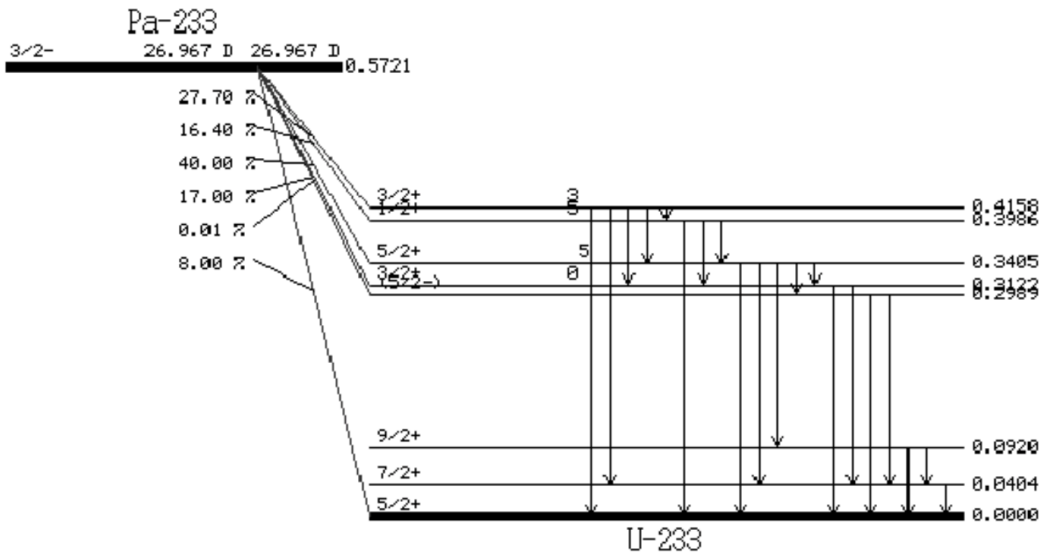

Figure 113: ^{233}Pa Decay Scheme (*Ultra Sensitive Neutron Activation Measurements of 232Th in Copper*, n.d.)

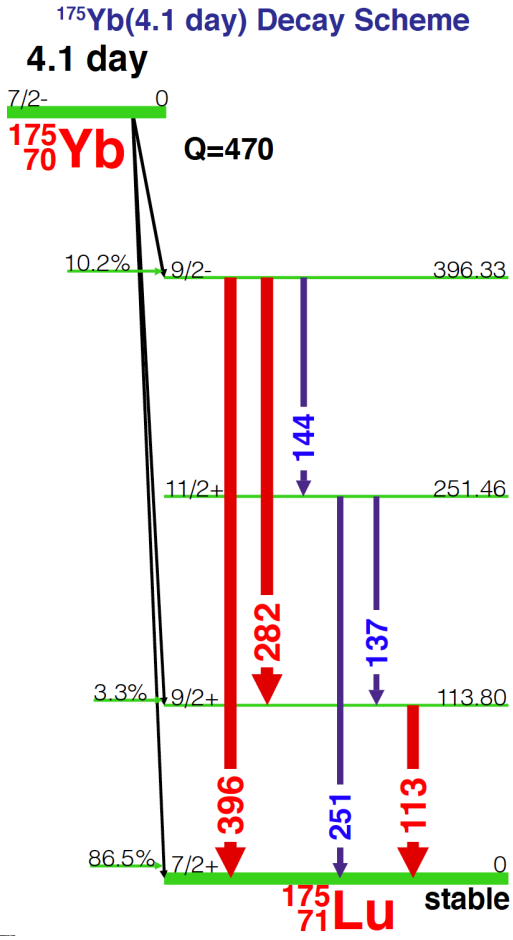

GAMMA-RAY ENERGIES AND INTENSITIES

Nuclide: ^{175}Yb — Half Life: 4.185(1) day

Detector: 4.55 cm^2 x 8 mm Ge (Li) — Method of Production: ^{174}Yb(n,γ)

E_γ (keV)	σ E_γ	I_γ (rel)	I_γ (%)	σ I_γ	S
113.805	0.004	25.0	1.88	0.24	1
137.658	0.006	2.1	0.103	0.015	3
144.863	0.005	5.1	0.33	0.04	2
251.474	0.017	1.7	0.084	0.011	3
282.522	0.014	47.0	3.0	0.4	1
396.329	0.020	100.	6.4	0.8	1

E_γ, σE_γ, I_γ, σI_γ - 1998 ENSDF Data

Figure 114: ^{175}Yb Decay Schem

References

Bonolis, L. (2011). Walther Bothe and Bruno Rossi: The birth and development of coincidence methods in cosmic-ray physics. *American Journal of Physics*, *79*(11), 1133–1150. https://doi.org/10.1119/1.3619808

Bramlitt, E. T. (1966). Gamma-Gamma Coincidence Counting Applied to Chlorine Analysis by Neutron Activation. *Analytical Chemistry*, *38*(12), 1669–1674. https://doi.org/10.1021/ac60244a010

Brennan, C., & Landsberger, S. (2019). Interferences in the determination of lutetium using neutron activation analysis. *Journal of Radioanalytical and Nuclear Chemistry*, *322*(2), 1201–1205. https://doi.org/10.1007/s10967-019-06674-8

Britton, R., Jackson, M. J., & Davies, A. V. (2015). Quantifying radionuclide signatures from a γ-γ coincidence system. *Journal of Environmental Radioactivity*, *149*, 158–163. https://doi.org/10.1016/j.jenvrad.2015.07.025

Canion, B., & Landsberger, S. (2013). Trace analysis and leaching dynamics of volcanic ash using NAA and ICP-MS. *Journal of Radioanalytical and Nuclear Chemistry*, *296*(1), 375–378. https://doi.org/10.1007/s10967-012-2069-3

Cooper, J. A. (1971). Radioanalytical Applications of Gamma-Gamma Coincidence Techniques with Lithium-Drifted Germanium Detectors. *Analytical Chemistry*, *43*(7), 838–845. https://doi.org/10.1021/ac60302a017

Crane, T. W. (1980). *Measurement of Uranium and Plutonium in Soiid Waste by Passive Photon or Neutron Counting and Isotopic Neutron Source Interrogation*. 1–96.

Crouthamel, C. E. (1970). *APPLIED GAMMA-RAY SPECTROMETRY* (F. Adams & R. Dams, Eds.; Second).

Drescher, A., Yoho, M., & Landsberger, S. (2018). Gamma–gamma coincidence in neutron activation analysis. *Journal of Radioanalytical and Nuclear Chemistry*, *318*(1), 527–532. https://doi.org/10.1007/s10967-018-6033-8

Drescher, A., Yoho, M., Landsberger, S., Durbin, M., Biegalski, S., Meier, D., & Schwantes, J. (2017). Gamma-gamma coincidence performance of LaBr3:Ce scintillation detectors vs HPGe detectors in high count-rate scenarios. *Applied Radiation and Isotopes*, *122*(January), 116–120. https://doi.org/10.1016/j.apradiso.2017.01.012

Egozi, C., Martinez, F., Luna, B. de, Terry, J., & Landsberger, S. (2020). A PRELIMINARY INVESTIGATION FOR THE USE OF DIGITAL GAMMA-GAMMA COINCIDENCE SPECTROMETRY TO DETERMINE ^{239}Pu. *4*, 1–4. https://doi.org/10.21175/RadProc.2020.00

Hatsukawa, Y., Miyamoto, Y., Toh, Y., Oshima, M., Hosein Mahmudy Gharaie, M., Goto, K., & Toyoda, K. (2007). High-sensitive elemental analysis using multi-parameter coincidence spectrometer: GEMINI-II. *Journal of Radioanalytical and Nuclear Chemistry*, *272*(2), 273–276. https://doi.org/10.1007/s10967-007-0514-5

Helmer, R. G., Davidson, J. R., Gehrke, R. J., & van der Luen, C. (1998). *GAMMA-RAY SPECTRUM CATALOGUE*.

Horne, S., & Landsberger, S. (2012). Selenium and mercury determination in biological samples using gamma-gamma coincidence and Compton suppression. *Journal of Radioanalytical and Nuclear Chemistry*, *291*(1), 49–53. https://doi.org/10.1007/s10967-011-1268-7

Jakůbek, J., Nuiten, P., Pluhař, J., Pospíšil, S., Šiňor, M., Štekl, I., Timorácký, S., & Vobecký, M. (1998). Coincidence gamma-gamma spectroscopy system for instrumental neutron activation analysis. *Nuclear Instruments and Methods in Physics Research, Section A: Accelerators, Spectrometers, Detectors and Associated Equipment*, *414*(2–3), 261–264. https://doi.org/10.1016/S0168-9002(98)00497-5

Kaihola, L. (2011). Low Level Liquid Scintillation Counting of Radioactivity in Food Products.

Kajrys, G., Landsberger, S., Lecomte, R., Paradis, P., & Monaro, S. (1982). Level Structure of 97Tc Investigated via the 97Mo(p,n) Reaction. *Physical Review*, *C26*, 1451–1461.

Kirkpatrick, J., & Young, B. (2009). Poission Low-Count Spectra.pdf. *IEEE TRANSACTIONS ON NUCLEAR SCIENCE*, *56*(3), 1278–1282.

Knoll, G. F. (2010). Radiation Detection and Measurement (4th ed.). John Wiley & Sons Ltd.

Landsberger, S. (1994). Chemical Analysis by Nuclear Methods (Zeev. B. Alfassi, Ed.; Issue 1). John Wiley & Sons Ltd.

Landsberger, S., & Peshev, S. (1996). Compton Suppression Neutron Activation Analysis: Past, Present and Future. *Journal of Radioanalytical and Nuclear Chemistry*, *202*, 203–226.

Landsberger, S., & Simsons, A. (1987). QUANTIFICATION OF URANIUM , THORIUM AND GADOLINIUM SPECTRAL INTERFERENCES IN INSTRUMENTAL NEUTRON ACTIVATION ANALYSIS OF SAMARIUM. *Chemical Geology*, *62*, 223–226.

Landsberger, S., & Wu, D. (1995). A COMPREHENSIVE STUDY FOR THE DETERMINATION OF FORTY EIGHT ELEMENTS IN THE CERTIFICATION OF A HAZARDOUS STANDARD REFERENCE MATERIAL. *Science*, *193*(1), 49–59.

Landsberger, S., & Yellin, J. (2018). Minimizing Sample Sizes while Achieving Accurate Elemental Concentrations in Neutron Activation Analysis of Precious Pottery. In *Journal of Archaeological Science: Reports*.

Marković, N., Roos, P., & Nielsen, S. P. (2017). Digital gamma-gamma coincidence HPGe system for environmental analysis. *Applied Radiation and Isotopes*, *126*(December 2016), 194–196. https://doi.org/10.1016/j.apradiso.2016.12.017

Niese, S. (1996). Application of low-level counting techniques for the investigation of the impact of uranium mining as well as remediation on the environment. *Applied Radiation and Isotopes*, *47*(9–10), 1109–1112.

Niese, S., & Kohler, M. (1996). Low-level counting techniques in the underground laboratory 'Telsenkeller" in Dresden. *PROCEEDINGS OF A WORKSHOP ROSSENDORF / DRESDEN,* 34–38.

Rossi, B. (1930). Method of Registering Multiple Simultaneous Impulses of Several Geiger's Counters. *Nature*, *125*(3156), 636. https://doi.org/10.1038/125636a0

Sampson, T. (1991). Plutonium Isotopic Composition by Gamma-Ray Spectroscopy. In *Passive Nondestructive Assay of Nuclear Materials (PANDA)* (Issue September). http://www.lanl.gov/orgs/n/n1/panda/

Smith, J. K., MacLean, A. D., Ashfield, W., Chester, A., Garnsworthy, A. B., & Svensson, C. E. (2019). Gamma–gamma angular correlation analysis techniques with the GRIFFIN spectrometer. *Nuclear Instruments and Methods in Physics Research, Section A: Accelerators, Spectrometers, Detectors and Associated Equipment*, *922*, 47–63. https://doi.org/10.1016/j.nima.2018.10.097

Stokley, M. B., & Landsberger, S. (2018). A Non-Destructive Analytical Technique for Low Level Detection of Praseodymium Using Epithermal Neutron Activation Analysis and Compton Suppression Gamma-Ray Spectroscopy. *Journal of Radioanalytical and Nuclear Chemistry*, *318*, 369–373.

Tomlin, B. E., Zeisler, R., & Lindstrom, R. M. (2008). Γ Γ Coincidence Spectrometer for Instrumental Neutron-Activation Analysis. *Nuclear Instruments and Methods in Physics Research, Section A: Accelerators, Spectrometers, Detectors and Associated Equipment*, *589*(2), 243–249. https://doi.org/10.1016/j.nima.2008.02.094

Ultra Sensitive Neutron Activation Measurements of 232Th in Copper. (n.d.). Retrieved October 20, 2021, from https://www.researchgate.net/figure/Decay-scheme-of-233-Pa-1_fig1_253988900

University of Missouri. (2012). *Analytical Chemistry Group - Neutron Activation Analysis*. Curators of the University of Missouri DMCA. https://acg.missouri.edu/NAA.html

Usman, S., & Patil, A. (2018). Radiation detector deadtime and pile up: A review of the status of science. *Nuclear Engineering and Technology*, *50*(7), 1006–1016. https://doi.org/10.1016/j.net.2018.06.014

Vobecký, M., Jakůbek, J., Granja Bustamante, C., Koníček, J., Pluhař, J., Pospíšil, S., & Rubáček, L. (1999). Multielement instrumental activation analysis based on gamma-gamma coincidence spectroscopy. *Analytica Chimica Acta*, *386*(1–2), 181–189. https://doi.org/10.1016/S0003-2670(99)00005-7

Wangen, L. E., Gladney, E. S., & Hensley, W. K. (1980). Determination of Selenium in Environmental Standard Reference Materials by a γ—γ. Coincidence Method Using Lithium-Drifted Germanium Detectors. *Analytical Chemistry*, *52*(4), 765–767. https://doi.org/10.1021/ac50054a037

Westphal, G. P. (2008). Review of loss-free counting in nuclear spectroscopy. *Journal of Radioanalytical and Nuclear Chemistry*, *275*(3), 677–685. https://doi.org/10.1007/s10967-007-7090-6

XIA LLC. (2019). *Pixie-16 User Manual* (Issue 3.06). https://www.xia.com/Manuals/Pixie16_UserManual.pdf

Yoho, M., & Landsberger, S. (2016). Determination of Selenium in coal fly ash via $γ$–$γ$ coincidence neutron activation analysis. *Journal of Radioanalytical and Nuclear Chemistry*, *307*(1), 733–737. https://doi.org/10.1007/s10967-015-4209-z

Zeisler, R., Cho, H., Junior, I. S. R., Shetty, M. G., & Turkoglu, D. (2017). On neutron activation analysis with γγ coincidence spectrometry. *Journal of Radioanalytical and Nuclear Chemistry*, *314*(1), 513–519. https://doi.org/10.1007/s10967-017-5342-7

Zeisler, R., Mackey, E. A., Lamaze, G. P., Stover, T. E., Spatz, R. O., & Greenberg, R. R. (2006). NAA methods for determination of nanogram amounts of arsenic in biological samples. *Journal of Radioanalytical and Nuclear Chemistry*, *269*(2), 291–296.

Zhang, W., Ungar, K., Stukel, M., & Mekarski, P. (2014). A gamma-gamma coincidence/anticoincidence spectrometer for low-level cosmogenic 22Na/7Be activity ratio measurement. *Journal of Environmental Radioactivity*, *130*, 1–6. https://doi.org/10.1016/j.jenvrad.2013.12.018